العنوان:	Experimental and Numerical Study of Natural Convection Heat Transfer from Rectangular Fin Arrays
المؤلف الرئيسي:	Mohamad, Hamza Ashur Milad
مؤلفين آخرين:	Abd Allatif, Ahmed Mohamed، El Bakoush, Taib A(Advisor، Co-Advisor)
التاريخ الميلادي:	2007
موقع:	Al Khums
الصفحات:	1 - 155
رقم MD:	766381
نوع المحتوى:	رسائل جامعية
اللغة:	English
الدرجة العلمية:	رسالة ماجستير
الجامعة:	جامعة المرقب
الكلية:	كلية الهندسة
الدولة:	ليبيا
قواعد المعلومات:	Dissertations
مواضيع:	المصفوفة ، الحاسب الآلي، الحمل الحراري
رابط:	https://search.mandumah.com/Record/766381

CHAPTER 1

INTRODUCTION

INTRODUCTION

1.1 Background

The needs for buoyancy driven ventilation appear in a variety of engineering applications, ranging from cooling of electronic components and solar energy applications to cooling of nuclear reactor fuel elements. For an efficient application of natural convection to cooling processes, it is necessary to understand the mechanisms involved. In the free-convection cooling of electronic and thermoelectric devices, as well as in improving the heat transfer in radiators for air conditioning and in other heat exchangers, finned surfaces are extensively used.

Compared to a bare plate, a finned surface increases the heat transfer area. However, with the fins the flow rate reduced. Hence, if not properly designed it is possible that no improvement achieved in terms of overall heat transfer. Therefore, only if the fins properly designed, they are very attractive for these applications, since they offer an economical, trouble-free solution to the problem.

Energy dissipated by electronic equipment transferred to heat sinks by conduction and transferred from the heat sink to the ambient air by natural or forced convection, depending on the power dissipation requirements. Natural convection is the preferred mode of heat transfer since it involves no moving parts, like the electronic components themselves. However, in the natural convection mode the components are likely to run at a higher temperature and thus undermine reliability. A properly selected heat sink may considerably lower the operation temperature of the components and thus reduce the risk of failure.

Extended surfaces, which are popularly known as fins, are extensively used in air-cooled automobile engines and in air-cooled aircraft engines. Fins are also used for the cooling of computer processors, and other electronic devices. Fins are used in the cooling of oil carrying pipe line which runs several hundreds of miles. Heat pipes are also used along with fins to enhance cooling rate.

A great deal of research effort has been developed for developing apparatus and performing experiments to define the conditions under which an augmentive technique will improve heat transfer. The more effective and feasible techniques have graduated from laboratory to full-scale industrial equipment.

The techniques of heat transfer augmentations studies are classified according to Bergles[1] classification as the following:

1- Passive methods operate without increase of the consumption. They lie in the introduction of finned, rough or otherwise developed surfaces on the side of a fluid of a low heat transfer coefficient, as well as turbulizers, rods, and swirls devices of eliminating the boundary layer.

2- Active methods of heat transfer augmentation employ supplementary external power. They employ mechanical devices to mix or to scrape the heat carrier from the surface, as well as vibration and rotation of the surfaces itself, to decrease the thickness of the boundary layer and to increase the rate of wetting, which results in heat transfer augmentation. Sound vibrations, may be introduced in the fluid, from 1 HZ to ultrasonic. An electric field may be introduced in the system, to increase convective motion of the fluid through specific forces in

the dielectric fluid. The heated fluid may be sucked a way through a porous layer.

Among the passive augmentative techniques in use today are:

1- Surface promoters, distributed, isolated, or machined.
2- Displaced promoters, by placed thin rings or discs, coil, or springs, and twisted tapes.
3- Vortex flow, which reffered to as turbulence promoters.
4- Extended surfaces, continuous or interrupted, internal or external, and straight or spiral.

1.2 Objectives

The objective of this thesis is to study the natural convection heat transfer from a rectangular fin arrays. In the first part of the present work, experimental investigations were performed to determine the heat transfer characteristics from a longitudinal fin arrays. Effects of fin spacing, fin height, model orientation angle, and temperature difference between fin and surroundings on the free convection heat transfer from fin arrays were carried out. During the experiments, the fin spacing (S) was varied from 3.4 to 33 mm, fin height (H) from 15 to 60 mm, orientation angle (Φ) from 0° to 180°, and temperature difference between fin and surrounding (ΔT) from 35 to 95 °C.

In the second part of present work, numerical model (Fluent) to predict the fluid motion that occurs in natural convection heat transfer from fin arrays. The three-dimensional elliptic governing equations solved using finite volume based computational fluid dynamics (CFD) code. A large number of runs were carried out for a systematic theoretical investigation of the effects of fin spacing, fin height, orientation angle and temperature

difference between fin and surroundings on the heat transfer processes involved.

In the third part of the present work is to compare the experimental results with the numerical results verification the numerical solution, and to derive empirical correlations between Nussult number, Rayighly number fin spacing, fin height, orientation angle, and temperature difference between the fin and surroundings.

العنوان:	Experimental and Numerical Study of Natural Convection Heat Transfer from Rectangular Fin Arrays
المؤلف الرئيسي:	Mohamad, Hamza Ashur Milad
مؤلفين آخرين:	Abd Allatif, Ahmed Mohamed، El Bakoush, Taib A(Advisor، Co-Advisor)
التاريخ الميلادي:	2007
موقع:	Al Khums
الصفحات:	1 - 155
رقم MD:	766381
نوع المحتوى:	رسائل جامعية
اللغة:	English
الدرجة العلمية:	رسالة ماجستير
الجامعة:	جامعة المرقب
الكلية:	كلية الهندسة
الدولة:	ليبيا
قواعد المعلومات:	Dissertations
مواضيع:	المصفوفة ، الحاسب الآلي، الحمل الحراري
رابط:	https://search.mandumah.com/Record/766381

CHAPTER 2

THEORETICAL BACKGROUND

THEORITICAL BACKGROUND

2.1 Introduction

This chapter presents a review of the theoretical analysis and equations of heat transfer especially for convection heat transfer on surfaces.

2.2 Natural Convection Mode

In natural convection, or free convection, the fluid flows “naturally” (by itself), as it is driven by the affect of buoyancy. This effect is distributed throughout the fluid, and is associated with the general tendency of fluids to expand, when heated at constant pressure. The layer that feels the warm vertical wall (see Fig. 2-1) becomes lighter than the rest of the fluid. Its lightness forces it to flow upward, to sweep the wall and to collect heat transfer from the wall in a manner that reminds us of the boundary layer of this time; however, the flow is a vertical. Jet parallel to the wall, whereas the fluid situated far from the wall is stagnant.[33]

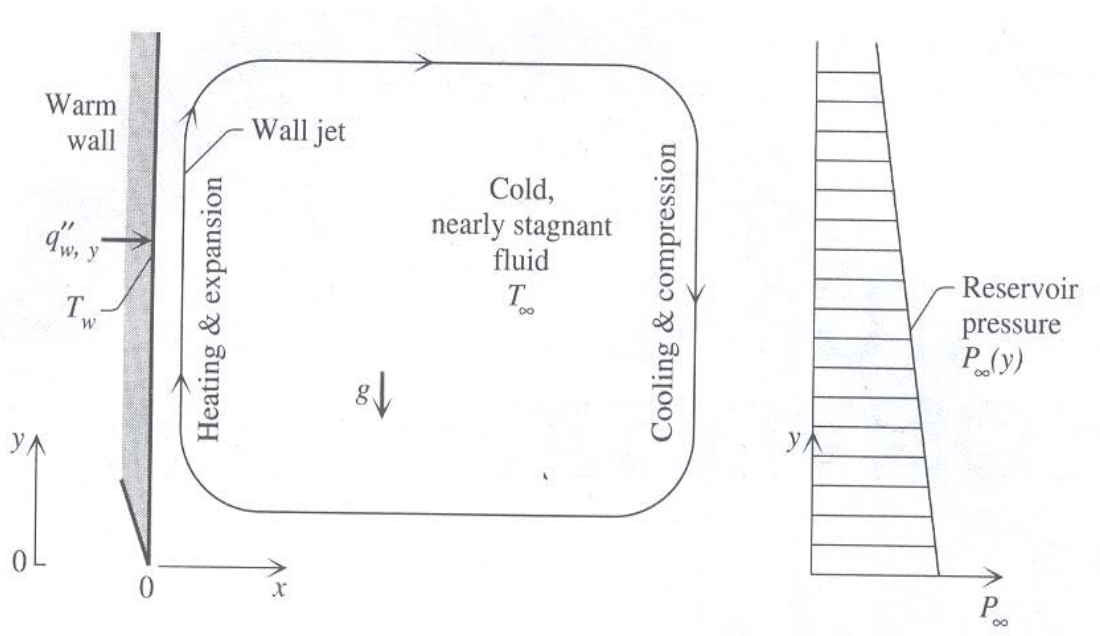

Fig. 2-1. Wall jet driven by buoyancy along a heated wall, and the pressure distribution in the reservoir of stagnant fluid.

In free convection, fluid motion is due to buoyancy forces within the fluid, while in forced convection it externally imposed. Buoyancy is due to the combined presence of a fluid density gradient and a body force that is proportional to the density. In practice, the body force is usually gravitational, although it may be a centrifugal force in rotating fluid machinery or a Carioles force in atmospheric and oceanic rotational motions. There are also several ways in which a mass density gradient may arise in a fluid, but for the most common situation it is due to the presence of a temperature gradient. We know that the density of gases and liquids depends on temperature, generally decreases (due to fluid expansion) with the increasing fluid temperature ($\partial\rho/\partial T < 0$).

To understand nature of free heat transfer mode, consider the conditions of Fig. (2-2). A fluid is enclosed by two large, horizontal plates of different temperature ($T_1 \neq T_2$). In case (a) the temperature of the lower plate exceeds that of the upper plate, and the density decreases in the direction of the gravitational force. If the temperature difference exceeds a critical value

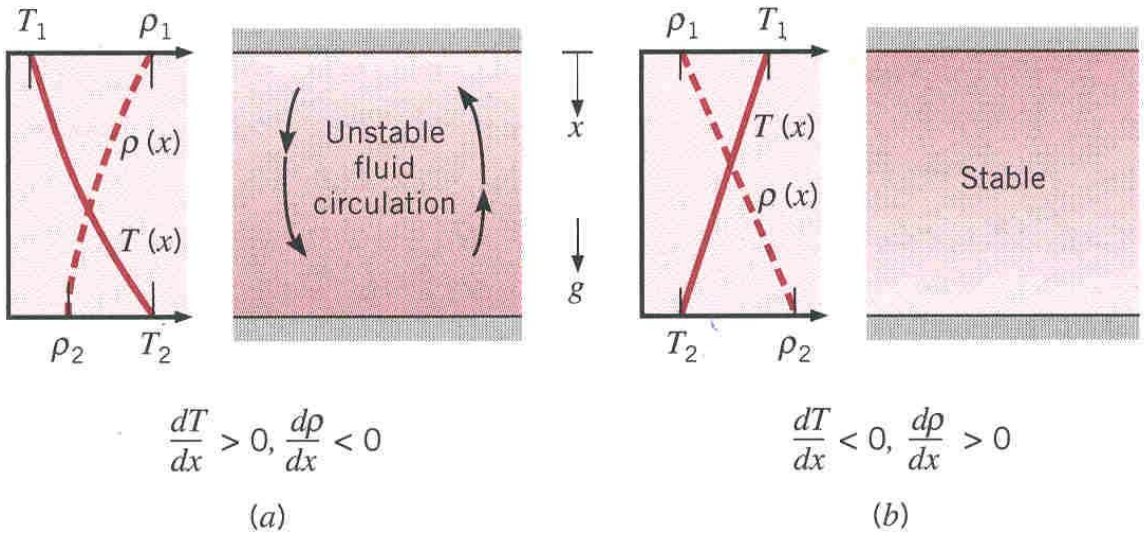

Fig. 2-2. Conditions in a fluid between large horizontal plates at different temperatures. (a) Unstable temperature gradient. (b) Stable temperature gradient.

conditions are unstable and buoyancy forces are able to overcome the retarding influence of viscous forces. The gravitational force on the denser fluid in the upper layers exceeds that acting on the lighter fluid in the lower layers, and the designated circulation pattern will exist. The heavier fluid will descend, warmed in the process, while the lighter fluid will rise, cooling as it moves. However, this condition does not characterize case (b), for which $T_1 > T_2$ and the density on longer decreases in the direction of the gravitational force. Conditions are now stable, and there is no bulk fluid motion. In case (a) heat transfer occurs from the bottom to the top surface by free convection; for case (b) heat transfer (from top to bottom) occurs by conduction.

Free convection flows may classify according to whether the flow is bounded by a surface. In the absence of an adjoining surface, free boundary

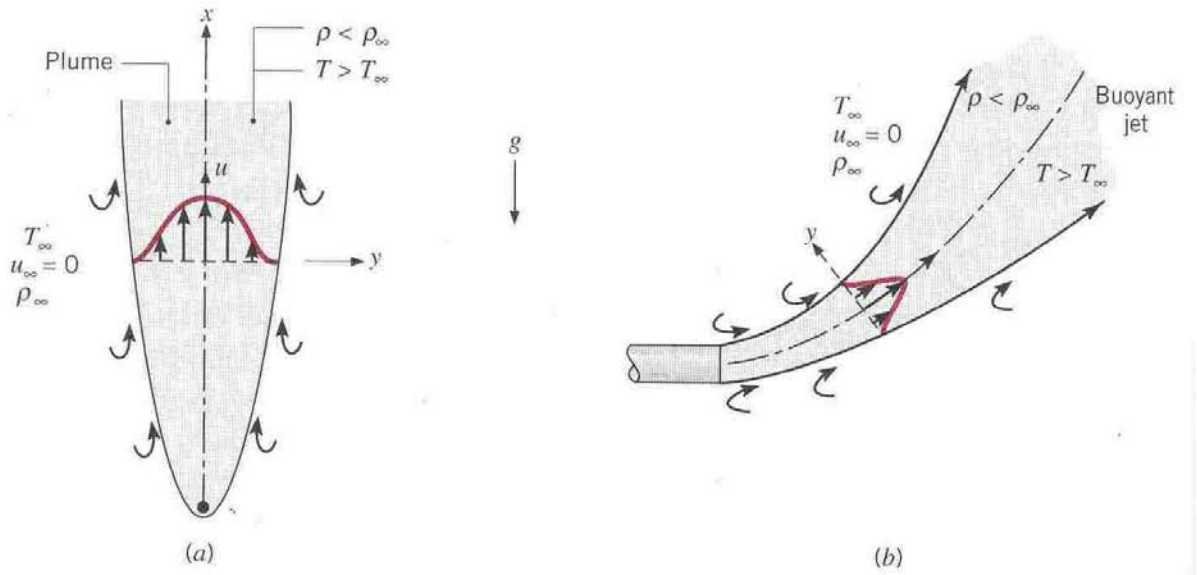

Fig. 2-3. Buoyancy driven free boundary layer flows in an extensive, quiescent medium. (a) Plume formation above a heated wire. (b) Buoyant jet associated with a heated discharge

flows may occur in the form of a plume or a buoyant jet (Fig. 2-3). A plume is associated with fluid rising from a submerged heated object. Consider the heated wire of Fig. (2-3a), which is immersed in an extensive, quiescent fluid. Fluid that is heated by the wire rises due to buoyancy forces, entraining fluid from the quiescent region. Although the width of the plume increases with distance from the wire, the plume itself will eventually dissipate as a result of viscous effects and a reduction in the buoyancy force caused by cooling of the fluid in the plume. The distinction between a plume and a buoyant jet is generally made on the basis of the initial fluid velocity. This velocity is zero for the plume, but finite for the buoyant jet. Fig. (2-3b) shows a heated fluid being discharged as a horizontal jet into a quiescent medium of lower temperature. The vertical motion that the jet begins to assume is due to the buoyancy force.[34]

2.3 Boundary Layer Equation

To introduce the concept of a boundary layer, consider flow over the flat plate of Fig. (2-4). When fluid particles make contact with the surface,

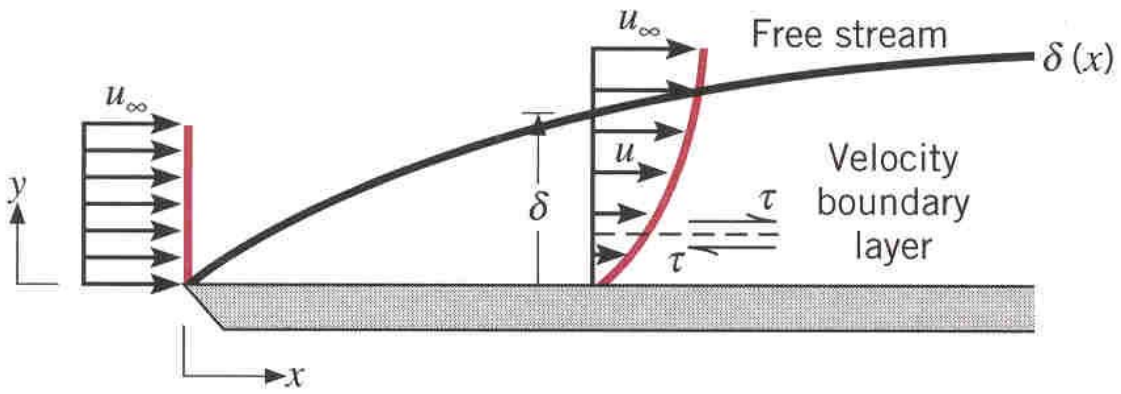

Fig. 2-4. Velocity boundary layer developments on a flat plate.

they assume zero velocity. These particles then act to retard the motion of particles in the next layer, and so on until, at a distance y = δ from the surface, the effect becomes negligible. This retardation of fluid motion is associated with shear stresses τ acting in planes that are parallel to the fluid velocity (Figure (2-4)). With increasing distance y from the surface, the x velocity component of the fluid, u, must then increase until it approaches the free stream value u_∞.

The quantity δ is value of y for which u = 0.99 u_∞. The boundary layer velocity profile refers to the manner in which u varies with y through the boundary layer. Accordingly, the fluid flow is characterized by two distinct regions, a thin fluid layer (the boundary layer) in which velocity gradients and shear stresses are large and a region outside the boundary layer in which velocity gradients and shear stresses are negligible. With increasing distance from the leading edge, the effects of viscosity penetrate further into the free stream and the boundary layer grows (δ increases with x). because it pertains to the fluid velocity, the foregoing boundary layer may be referred to more specifically as the velocity boundary layer. It develops whenever there is fluid flow over a surface, and it is of fundamental importance to problems involving convection transport. In fluid mechanics its significance to the engineer stems from its relation to the surface shear stress τ_s, and hence to surface frictional effects. For external flows it provides the basis determining the local friction coefficient.

$$C_f = \frac{\tau_s}{\rho u_\infty^2 / 2} \tag{2-1}$$

a key dimensionless parameter from which the surface frictional drag may be determined. Assuming a Newtonian fluid, the surface shear stress may evaluate from knowledge of the velocity gradient at the surface by equation

$$\tau_s = \mu \frac{\partial u}{\partial y}\Big|_{y=0} \qquad (2\text{-}2)$$

Where, μ: is a fluid property known as the dynamic viscosity.[34]

In three rectangular Cartesian coordinate directions, we assume that the fluid is in compressible, steady, laminar flow of air with constant properties except for density which is taken as a function of temperature only, ρ = ρ(T) and radiation heat transfer is negligible .With these assumptions the non-dimensional governing equation are .

(Conservation of mass)

$$\frac{\partial(\rho u)}{\partial x} + \frac{\partial(\rho v)}{\partial y} + \frac{\partial(\rho w)}{\partial z} = 0 \qquad (2\text{-}3)$$

(Conservation of momentum)

$$\frac{\partial(\rho u^2)}{\partial x} + \frac{\partial(\rho uv)}{\partial y} + \frac{\partial(\rho uw)}{\partial z} = -\frac{\partial(Pm)}{\partial x} + \rho\nu\left(\frac{\partial^2 u}{\partial x^2} + \frac{\partial^2 u}{\partial y^2} + \frac{\partial^2 u}{\partial z^2}\right) \qquad (2\text{-}4)$$

$$\frac{\partial(\rho vu)}{\partial x} + \frac{\partial(\rho v^2)}{\partial y} + \frac{\partial(\rho vw)}{\partial z} = -\frac{\partial(Pm)}{\partial y} + \rho\nu\left(\frac{\partial^2 v}{\partial x^2} + \frac{\partial^2 v}{\partial y^2} + \frac{\partial^2 v}{\partial z^2}\right) + g(\rho - \rho_a) \qquad (2\text{-}5)$$

$$\frac{\partial(\rho wu)}{\partial x} + \frac{\partial(\rho wv)}{\partial y} + \frac{\partial(\rho w^2)}{\partial z} = -\frac{\partial(Pm)}{\partial z} + \rho\nu\left(\frac{\partial^2 w}{\partial x^2} + \frac{\partial^2 w}{\partial y^2} + \frac{\partial^2 w}{\partial z^2}\right) \qquad (2\text{-}6)$$

(Conservation of energy)

$$\frac{\partial(\rho uT)}{\partial x} + \frac{\partial(\rho vT)}{\partial y} + \frac{\partial(\rho wT)}{\partial z} = \frac{\nu}{\mathrm{Pr}}\left(\frac{\partial^2 T}{\partial x^2} + \frac{\partial^2 T}{\partial y^2} + \frac{\partial^2 T}{\partial w^2}\right) \qquad (2\text{-}7)$$

2.4 The Thermal Boundary Layer

Just as a velocity boundary layer develops when there is fluid flow over a surface, a thermal boundary layer must develop if the fluid free stream and surface temperatures differ. Consider flow over an isothermal flat plate Fig. (2-5). At the leading edge the temperature profile is uniform,

with T(y) = T_∞. However, fluid particles that come into contact with the plate achieve thermal equilibrium at the plate surface temperature. In turn these particles exchange energy with those in the adjoining fluid layer, and temperature gradients develop in the fluid. The region of the fluid in which these temperature gradients exist is the thermal boundary layer, and its thickness δ_t is typically defined as the value of y for which the ratio $\{(T_s - T)/(T_s - T_\infty)\}=0.99$. With increasing distance from the leading edge, the effects of heat transfer penetrate further into the free stream and the thermal boundary layer grows.

The relation between conditions in this boundary layer and the convection heat transfer coefficient may readily be demonstrated. At any distance x from the leading edge, the local heat flux may be obtained by applying Fourier's law to the fluid at y = 0.

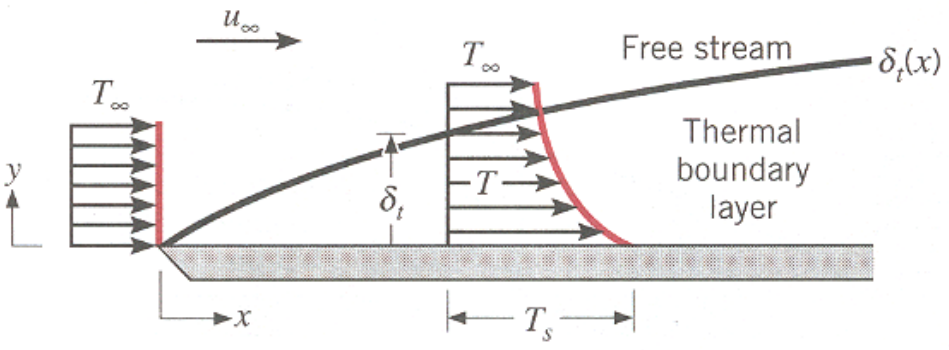

Fig. 2-5. Thermal boundary layer developments on an isothermal flat plate

That is,

$$q_s'' = -k_f \left.\frac{\partial T}{\partial y}\right|_{y=0} \qquad (2\text{-}8)$$

This expression is appropriate because, at the surface, there is no fluid motion and energy transfer occurs only by conduction. By combining Equation (2-8) with Newton's law of cooling Equation (2-9),

$$q'' = h(T_s - T_\infty) \qquad (2\text{-}9)$$

We then obtain :

$$h = \frac{-k_f \left. \partial T / \partial y \right|_{y=0}}{(T_s - T_\infty)} \qquad (2\text{-}10)$$

Hence conditions in the thermal boundary layer, which strongly influence the wall temperature gradient $\partial T/\partial y|_{y=0}$, determine the rate of heat transfer across the boundary. Since (T_s - T_∞) is a constant, independent of x, while δ_t increases with increasing x, temperature gradients in the boundary layer must decrease with increasing x. Accordingly, the magnitude of $\partial T/\partial y|_{y=0}$ decreases with increasing x, and it follows that q_s" and h decrease with increasing x.[34]

2.5 Empirical Correlation

In this section we summarize empirical correlation that has been developed for common immersed (external flow) geometries. The correlations are suitable for most engineering calculation and are generally of the form

$$\overline{Nu_L} = \frac{\overline{hL}}{k} = cRa_L^n \qquad (2\text{-}11)$$

where the Rayleigh number,

$$Ra_L = \Pr Gr_L = \frac{g\beta(T_s - T_\infty)L^3}{\alpha\nu} \qquad (2\text{-}12)$$

Where Re_L is based on the characteristic length L .Typically, n=¼ and n=⅓ for laminar and turbulent flows, respectively. Note that all properties are evaluated at the film temperature, $T_f = (T_S + T_\infty)/2$, Equation (2-11) have been developed for vertical plate and the coefficient (C) and exponent (n) depend on the Rayleigh number range.

2.5.1The vertical plate

A correlation that may be applied over the entire range of Ra_L has been recommended by Churuhill and Chu[4] and is of the form .

$$\overline{Nu}_L = \left\{ 0.825 + \frac{0.387 Ra_L^{1/6}}{\left[1 + (0.492/\mathrm{Pr})^{9/16}\right]^{\frac{8}{27}}} \right\}^2 \qquad (2\text{-}13)$$

Although is suitable for most engineering calculation, slightly better accuracy may be obtained for laminar flow by using Equation (2.14).

$$\overline{Nu}_L = \left\{ 0.68 + \frac{0.670 Ra_L^{1/4}}{\left[1 + (0.492/\mathrm{Pr})^{9/16}\right]^{\frac{4}{9}}} \right\}^2 \qquad Ra_L \le 10^9 \qquad (2\text{-}14)$$

for an isothermal plate (constant T_S).

2.5.2 Inclined and horizontal plates

For a vertical plate, heated (or cooled) relative to an ambient fluid, the plate is aligned with the gravitational vector, and the buoyancy force acts exclusively to induce fluid motion in the upward (or downward) direction. However, if the plate is inclined with respect to gravity, the buoyancy force has a component normal, as will as parallel, to the plate surface. With a reduction in the buoyancy force parallel to the surface, there is a reduction in fluid velocities along the plate, and one might expect there to be an attendant reduction in convection heat transfer. Whether, in fact, there is such a reduction depends on whether one is interested in heat transfer from the top or bottom surface of the plate.

As shown in Fig. (2-6a), if the plate is cooled, the *y* component of the buoyancy force, which is normal to the plate, acts to maintain the descending boundary layer flow in contact with the top surface of the plate. Since the x component of the gravitational acceleration is reduced to g cos

θ, fluid velocities along the plate are reduced and there is an attendant reduction in convection heat transfer to the top surface. However, at the

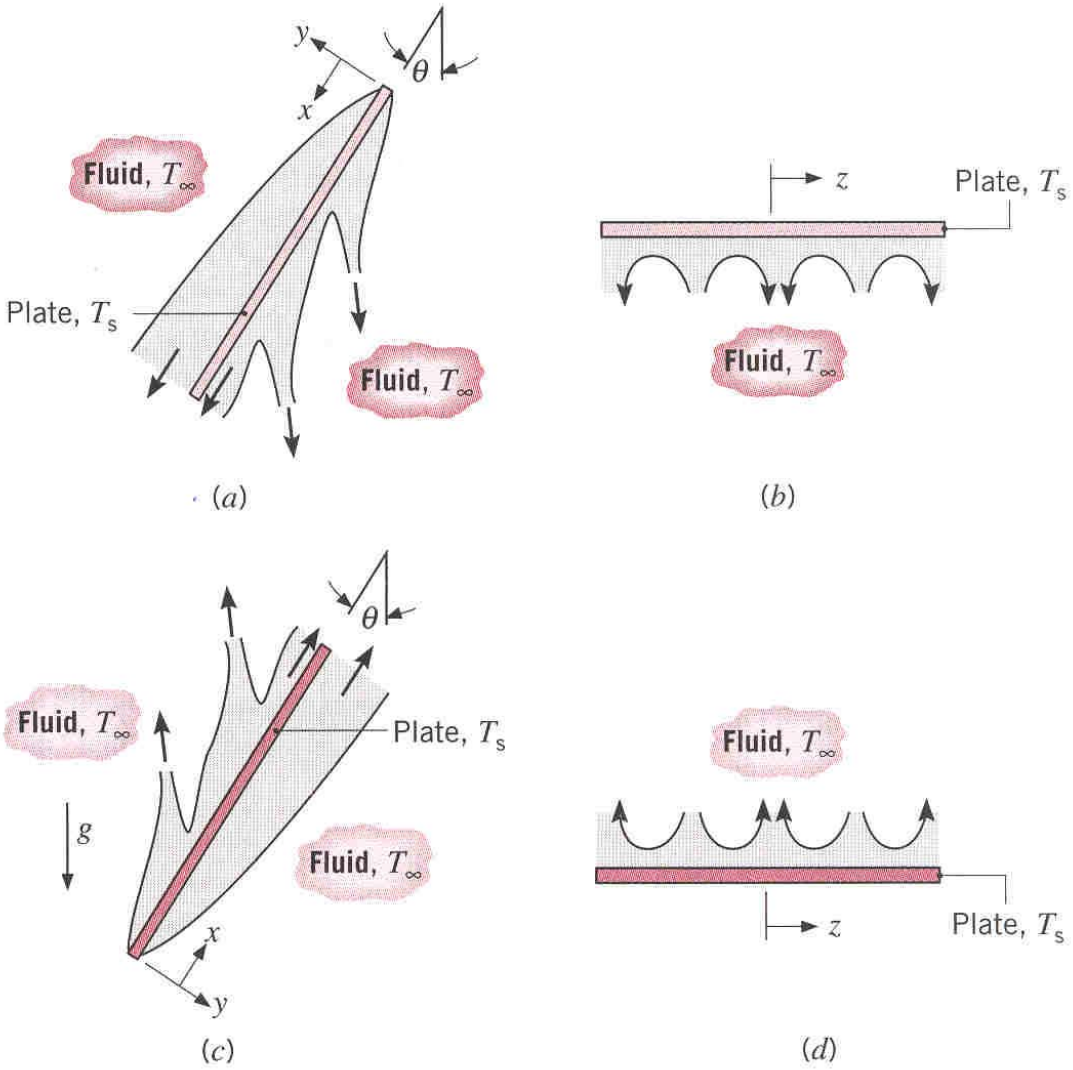

Fig. 2-6. Buoyancy driven flows on an inclined plate : (a)side view of flows at top and bottom surfaces of a cold plate ($T_s<T_\infty$), (b) end view of flow at bottom surfaces of cold plate, (c) side view of flows at top and bottom surfaces of a hot plate ($T_s<T_\infty$),and (d) end view of flow at top surface of hot plate.

bottom surface, the y component of the buoyancy force acts to move fluid

from the surface, and boundary layer development is interrupted by the discharge of parcels of cool fluid from the surface Fig. (2-6a). The resulting flow is three-dimensional, and, as shown by the span wise (z-direction) variations of Fig. (2-6b), the cool discharged from the bottom surface is continuously replaced by the warmer ambient fluid. The displacement of cool boundary layer fluid by the ambient and the attendant reduction in the thermal boundary layer thickness act to increase Convection heat transfer to the bottom surface. In fact, heat transfer enhancement due to the three-dimensional flow typically exceeds the reduction associated with the reduced *x* component of g, and the combined effect is to increase heat transfer to the bottom surface. Similar trends characterize a heated plate Fig. (2-6c) and (d), and the three-dimensional flow is now associated with the upper surface, from which parcels of warm fluid are discharged. Such flows have been observed by several investigators.

In an early study of heat transfer from inclined plates. Rich [2] suggested that convection coefficients could be determined from vertical plate correlation, Equations (2-13) and (2-14) if g is replaced by g cos θ in computing the plate Rayleigh number. Since then, however, it has been determined that this approach is only satisfactory for the top and bottom surfaces of cooled and heated plates, respectively, it is not appropriate for the top and bottom surfaces of heated and cooled plates, respectively, where the three-dimensionality of the flow has limited the ability to de-velop generalized correlations. At the top and bottom surfaces of cooled and heated inclined plates, respectively it is therefore recommended that, for $0 \leq \theta \leq 60^{\circ}$, g be replaced by g cos θ and that equation be used to compute the average Nusselt number. For the opposite surfaces, no recommendations are made and the literature should be consulted. If the plate is horizontal, the buoyancy force is exclusively normal to the surface. As for the inclined plate, flow patterns and heat transfer depend strongly on

whether the surface is cooled or heated and on whether it is facing upward or downward, For a cold surface facing upward (Fig. 2-7a) and a hot surface facing downward Fig. (2-7d), the tendency of the fluid to descend

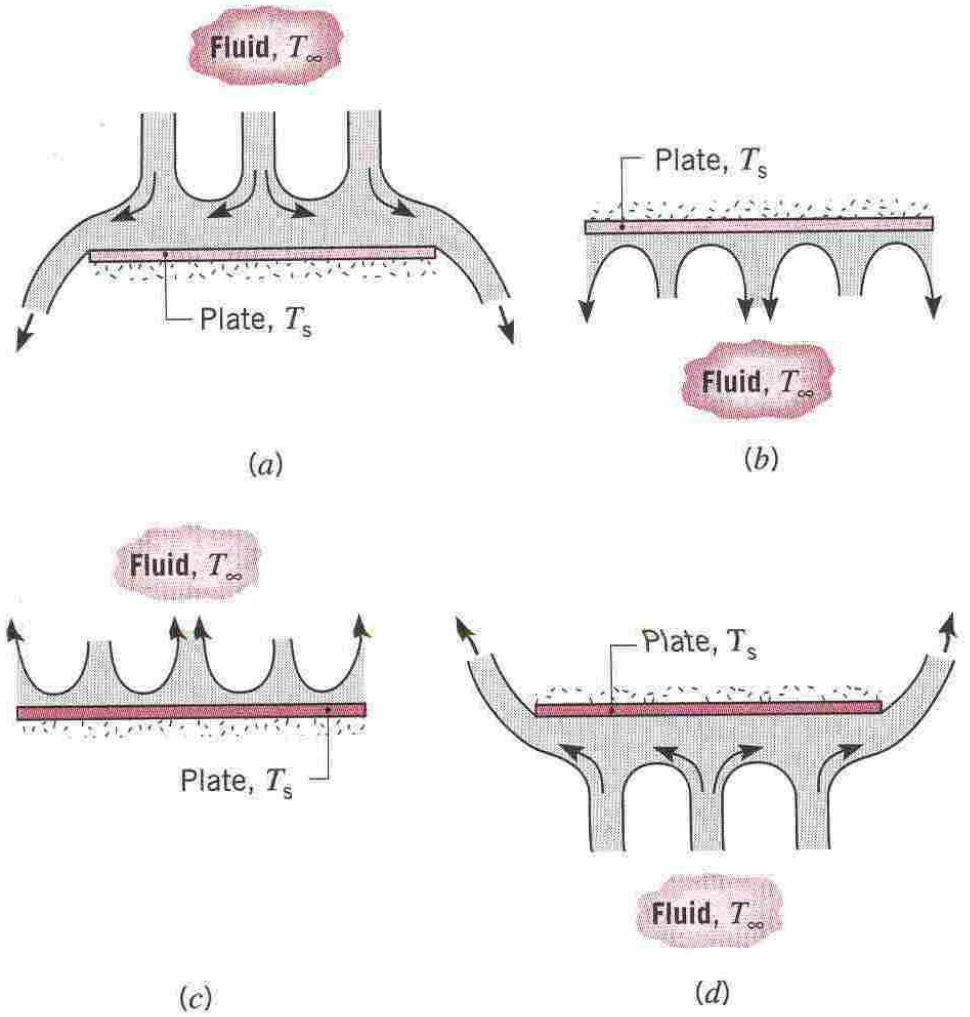

Fig. 2-7. Buoyancy- driven flows on horizontal cold ($T_s<T_\infty$) and hot ($T_s>T_\infty$) plates : (a)Top surface of cold plate, (b)bottom surfaces of cold plate, (c) top surface of a hot plate, and (d) bottom surface of hot plate.

and ascend, respectively, is impeded by the plate. The flow must move horizontally before it can descend or ascend from the edges of the plate,

and convection heat transfer is somewhat ineffective. In contrast, for a cold surface facing downward Fig. (2-7b) and a hot surface facing upward Fig. (2-7c), flow is of the mass dictates that cold (warm) fluid descending (ascending) from a surface be replaced by ascending (descending) warmer (cooler) fluid from the ambient and heat transfer is much more effective. Although correlations suggested be McAdams[3] are widely used for horizontal plates, improved accuracy may be obtained by altering the form of the characteristic length,

$$L \equiv \frac{A_s}{P} \tag{2-15}$$

Where A_S and P are the plate surface area and perimeter, respectively, recommended correlations for the average Nusselt number are.

Upper surface of heated plate or lower surface of cooled plate:

$$\overline{Nu_L} = 0.54 Ra_L^{1/4} \qquad \left(10^4 \le Ra_L \le 10^7\right) \tag{2-16}$$

$$\overline{Nu_L} = 0.15 Ra_L^{1/3} \qquad \left(10^7 \le Ra_L \le 10^{11}\right) \tag{2-17}$$

Lower surface of Heated Plate or Upper Surface of Cooled Plate:

$$\overline{Nu_L} = 0.27 Ra_L^{1/4} \qquad \left(10^5 \le Ra_L \le 10^{10}\right) \tag{2-18}$$

2.5.4 Natural convection cooling of finned surfaces

Finned surfaces of various shapes, called heat sinks, are frequently used in the cooling of electronic devices. Energy dissipated by these devices is transferred to the heat sinks by conduction and from the heat sinks to the ambient air by natural or forced convection, depending on the power dissipation requirements. Natural convection is the preferred mode of heat transfer since it involves no moving parts, like the electronic components themselvesRef [35]. However in the natural convection mode, the components are more likely to run at a higher temperature and thus

undermine reliability. A properly selected heat sink may considerably lower the operation temperature of the components and thus reduce the risk of failure. Natural convection from finned surfaces of rectangular shape has been the subject of numerous studies, mostly experimental. Bar-Cohen and Rohsenow [5] have compiled the available data under various boundary conditions, and develop correlations for the Nusselt number and optimum spacing.

2.6 The Governing Equations of Natural Convection Heat Transfer

The basic equations that govern convective processes are obtained from the conservation laws for mass, momentum and energy. Considering a given location in the flow, if ρ is the density of fluid and V the local velocity, the conservation of mass gives .{Rate of mass flow into the control volume}= {Rate of mass flow out of the control volume}

$$\frac{\partial \rho}{\partial t} + \nabla.\left(\rho \bar{v}\right) = 0 \qquad (2\text{-}21)$$

therefore, for steady flow, this equation, which is also known as the continuity equation, may be written as:

$$\nabla.\left(\rho \bar{v}\right) = 0 \qquad (2\text{-}22)$$

And if the density is constant:

$$\nabla.\bar{v} = 0 \qquad (2\text{-}23)$$

In many convection processes the variation in pressure and temperature is small enough to allow the density to be taken as constant. In such cases the preceding equation applies. In the Cartesian coordinate system the equation is.

$$\frac{\partial u}{\partial x} + \frac{\partial v}{\partial y} + \frac{\partial w}{\partial z} = 0 \qquad (2\text{-}24)$$

Where *u*, *v*, *w*, are the velocity components in *x*, *y* and *z* directions, respectively. Therefore the continuity equation, for two dimensional is

$$\frac{\partial u}{\partial x}+\frac{\partial v}{\partial y}=0 \qquad (2\text{-}25)$$

The principle of conservation of momentum, which equates the rate of change of momentum to the forces applied gives:

$$(M_x) \qquad \rho\left(u\frac{\partial u}{\partial x}+v\frac{\partial u}{\partial y}\right)=-\frac{\partial P}{\partial x}+\mu\left(\frac{\partial^2 u}{\partial x^2}+\frac{\partial^2 u}{\partial y^2}\right) \qquad (2\text{-}26)$$

$$(M_y) \qquad \rho\left(u\frac{\partial v}{\partial x}+v\frac{\partial v}{\partial y}\right)=-\frac{\partial P}{\partial y}+\mu\left(\frac{\partial^2 v}{\partial x^2}+\frac{\partial^2 v}{\partial y^2}\right)-\rho g \qquad (2\text{-}27)$$

(Convection term) = (pressure term) + (viscous term) - (Buoyancy force term)

Where, the body force per unit volume and may arise from gravitational, electrical, magnetic or some other body force field. And the gravity force is the only body force we shall consider it. The two-dimensional frame x-y is oriented in the usual way that Cartesian systems are drawn, with y pointing upward and x pointing horizontally as shown in Fig. (2-9). the gravitational acceleration (g) points in the negative (y) direction. Which the body forces components are: X = 0 and Y = - ρ *g*

μ is the coefficient of viscosity

P is the local pressure.

We assume that this wall layer of thickness δ_T and height y is slender.

$$\delta_T << y \qquad (2\text{-}28)$$

So-all the longitudinal curvature terms $\frac{\partial^2}{\partial y^2}$ can be neglected in favor of the transversal curvature terms of type $\frac{\partial^2}{\partial x^2}$. This simplification occurs on the right side of equation eqn. (2-26), eqn. (2-27). And the pressure inside the boundary layer P(x) must be the same as the pressure outer edge of the

boundary layer p_∞, which is constant. This means that the pressure gradient term that appears in eqn. (2-26) is zero.

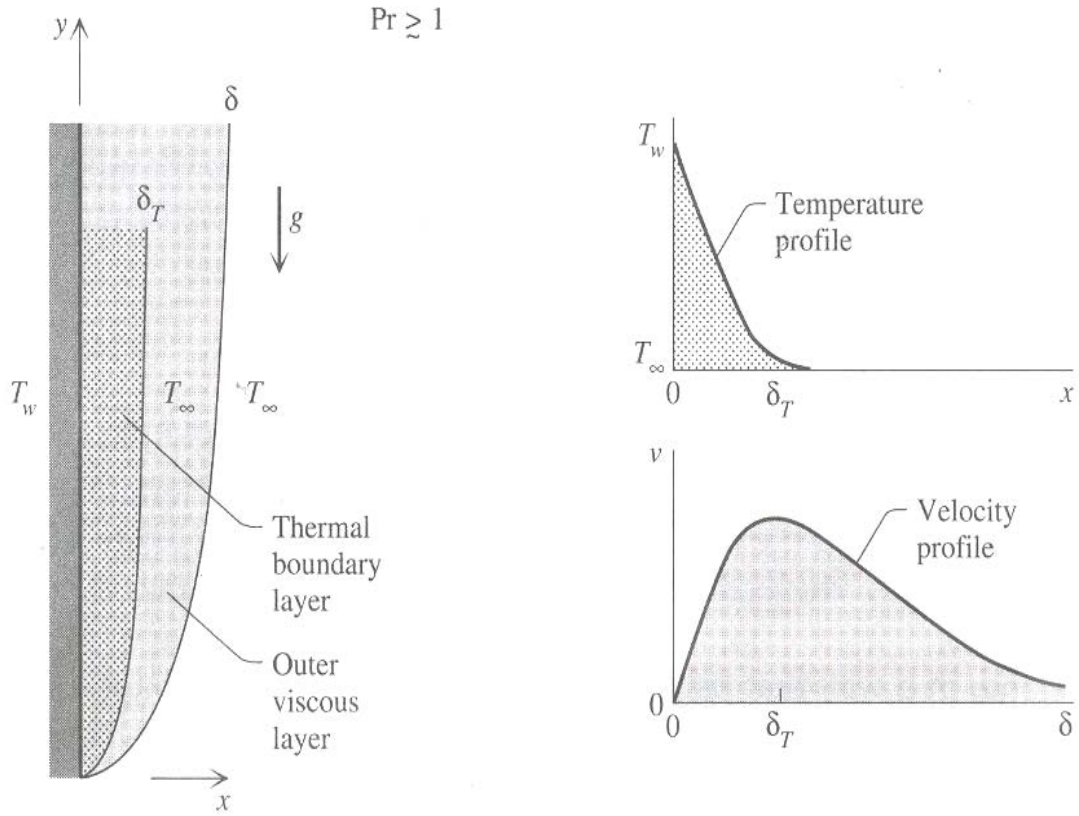

Fig. 2-9. The structure of the thermal and velocity boundary layers over a heated vertical wall

$$\frac{\partial p}{\partial x} \cong \frac{dp}{dx} = \frac{dp_\infty}{dx} = 0 \qquad (2\text{-}29a)$$

$$p(x,y) \cong p(y) = p_\infty(y) \qquad (2\text{-}29b)$$

The distribution of pressure in the reservoir is hydrostatic.

$$\frac{dp_\infty}{dy} = -p_\infty g \qquad (2\text{-}30)$$

In view of eq. (2-29) and (2-30), It is easy to see that the longitudinal pressure gradient $(\partial P/\partial y)$ in eqn. (2-27) can be replaced by the quantity $-\rho_\infty g$ in which ρ_∞ is the density of reservoir fluid.

$$\rho\left(u\frac{\partial v}{\partial x}+v\frac{\partial v}{\partial y}\right)=\mu\left(\frac{\partial^2 v}{\partial x^2}\right)-(\rho_\infty-\rho)g$$

(2-31)

There is only one momentum equation now eqn. (2-31). Because the other one eqn. (2-26) was invoked to write eqn. (2-29), that is, to eliminate *P* as one of the unknowns of the problem.

Avery important approximation employed in natural convection flows is the Boussinesq approximation which assumes a linear dependence of the density on the temperature and neglects the density variation in the continuity equation. There fore

$$(\rho_\infty-\rho)\approx\rho\beta(T-T_\infty) \qquad (2\text{-}32)$$

Where ρ_∞ is the density in the ambient medium temperature and β is the coefficient of thermal expansion.

Given by : $\beta=-\frac{1}{\rho}\left(\frac{\partial\rho}{\partial T}\right)_p$ (2-33)

$$\underbrace{u\frac{\partial v}{\partial x}+v\frac{\partial v}{\partial y}}_{Inertia}=\underbrace{\nu\frac{\partial^2 v}{\partial x^2}}_{Friction}+\underbrace{g\beta(T-T_\infty)}_{Buoyancy} \qquad (2\text{-}34)$$

$$u\frac{\partial T}{\partial x}+v\frac{\partial T}{\partial y}=\alpha\frac{\partial^2 T}{\partial y^2} \qquad (2\text{-}35)$$

The pressure work term, and the viscous dissipation term are generally negligible in natural, convection flows. Due to the low velocity levels encountered.

The set of governing equation is then:-

$$\frac{\partial u}{\partial x}+\frac{\partial v}{\partial y}=0 \qquad (2\text{-}36)$$

$$\underbrace{u\frac{\partial v}{\partial x}+v\frac{\partial v}{\partial y}}_{Inertia}=\underbrace{\nu\frac{\partial^2 v}{\partial x^2}}_{Friction}+\underbrace{g\beta(T-T_\infty)}_{Buoyancy} \tag{2-37}$$

$$u\frac{\partial T}{\partial x}+v\frac{\partial T}{\partial y}=\alpha\frac{\partial^2 T}{\partial y^2} \tag{2-38}$$

2.7 Heat Transfer From Extended Surfaces

The term extended surface is commonly used in reference to a solid that experiences energy transfer by Conduction within its boundaries, as well as energy transfer by convection (and/or radiation) between its boundaries and the surroundings. Such a system is shown schematically in Fig. (2-10). A strut is used to provide mechanical support to two walls that are at different temperatures A temperature gradient in the *x* direction sustains heat transfer by conduction internally, at the same time that there is energy transfer by convection from the surface.

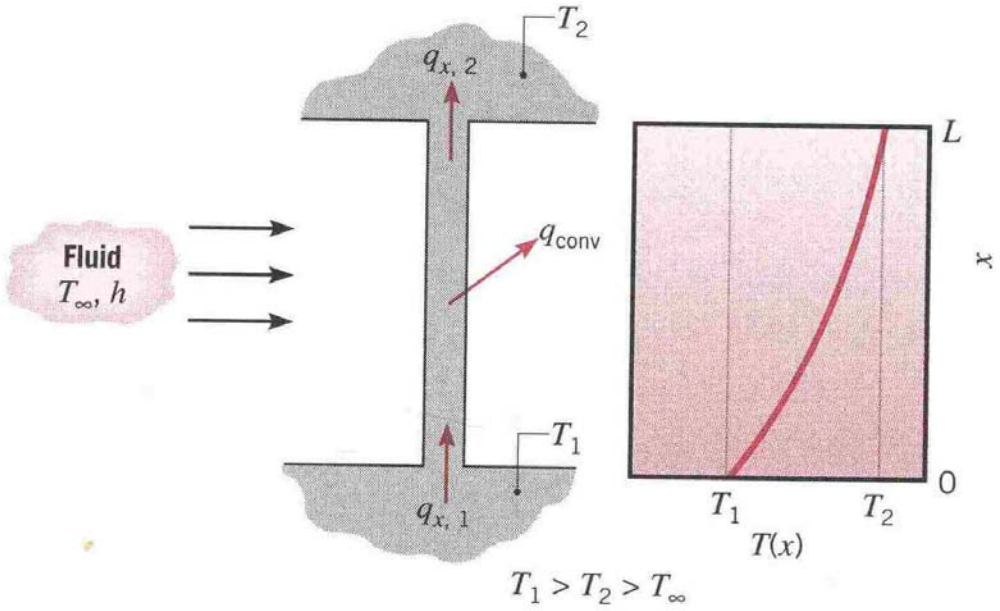

Fig. 2-10. Combined conduction and convection in a structural element.

Although there are many different situations that involve combined conduction—convection effects, the most frequent application is one in

which an extended surface is used specifically to *enhance* the heat transfer rate between a solid and an adjoining fluid. Such an extended surface is termed a fin.

Consider the plane wall of Fig. (2.11a). If T_s is fixed, there are two ways in which the heat transfer rate may be increased. The convection coefficient *h* could be increased by increasing the fluid velocity, and/or the fluid temperature T_∞ could be reduced. However, many situations

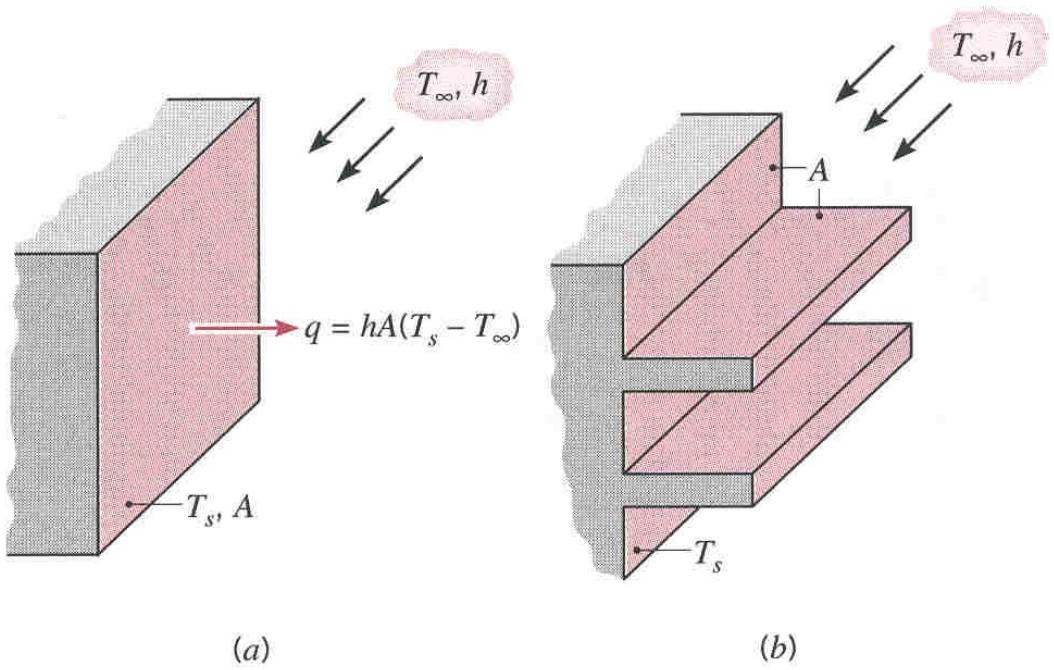

Fig. 2-11. Use of fins to enhance heat transfer from a plane wall. (a) Bare surface (b).Finned Surface.

would be encountered in which increasing *h* to the maximum possible value is either insufficient to obtain the desired heat transfer rate or the associated costs are prohibitive. Such costs are related to the blower or pump power requirements needed to increase *h* through increased fluid

motion. Moreover, the second option of reducing T_∞ is often impractical. Examining Fig. (2.11b), however, we see that there exists a third option. That is, the heat transfer rate may be increased by increasing the surface area across which the convection occurs. This may be done by employing fins that extend from the wall into the surrounding fluid. The thermal conductivity of the fin material has a strong effect on the temperature distribution along the fin and therefore influences the degree to which the heat transfer rate is enhanced. Ideally, the fin material should have a large thermal conductivity to minimize temperature variations from its base to its tip. In the limit of infinite thermal conductivity, the entire fin would be at the temperature of the base surface, thereby providing the maximum possible heat transfer enhancement. There are several fin applications.

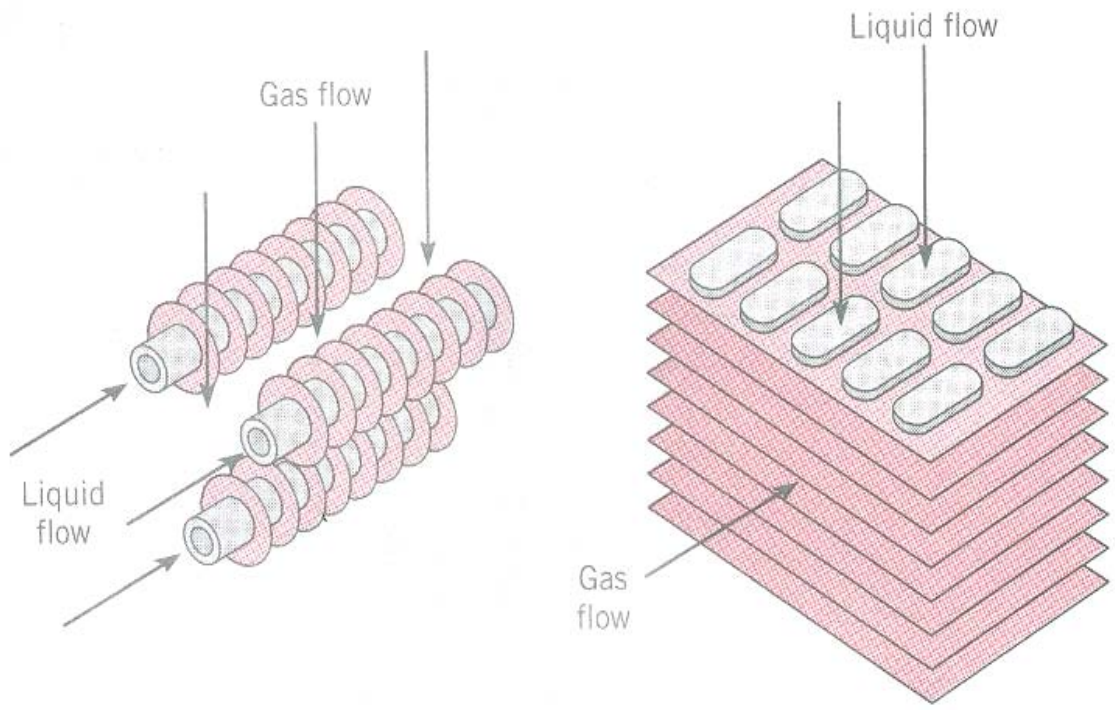

Fig. 2-12. Schematic of typical finned tube heat exchangers.

Consider the arrangement for cooling engine heads on motorcycles and lawnmowers or for cooling electric power transformers. Consider also the

tubes with attached fins used to promote heat exchange between air and the working fluid of an air conditioner Two common finned-tube arrangements are shown in Fig. (2.12). Different fin configurations are illustrated in Fig.(2.13). A straight fin is any extended surface that is attached to a plane wall. It may be of uniform cross-sectional area, or its cross-sectional area may vary with the distance x from the wall. An annular fin is one that is circumferentially attached to a cylinder, and its cross section varies with radius from the centerline of the cylinder. The foregoing fin types have rectangular cross sections, whose area may be expressed as a product of the fin thickness t and the width w for straight fins or the circumference $2\pi r$ for annular fins. In contrast a pin fin, or spine, is an extended surface of circular cross section. Pin fins may also be of uniform or non uniform cross section.

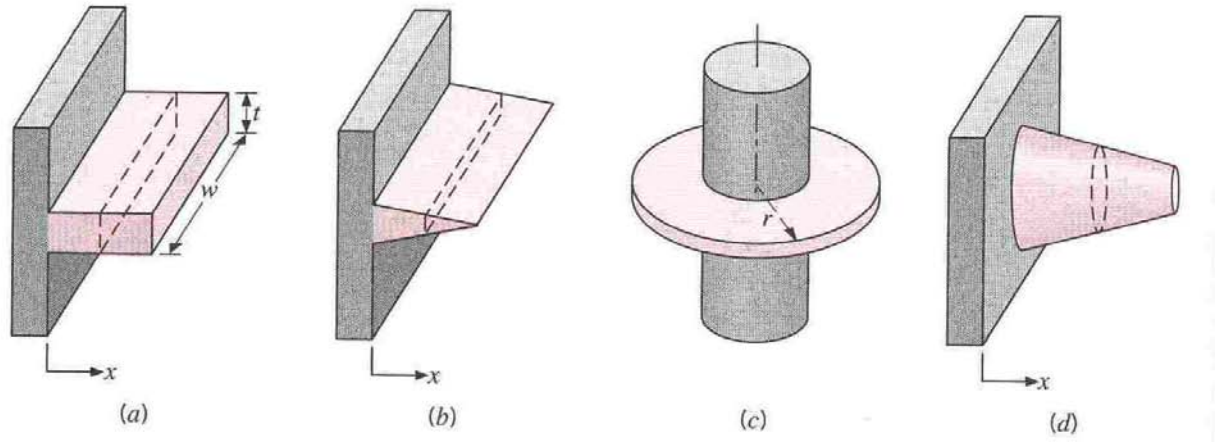

Fig. 2-13. Fin configurations. (a) Straight fin of uniform cross section. (b) Straight fin of non uniform cross section. (c) Annular fin. (d) Pin Fin.

In any application, selection of a particular fin configuration may depend on space, weight, manufacturing and cost considerations as well as on the extent to which the fins reduce the surfaces convection coefficient and increase the pressure drop associated with flow over the fins.

العنوان:	Experimental and Numerical Study of Natural Convection Heat Transfer from Rectangular Fin Arrays
المؤلف الرئيسي:	Mohamad, Hamza Ashur Milad
مؤلفين آخرين:	Abd Allatif, Ahmed Mohamed، El Bakoush, Taib A(Advisor، Co-Advisor)
التاريخ الميلادي:	2007
موقع:	Al Khums
الصفحات:	1 - 155
رقم MD:	766381
نوع المحتوى:	رسائل جامعية
اللغة:	English
الدرجة العلمية:	رسالة ماجستير
الجامعة:	جامعة المرقب
الكلية:	كلية الهندسة
الدولة:	ليبيا
قواعد المعلومات:	Dissertations
مواضيع:	المصفوفة ، الحاسب الآلي، الحمل الحراري
رابط:	https://search.mandumah.com/Record/766381

CHAPTER 4

EXPERMENTAL TEST RIG AND MEASURING INSTRUMENTS

EXPERIMENTAL TEST RIG AND MEASURING INSTRUMENTS

4.1 Introduction

This chapter presents a full design steps and description of the experimental test apparatus. The measuring instruments and the errors associated with them are also discussed.

4.2 Experimental Test Rig

The description of the experimental apparatus is facilited by reference to Fig. (4-1), which displays a schematic layout of a representative fin arrays. The test rig consisted of base plate, array of parallel longitudinal fins, heating unit and layers of thermal insulation. Fig. (4-2) shows a photograph of the test rig.

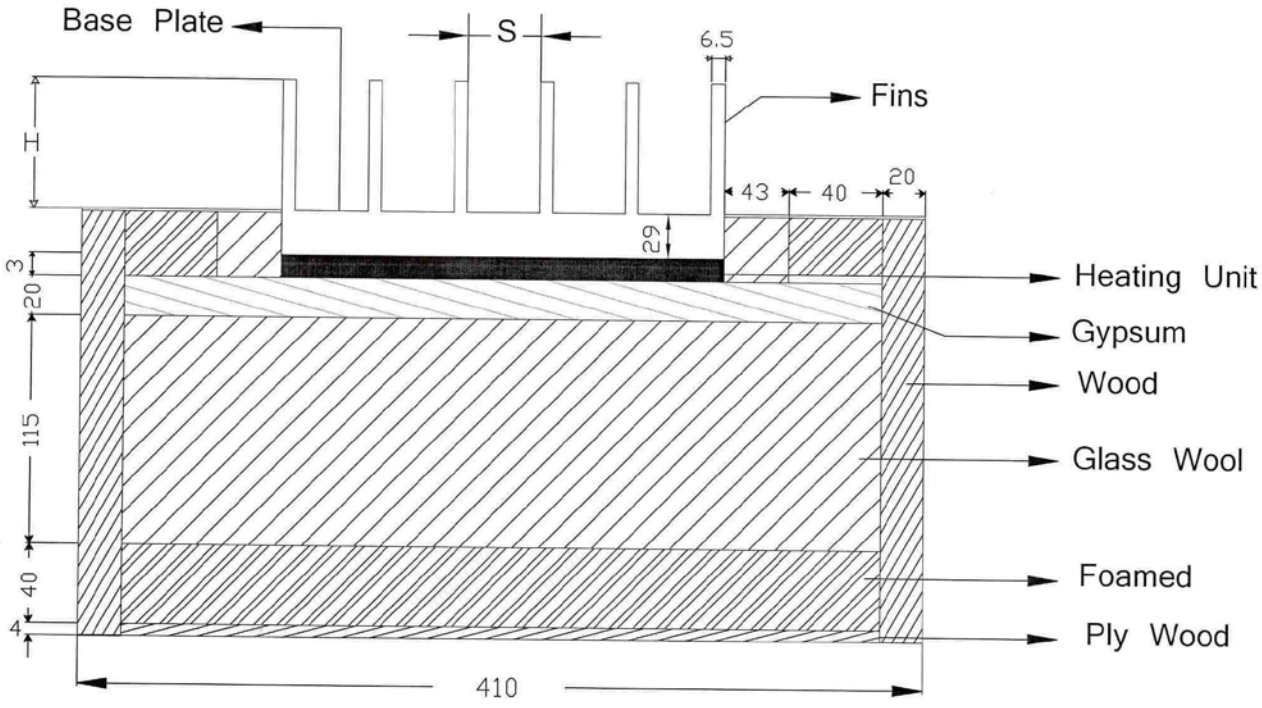

Fig. 4-1. Schematic diagram of the test rig.

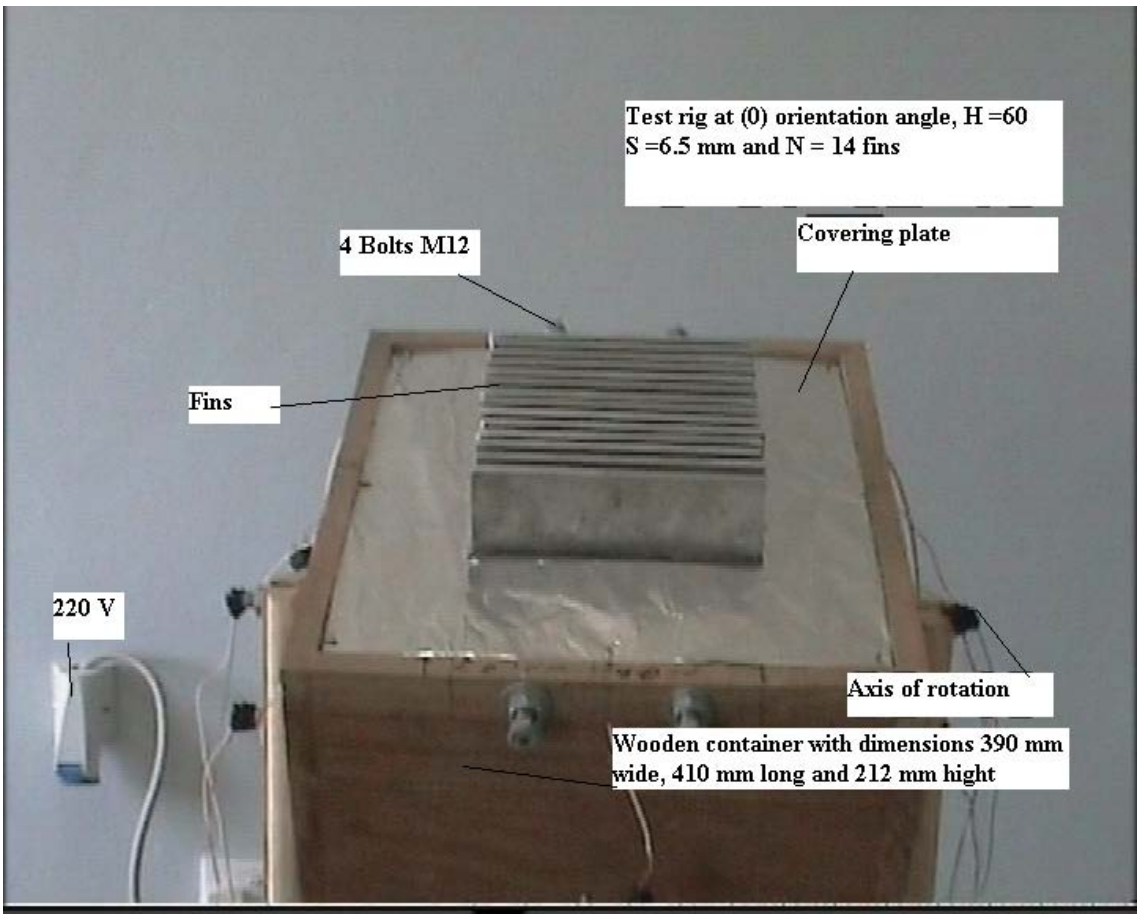

Fig. 4-2. Photograph of the test rig.

4.2.1 Base plate

The base plate is made from pure aluminum metal, which has high thermal conductivity with 204 mm long, 186 mm wide and 29 mm height. Eight rectangular slots of 6.5 mm wide and 15 mm high and with different lengths (35 and 60 mm) are milled in bottom side of the base plate. They are used to embed eight thermocouples distributed over the base plate to measure the temperature of the base plate, as shown in Fig. (4-3).

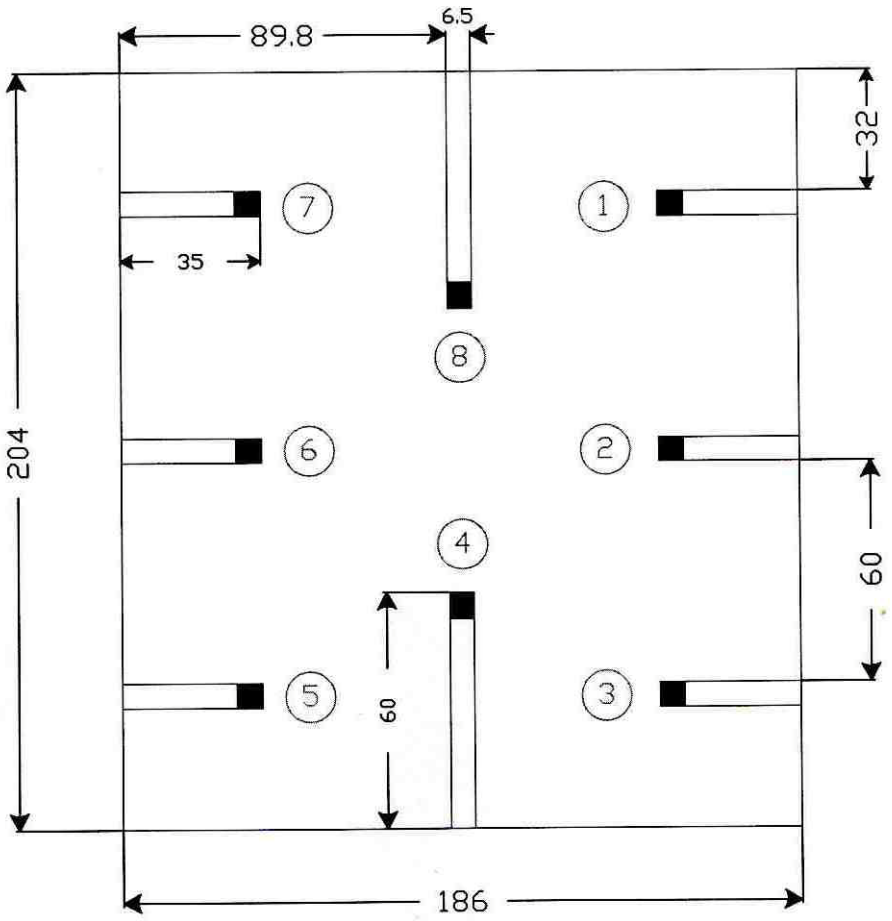

Fig. 4-3. Locations of the thermocouples over base plate

4.2.2 Tested fins

The tested fins are made from pure aluminum with a highly polished surface to minimize heat radiation. The fins are of the rectangular type with (t) thickness, (H) high and (L) long. During all experiments, the fins thickness (t) was 6.5 mm and the length of fins (L) was 186 mm. The fins were glued vertically upward to the upper surface of the base plate. The glue layer (Epoxy) was made very thin so that the resistance to heat transfer from heating base plate is minimized in addition to the fact that the glue itself is a good conductive material. The fins are distributed along the upper surface of the base plate at a different inter-fin spacing S (the distance between the centers of two adjacent fins).

4.2.3 Heating unit

The main target of the heating unit is to provide a heat flow through the lower surface of the base plate to the fins, the heater is a nickel chromium resistance tap 3 mm wide, 0.15 mm thickness and its resistance is 2.99 Ohms per meter. It was wound uniformly round the mica plate (electrical insulation) with 2 mm pitch. The upper and bottom heater surfaces are covered by using mica plate of 0.8 mm thickness. The heating unit is fixed with the lower surface of the base plate by small screws to make good contact between them. The electrical power input to the heater was controlled by autotransformer (varic) to obtain constant heat flux along the base plate and measured by a digital wattmeter.

4.2.4 Thermal insulation

The lower surface of the heater and the sides of base plate were isolated thermally. The insulation of the lower surface of the heater made of calcium silicate (Gypsum) of thickness 2 cm, glass wool of thickness 11.5 cm, foamed with thickness 4 cm and ply wood 0.4 cm thickness as shown in Fig. (4-4). The sides of the heated base plate were isolated via glass wool of thickness 4.3 cm and foamed of thickness 4 cm. Table 4-1 shows the thermal conductivity of the insulation material.

Table (4-1) Thermal conductivity of insulation materials.

Insulation material	Thermal conductivity K (W/m.K)
Calcium silicate (Gypsum)	0.17
Glass wool	0.04
Foamed	0.031
Ply wood	0.12
Hard wood	0.16

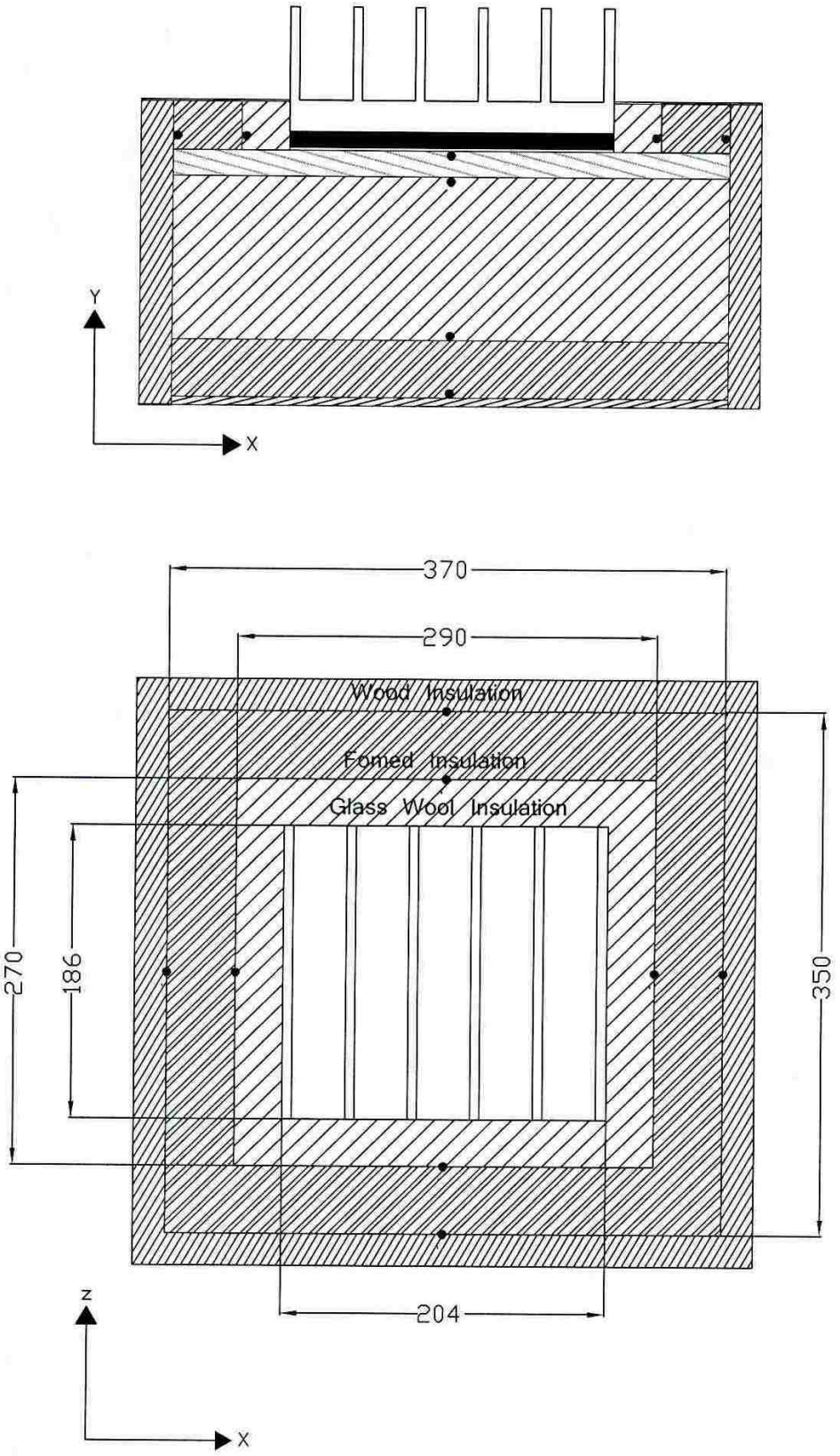

Fig. 4-4. The locations of thermocouples in the thermal insulation.

Four thermocouples were located at various points to measure losses from the lower surface of the heater. Also; eight thermocouples were located at different locations to measure heat losses from sides of base plate as shown in Fig. (4-4).

4.3 Wooden Container

The wooden container was fabricated from wooden plate with 20 mm thickness. The container dimensions were 390 mm wide, 410 mm long and 212 mm height as shown in Fig. (4-5). Four bolts of 12 mm diameter are

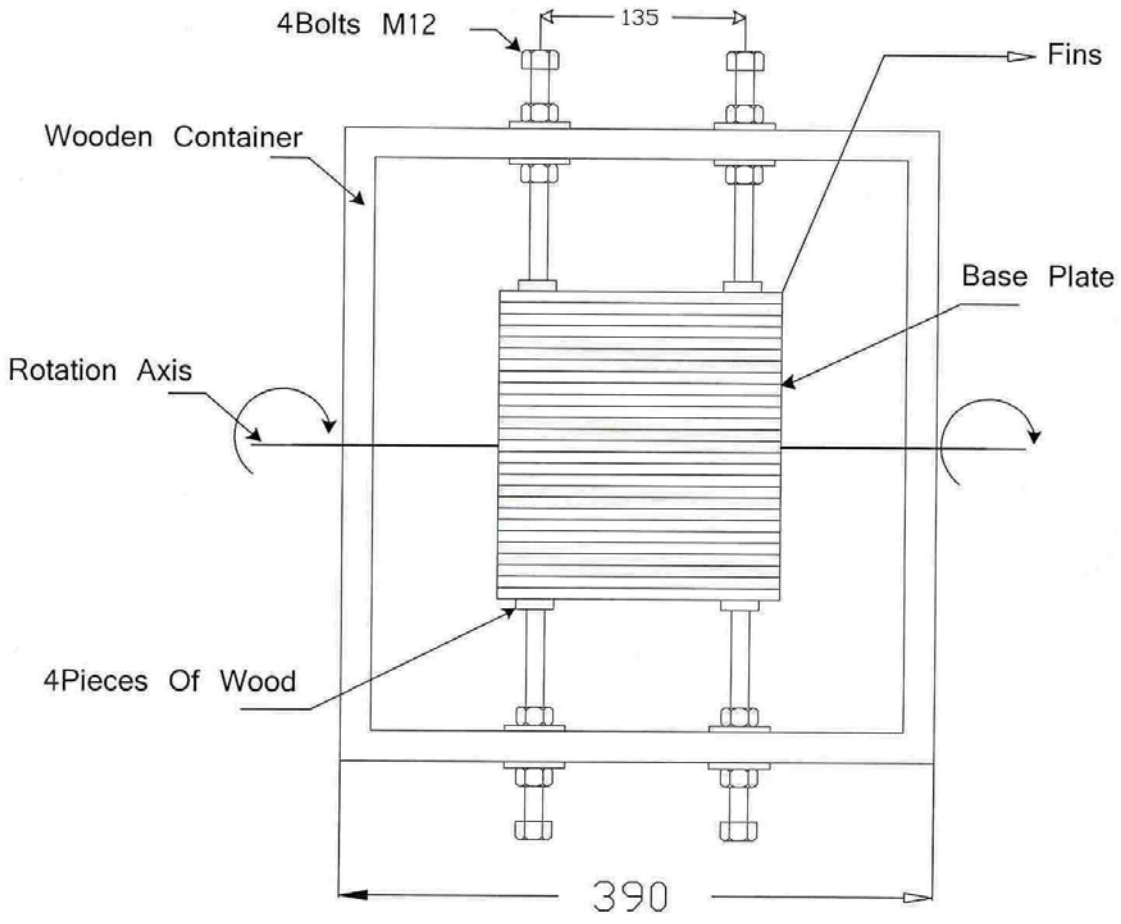

Fig. 4-6. Schematic diagram of the wooden container.

used to fix the test model in the wooden container. Four pieces of wood are fixed in the tip of the bolts to prevent heat transfer from the test model to the bolts as shown in Fig. (4-5). The wooden container with the test model was mounted on the wooden frame to rotate the test model at the desired orientation angle around Z axis(normal to the paper). The orientation angle (Φ) was adjusted via a protractor was fixed on one side of the wooden container and a pointer was fixed on the wooden frame. Description of orientation angle is shown in Fig (4-6).

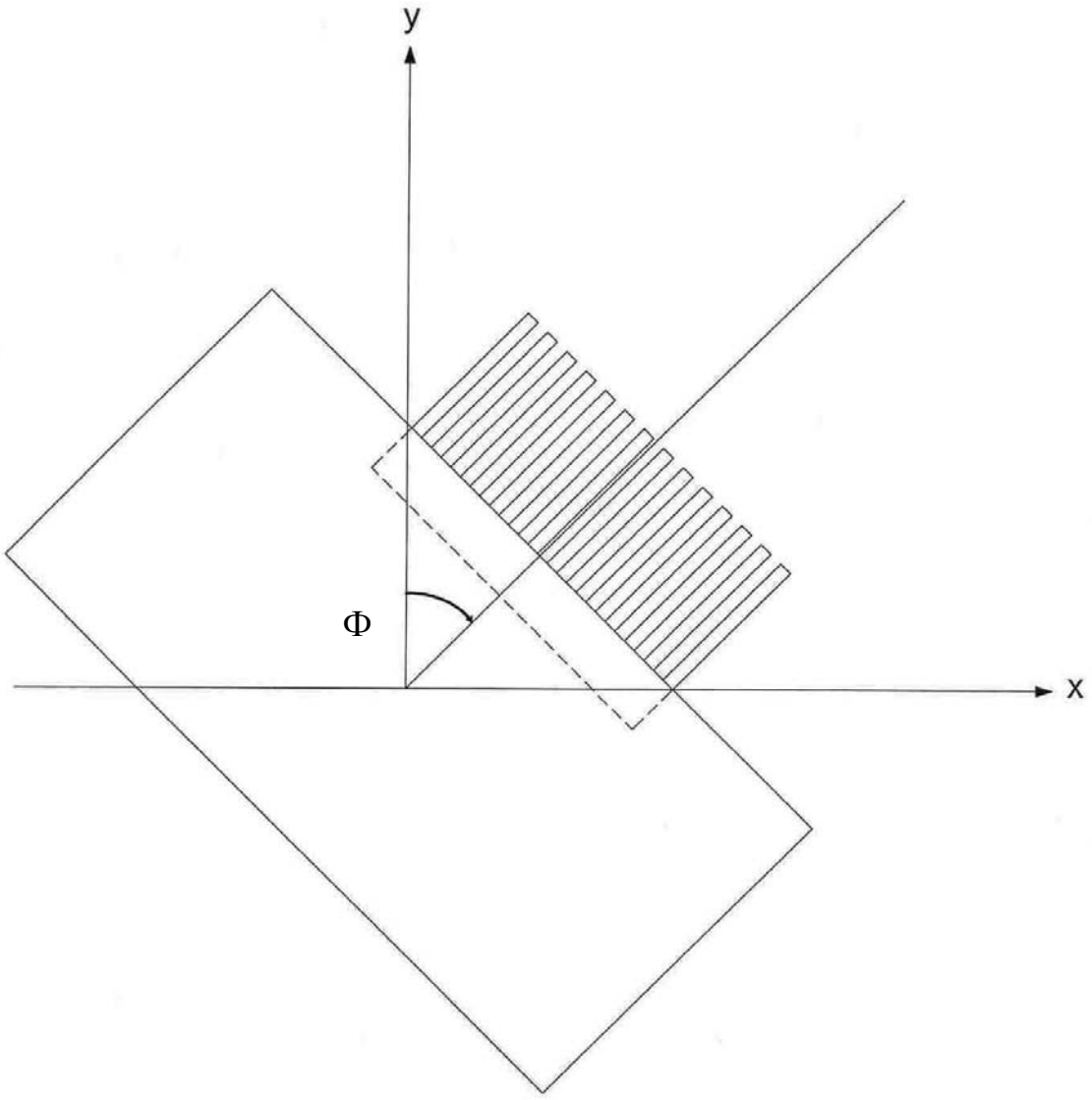

Fig. 4-6. Schematic illustration of the orientation angle of the test model.

4.4 Measuring Instruments Description and Calibration

In the following sections of this chapter, the measuring devices used in present study discussed. These include thermocouples, digital thermometer, digital wattmeter and mercury thermometer. Fig. (4-7) shows a photograph of the measuring devices.

4.4.1 The thermocouples

The thermocouple is of copper constant (type T) wires with 0.3 mm diameter; the ends of both wires were twisted and then fused together by means of an electric spark in medium free from oxygen. Thus forming a junction of the thermocouple with 0.5mm diameter. Eight thermocouples were embedded in the base plate to measure its temperature. Four thermocouples were distributed through the insulation layers under the heater to determine the conduction heat losses through the insulation layer. Eight thermocouples were distributed around the test model to determine the heat losses from its sides. The readings of the thermocouples were taken out by a digital thermometer.

4.4.2 Digital thermometer

The thermocouple readings were measured by a digital thermometer.The digital thermometer is (T) type, model number (JTC-905), with an accuracy of $\pm$ 0.5 C°.

4.5 Digital multi-meter

The digital multi-meter model number DW-6060 and serial number N 097398, is used to measure the electric power (Watt), the electrical voltage (Volt) and the electric current (Ampere) of accuracy 1.5 ٪ of full scale. It

has full scale reading 2 kW. The input voltage is ranging between 0 and 600 Volt, A.C. and the input current is from 0 to 10 Ampere A.C. The input power to the heater was measured directly by the digital multi-meter. The input voltage and input current to the heater were also measured, and the calculated input power can be checked with the readings of the digital multi-meter.

4.6 Mercury Thermometer

The laboratory air temperature was measured by using a standard mercury thermometer with full-scale range of 80^0 C, with an accuracy of $\pm$ 0.5 C°.

Fig. 4-7. Photograph of the measuring devices.

4.7 Calibration of Thermocouple

Special thermocouples were designed and prepared. Consequently it was necessary to calibrate the adopted thermocouples; ten junctions were chosen and calibrated by direct comparison using the standard method. In this method, two-standard mercury thermometers additional to ten junctions of the thermocouples were filled at the same level in isolated water field. The filled was heated and then the temperature is recorded gradually. And at the same time the field was cooled the calibration range is from 20C ° to 100C ° which covers the working rang of the present work. During the calibration, the thermocouples were connected to their extension wires and then to the digital thermometer. The observations of the calibration of the used thermocouples function are given in appendix (1) and Fig. (4-9) this figure shows the calibration curve of the used thermocouples in the calibration $T_{ture} = 1.0441T_{measured} + 0.7561$.

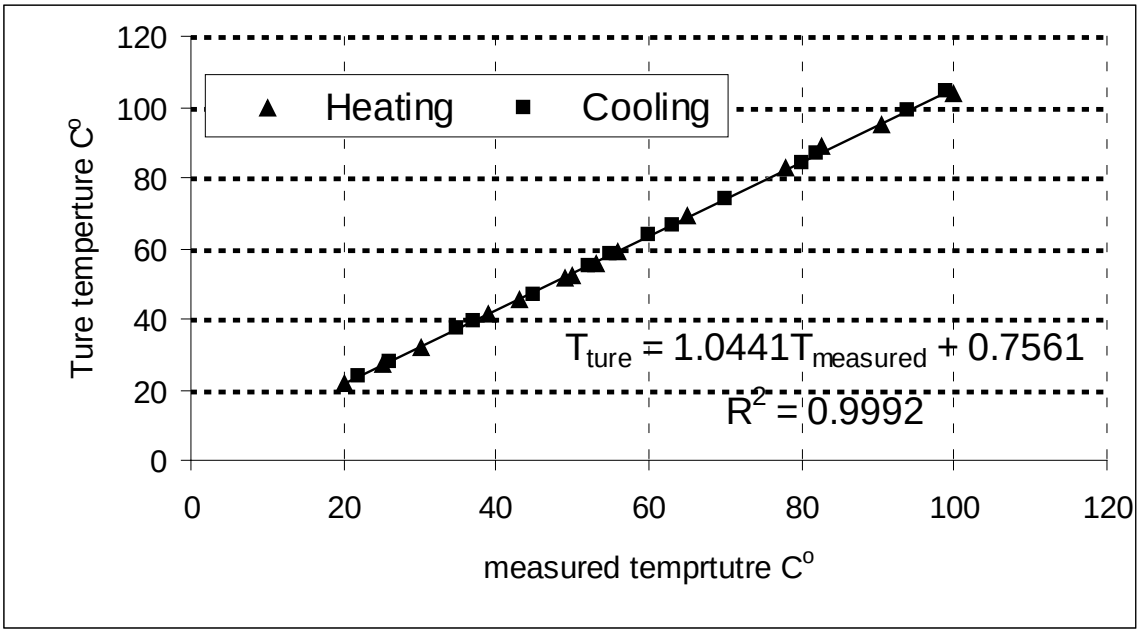

Fig. 4-8. The Calibration curve of thermocouples.

العنوان:	Experimental and Numerical Study of Natural Convection Heat Transfer from Rectangular Fin Arrays
المؤلف الرئيسي:	Mohamad, Hamza Ashur Milad
مؤلفين آخرين:	Abd Allatif, Ahmed Mohamed، El Bakoush, Taib A(Advisor، Co-Advisor)
التاريخ الميلادي:	2007
موقع:	Al Khums
الصفحات:	1 - 155
رقم MD:	766381
نوع المحتوى:	رسائل جامعية
اللغة:	English
الدرجة العلمية:	رسالة ماجستير
الجامعة:	جامعة المرقب
الكلية:	كلية الهندسة
الدولة:	ليبيا
قواعد المعلومات:	Dissertations
مواضيع:	المصفوفة ، الحاسب الآلي، الحمل الحراري
رابط:	https://search.mandumah.com/Record/766381

CHAPTER 5

EXPERMENTAL PROCUDER AND UNCERTAINTY ANALYSIS

EXPERIMENTAL PROCCEDURE AND UNCERTAINTY ANALYSIS

5.1 Introduction

In this chapter, the full experimental procedure and method of calculation will be introduced. This will be followed by sample of the calculation and uncertainty analysis of experimental results.

5.2 Measurements

The experimental measurements, which have been done through study:-

1. The power input to the model.
2. The heat loses to the surroundings.
3. The base plate temperature distribution at different orientation angle.
4. Ambient temperature of the air.

5.3 Experimental Procedure

There were two conditions that had to be satisfied before measurement is taken.

1. Steady-State condition.
2. Balancing condition.

The steady–State condition is satisfied if the power of the heater is constant (i.e. the current and the voltage of the heater were constant) and the change of all temperatures with time becomes negligible. Also the balancing condition was satisfied when heat lost through insulation is constant .The average time required to reach a satisfactory thermal steady state was (3-5 hrs). The steps involved in the experiment were as followed.

1. Choose the desired orientation angle Φ by using a pointer and protractor.
2. Make sure that all junctions between the copper wires and thermocouples wires are jointed well, (cold junction) because if there is another heating source like the beam solar radiation or cooling current, a natural convection current which passes through the wires directly and will make some errors in the reading.
3. The power input to the heater is adjusted to the desired value via an autotransformer (varic).
4. After (3-5) hours or more and when the steady state condition of the measurements is established ,the following data were recorded as:

(a) T_1, T_2, ... up to T_8 thermocouples readings giving the base plate temperature.

(b) T_9, T_{10}, … up to T_{13} thermocouples reading giving the temperature of the insulation layers under the heater.

(c) T_{14}, T_{15}, ... up to T_{21} thermocouples readings giving the temperature of insulation layers around test model.

(d) Near the test model the ambient temperature was recorded .

5.4 Methods of Calculation

The essential quantity, which was determined in the study is convective heat transfer. The total heat input from the heater (q_t) is distributed into the heat transferred by convection to the quiescent air (q_c) and the heat losses through the insulation to the surrounding the tested model (q_{lost}).

$$q_c = q_{total} - q_{lost} \tag{5-1}$$

$$q_{lost} = q_{bottom} + q_{edges} + q_{radiation} \tag{5-2}$$

Where, q_{bottom} = The heat lost by conduction from the bottom side of the heater. It is calculated from equation.

$$q_{bottom} = \frac{\Delta T}{\sum R_t} \qquad (5\text{-}3)$$

Where ΔT is the temperature difference between the heating unit temperature T_h and ambient air temperature T_∞.

$\sum R_t$ is the thermal resistance.

$$q_{bottom} = \frac{\Delta T}{\left[\left(L_G / A_b k_G\right) + \left(L_W / A_b k_W\right) + \left(L_F / A_b k_F\right) + \left(L_P / A_b k_P\right) + \left(1 / A_b h\right)\right]} \qquad \text{------ (5-4)}$$

k = Thermal conductivity of insulation material (as shown in Table 4-1).

A_b = Cross-sectional area of the base plate = $0.038 m^2$.

L_G, L_W, L_F and L_P = Insulation layer thickness of Gypsum, glass wool, foamed and ply wood respectively in (y) direction as shown in figure (4-4).

It was found that it represents about 1.8 ٪ of the total heat input for maximum heat input.

q_{edges} = The heat lost by conduction from four sides of the base plate.

The heat lost by conduction from the fourth edges of the base plate can be determined from eqn. (5-3).

It was found that it represents about 1.15 ٪ of the total heat input for maximum heat input.

And the heat transfer by a radiation can be calculated from.

$$q_{radiation} = E\sigma A_S\left(T_S^4 - T_{surr}^4\right) \qquad (5\text{-}5)$$

Where:

E = Emissivity of the tested model material (pure aluminum) =0.05 Ref. [34].

σ = Stefan – boltzmann constant = $5.67 \times 10^{-8} \left(\frac{W}{m^2 . K^4} \right)$.

A_s= total heat transfer surface area of the base plate and fins.

It was found that it represents a bout 3.4 ٪ of the total input power for maximum heat input.

By using these finding with the fact that the tested model was well insulated, the total heats lost was very small compared with the total heat input. For more accuracy is calculated for each analysis.

Consequently the total the heat transferred by convection to the ambient can be calculated from.

$$\therefore q_{convection} = q_{total} - q_{bottom} - q_{edges} - q_{radiation} \quad (5\text{-}6)$$

The heat transfer coefficient can be calculated from the equation :

$$h = \frac{q_{convection}}{A_s (T_s - T_\infty)} \quad (5\text{-}7)$$

Where, T_S is the average temperature of the base plate.

T_∞ is the ambient temperature.

A_s total heat transfer surface area of the base plate and fins.

The model Nussult number (Nu) can be determined from:

$$Nu_L = \frac{hL}{k_a} \quad (5\text{-}8)$$

The Rayleigh number can be calculated from.

$$Ra_L = \frac{g\beta(T_S - T_\infty)L^3}{\alpha\nu} \quad (5\text{-}9)$$

5.5 Uncertainty Analysis of Experimental Results

The uncertainty of measurements may be defined as the range within which the true value of quantities measured is likely to lie at a given probability. Errors are created due to the imperfection of human senses, inaccuracy of measuring instruments and impossibility of arranging quite exactly the required regime of measurements.

5.5.1Causes and types of experimental errors

Single-Simple data are those in which some uncertainties may not be discovered by repetition. Multi sample data are obtained in those instances where enough experiments are performed so that the reliability of the results can be assured by statistics.

Frequently cost will prohibit the collection of multisampling data and the experiment must content with single-sample data and prepared to extract as much information as possible from such experiments. The number of observation will then determine the success of this multisampling experiment in accordance with accepted statistical principles. If the experiment list knows what the error was, he could correct it and it would no longer be an error. In other words, the real errors in experimental data are those factors that are always vague to some extend and carry some amount of uncertainty. Our task is to determine just how certain a particular observation may be and to devise a consistent way of specifying the uncertainty in analytical form. A reasonable definition of experimental uncertainty may be taken as the possible value error may have, at this point we may mention some types of errors that may cause uncertainty in an experimental measurement.

First there can always be those gross blunders in apparatus or instrument construction which may invalidate the data. Hopefully, the careful experiment

list will be able to eliminate most of these errors. Second there may be certain fixed errors which will cause repeated reading to be in error by roughly the same amount but for some unknown reason. These fixed errors are sometimes called systematic errors or bias errors. Third there are random errors which may be caused by personal fluctuations in the apparatus or instruments, various influences of friction etc. In many instances it is very difficult to distinguish between fixed errors and random errors [37].

5.5.2 Uncertainty analysis

Suppose a set of measurements is mad and the uncertainty in each instrument may be expressed with some odds. These measurements are then used to calculate some desired result of the experiments:

$$W_R = \left[\left(\frac{\partial R}{\partial x_1} w_1 \right)^2 + \left(\frac{\partial R}{\partial x_2} w_2 \right)^2 + \left(\frac{\partial R}{\partial x_3} w_3 \right)^2 + ... + \left(\frac{\partial R}{\partial x_n} w_n \right)^2 \right]^{\frac{1}{2}} \quad (5\text{-}10)$$

Where $w_{1,}\, w_{2\,.....}\, w_n$ the uncertainties in the independent variable, and W_R is the uncertainty in the result.

The uncertainty of measurement is not confused with error. It may be defined as the range within which the true value of quantity measured is likely to lie at given of probability. By its very nature, it consists of the results of number of measurement, each of which carries an error. It expresses the variability, which always occurs when more than one measurement is made. The experiment quantities can be divided into simple and compound. The simple variables are those which can be measured directly by an instrument. and the compound variable is obtained from simple variables by combining them through calculations.

5.5.3 Uncertainty in simple variable.

5.5.3.1 Uncertainty in measuring the base plate temperature.

The average surface temperature of the tested model is about 94°C.

The accuracy of digital thermometer was $\pm 0.5^{\circ}C$.

The percentage relative uncertainty in the measuring of the base plate was:

$$\frac{W_{Ts}}{T_S} = \frac{0.5}{94} \times 100 = .532\ \%$$

Where, W_{Ts} is the uncertainty in the surface temperature.

5.5.3.2 Uncertainty in measuring the ambient air temperature.

The average temperature in the laboratory during the experiments was 29 °C.

The accuracy of mercury thermometer was $\pm 0.5^{\circ}C$.

Therefore the percentage relative uncertainty in measuring the ambient temperature was.

$$\frac{W_{T\infty}}{T_{\infty}} = \frac{0.5}{29} \times 100 = 1.724\ \%$$

Where, $W_{T\infty}$ is the uncertainty in the quiescent air temperature .Ref [37]

5.5.3.3 Uncertainty in measuring the heaters power.

The average power input to the heater during the experiments was 100 Watt; the accuracy of the Watt meter is ± 0.6 watt. Therefore the percentage relative uncertainty in measuring the electric power input to the heater is:

$$\frac{W_P}{P} = \frac{0.6}{100} \times 100 = 0.6\ \%$$

Where, W_P is the uncertainty in the electric power.

5.5.3.4 Uncertainty in measuring the orientation angle (Φ).

The average orientation angle during experiments was 90°. The uncertainty in measuring Φ was $\pm 0.5^{\circ}$. Therefore the percentage relative uncertainty in measuring the orientation angle was:

$$\frac{W_{\phi}}{\phi} = \frac{0.5}{90} \times 100 = 0.55\% .$$

Where, $W_{ß}$ is the uncertainty in the orientation angle.

5.5.4 Uncertainty in compound variables.

5.5.4.1 The uncertainty in heat transfer coefficient.

The heat transfer coefficient was calculated from equation (5-11)

$$h = \frac{q}{A_S (T_S - T_\infty)} \tag{5-11}$$

It is clear that h = h (q, T_s, T_∞). Then the uncertainty in heat transfer coefficient was calculated from the equation:

$$W_h = \left[\left(\frac{\partial h}{\partial q} W_q \right)^2 + \left(\frac{\partial h}{\partial T_s} W_{Ts} \right)^2 + \left(\frac{\partial h}{\partial T_\infty} W_{T\infty} \right)^2 \right]^{\frac{1}{2}} \tag{5-12}$$

From equation (5.11)

$$\frac{\partial h}{\partial q} = \frac{1}{A_S (T_S - T_\infty)} \tag{5-13}$$

$$\frac{\partial \mathrm{h}}{\partial \mathrm{T_s}} = \frac{\mathrm{q}}{\mathrm{A_S (T_S - T_\infty)^2}} \tag{5-14}$$

$$\frac{\partial \mathrm{h}}{\partial \mathrm{T_\infty}} = -\frac{\mathrm{q}}{\mathrm{A_S (T_S - T_\infty)^2}} \tag{5-15}$$

Substitution in eq (5.12)

$$W_h = \left[\left(\frac{hW_q}{hA_S(T_S - T_\infty)} \right)^2 + \left(\frac{-qhW_{Ts}}{A_S h(T_S - T_\infty)^2} \right)^2 + \left(\frac{qhW_{T\infty}}{A_S h(T_S - T_\infty)^2} \right)^2 \right]^{\frac{1}{2}} \quad (5\text{-}16)$$

$$W_h = \left[\left(\frac{hW_q}{q} \right)^2 + \left(\frac{-hW_{Ts}}{(T_S - T_\infty)} \right)^2 + \left(\frac{hW_{T\infty}}{(T_S - T_\infty)} \right)^2 \right]^{\frac{1}{2}} \quad (5\text{-}17)$$

$$\frac{W_h}{h} = \left[\left(\frac{W_q}{q} \right)^2 + \left(\frac{-W_{Ts}}{(T_S - T_\infty)} \right)^2 + \left(\frac{W_{T\infty}}{(T_S - T_\infty)} \right)^2 \right]^{\frac{1}{2}} \quad (5\text{-}18)$$

Where the average value of the $(T_s - T_\infty) = 65$ C°

$$\frac{W_h}{h} = \left[(0.6)^2 + \left(\frac{-0.53191}{65} \right)^2 + \left(\frac{1.72414}{65} \right)^2 \right]^{\frac{1}{2}}$$

$$\frac{W_h}{h} = 0.600642 \ \%$$

Where, W_h is the uncertainty in the heat transfer coefficient.

5.5.4.2 Uncertainty in Nusselt number

The Nusselt number was calculated from

$$\mathrm{Nu} = \frac{\mathrm{hL}}{\mathrm{k_a}} \quad (5\text{-}19)$$

It is clear that $Nu = f(h)$

Then the percentage relative uncertainty in Nusselt number is the same as for the heat transfer coefficient.

$$\frac{\mathrm{W_{Nu}}}{\mathrm{Nu}} = \frac{\mathrm{W_h}}{\mathrm{h}} = 0.60 \ \%$$

Where, W_{Nu} is the uncertainty in Nusselt number.

5.5.4.2 Uncertainty in Rayleigh number

The Rayleigh number was calculated from $Ra_L = \frac{g\beta(T_S - T_\infty)L^3}{\alpha\nu}$

It is clear that $Ra_L = f(T_{s,}T_\infty)$. Then the uncertainty in the Rayligh was calculated from the equation:

$$W_{RaL} = \left[\left(\frac{Ra_L}{T_s - T_\infty} W_{TS}\right)^2 + \left(-\frac{Ra_L}{T_s - T_\infty} W_{T\infty}\right)^2\right]^{\frac{1}{2}} \quad (5\text{-}20)$$

$$\frac{W_{RaL}}{Ra_L} = \left[\left(\frac{W_{TS}}{T_s - T_\infty}\right)^2 + \left(-\frac{W_{T\infty}}{T_s - T_\infty}\right)^2\right]^{\frac{1}{2}} \quad (5\text{-}21)$$

$$\frac{W_{RaL}}{Ra_L} = \left[\left(\frac{0.53191}{65}\right)^2 + \left(\frac{1.72414}{65}\right)^2\right]^{\frac{1}{2}} \quad (5\text{-}22)$$

$$\frac{W_{RaL}}{Ra_L} = 0.02776\%$$

Where W_{RaL} is the uncertainty in the Rayleigh number.

5.6 Sample of Calculations

As an example of the calculations of different items, the case of at orientation angle Φ=0°, H = 15 mm, S = 33 mm, A_S = 0.07259 m^2 ,L = 0.186 m

T_9	T_{10}	T_{12}	T_{14}	T_{15}	T_{16}	T_{17}	T_{18}
138 C°	44.5 C°	30 C°	36 C°	35 C°	34 C°	39 C°	52 C°
T_{19}	T_{20}	T_{22}	T_h	T_∞	T_b	power	
35 C°	37 C°	37 C°	153 C°	30 C°	104.3C°	66 W	

By using equations (5-3) and (5-4).

$\sum R_t = 118.5467$ K/W , $q_{bottom} = 1.037$ W

And the total heat transfer from the fourth sides of the base plate was calculated from equation (5-3).

$\sum R_{t\,2,4} = 495.9$ K/W

$\sum R_{t1,3} = 447.5$ K/W

$$q_{edges} = \left(\frac{2 \times \Delta T}{\sum R_{t_{1,3}}}\right) + \left(\frac{2 \times \Delta T}{\sum R_{t_{2,4}}}\right)$$

$q_{edges} = 0.63$ W

$q_{radiation} = 2.3$ W

From equation (5-6) $c_{onvection} = 62$ W

From equation (5-7) $h = 11.5 \ \frac{W}{m^2 \times K}$

Properties: Table A.4, air [32]. (T_f =340 K),

$\nu = 1.97884 \times 10^{-5} \frac{m^2}{s}$, $\alpha = 28.42 \times 10^{-6} \frac{m^2}{s}$,

$\beta = T_f{}^{-1} = 2.941176 \times 10^{-3} K^{-1}$, $k_a = 29.26 \times 10^{-3} \frac{W}{m.K}$.

From equation (5-8) $Nu_L = 72.48$

From equation (5-9) $Ra_L = 2.45 \times 10^7$

العنوان:	Experimental and Numerical Study of Natural Convection Heat Transfer from Rectangular Fin Arrays
المؤلف الرئيسي:	Mohamad, Hamza Ashur Milad
مؤلفين آخرين:	Abd Allatif, Ahmed Mohamed، El Bakoush, Taib A(Advisor، Co-Advisor)
التاريخ الميلادي:	2007
موقع:	Al Khums
الصفحات:	1 - 155
رقم MD:	766381
نوع المحتوى:	رسائل جامعية
اللغة:	English
الدرجة العلمية:	رسالة ماجستير
الجامعة:	جامعة المرقب
الكلية:	كلية الهندسة
الدولة:	ليبيا
قواعد المعلومات:	Dissertations
مواضيع:	المصفوفة ، الحاسب الآلي، الحمل الحراري
رابط:	https://search.mandumah.com/Record/766381

CHAPTER 6

NUMERICAL SOLUTION

NUMERICAL SOLUTION

In verification of the experimental results obtained for the test model, attempts to perform corresponding computations were made. The physical domain was defined and the governing equations were outlined. Considering the boundary condition posed by the physical domain, these equations were subjected to numerical computations following a well-recognized computational technique. The governing equations and computational procedure will be detailed in this chapter. The computational results will be presented and a comparison with experiment as well as with available results by previous investigators will be held.

6-1 Physical Domain

The computational domain for the present problem is shown in Fig. (6-1) an infinite number of fins with negligible thickness were assumed. The fin surfaces and fin array base were assumed to be at a constant heat flux. The computation domain which described in figure (6-1) was reduced to one quarter of one fin channel with an extension towards one open end, in agreement with the geometry and symmetry conditions of the problem. The simulated part is shown in figure (6-2) in more detail. The computational domain has been beyond the actual dimensions of the fin array in order to account for effects due to surrounding of the fin array. Computations were performed for fin of L/2, H being the height of the fin, and S/2 is (half spacing) width of the domain in x- direction. The domain length was L in the z- direction and the height of the domain 5H in y- direction. The present study investigates the effects of a wide range of geometrical parameters to the heat transfer from fin arrays. Effects due to change in fin height, fin spacing,

orientation angle and temperature difference between fin and surrounding are investigated.

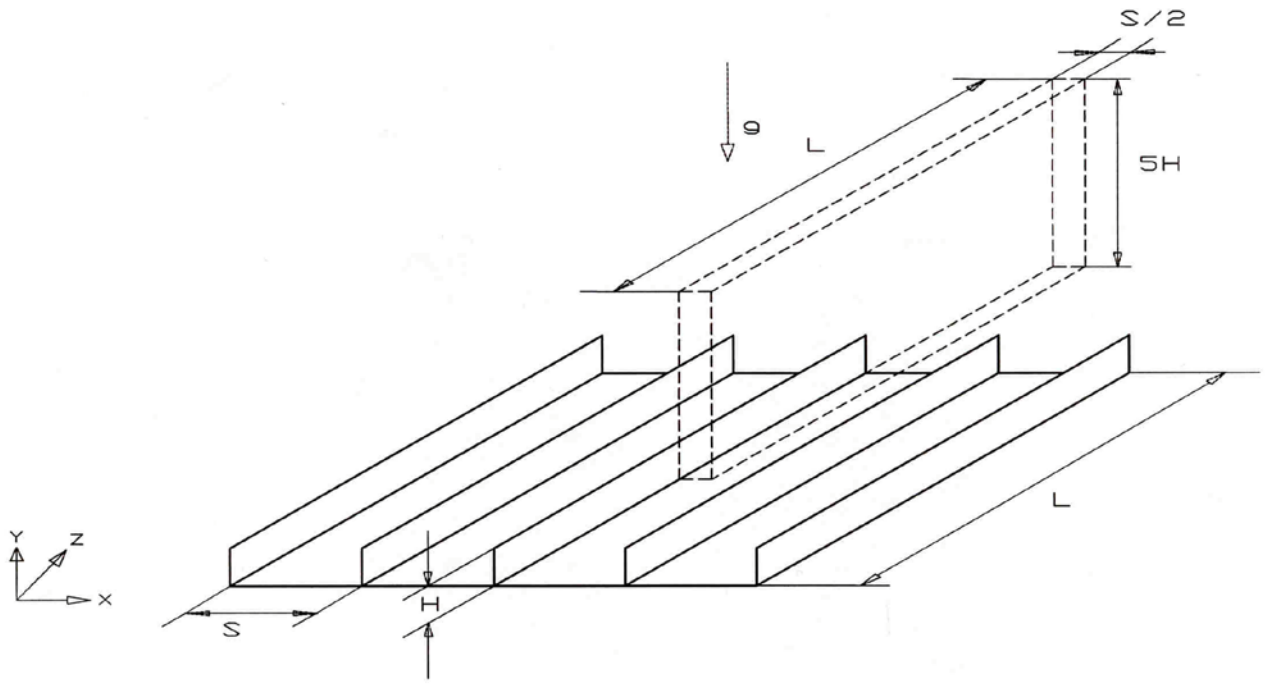

Fig. 6-1.Schematic drawing of the fin array under investigation

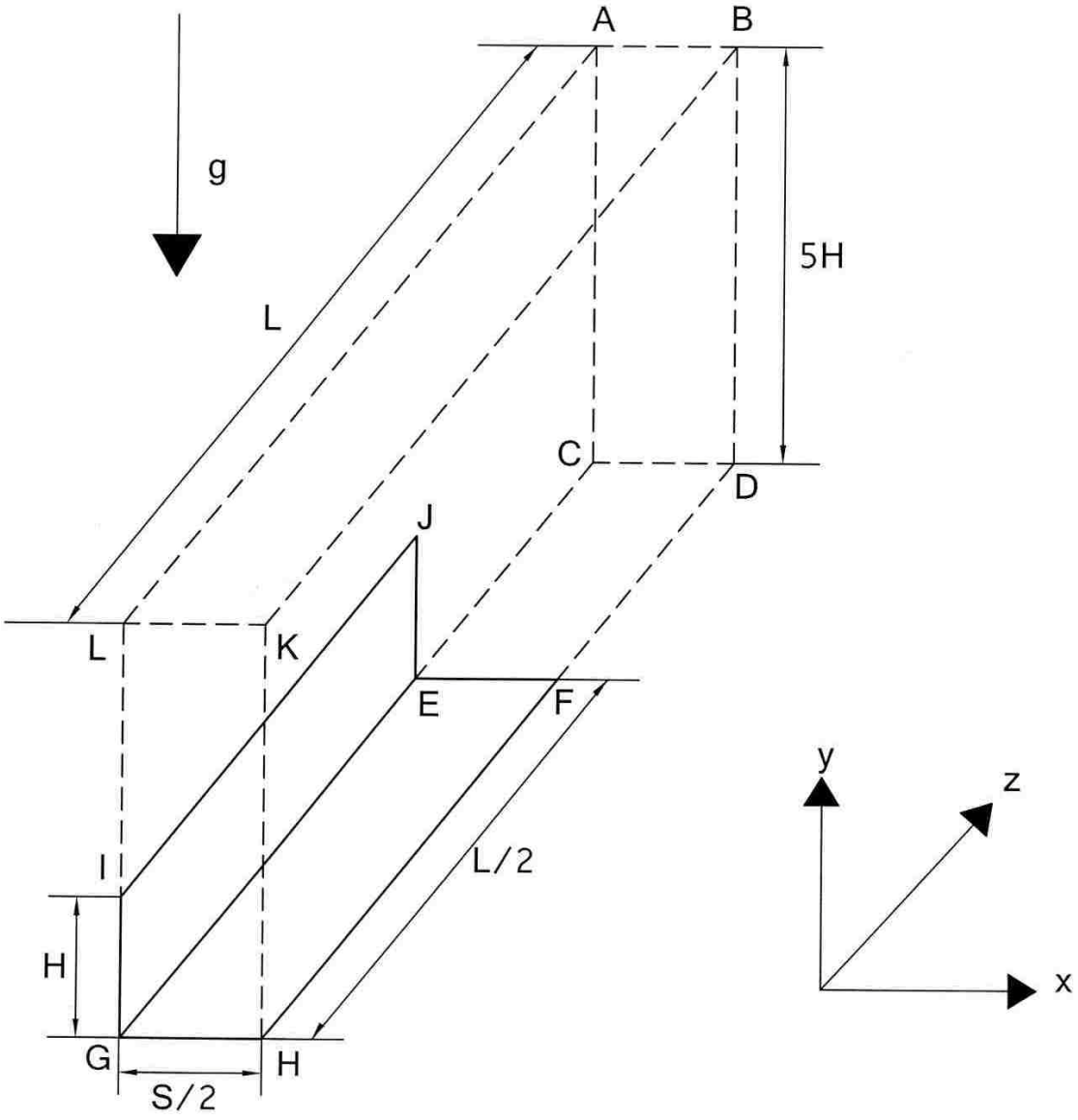

Fig. 6-2. Control volume for the numerical simulation of a hot finned surface.

6-2 Governing Equations

The flow around and heat transfer from fin arrays investigation was modeled by a set of elliptic partial differential equations. The three-dimensional continuity, momentum and energy equation in Cartesian coordinate are:

(Conservation of mass)

$$(6\text{-}1)\quad \frac{\partial(\rho u)}{\partial x}+\frac{\partial(\rho v)}{\partial y}+\frac{\partial(\rho w)}{\partial z}=0$$

(Conservation of momentum)

$$(6\text{-}2)\frac{\partial\left(\rho u^{2}\right)}{\partial x}+\frac{\partial(\rho uv)}{\partial y}+\frac{\partial(\rho uw)}{\partial z}=-\frac{\partial(P_{m})}{\partial x}+\rho\nu\left(\frac{\partial^{2}u}{\partial x^{2}}+\frac{\partial^{2}u}{\partial y^{2}}+\frac{\partial^{2}u}{\partial z^{2}}\right)$$

$$\frac{\partial(\rho vu)}{\partial x}+\frac{\partial\left(\rho v^{2}\right)}{\partial y}+\frac{\partial(\rho vw)}{\partial z}=-\frac{\partial(P_{m})}{\partial y}+\rho\nu\left(\frac{\partial^{2}v}{\partial x^{2}}+\frac{\partial^{2}v}{\partial y^{2}}+\frac{\partial^{2}v}{\partial z^{2}}\right)+g(\rho-\rho_{\infty})$$

$$\frac{\partial(\rho wu)}{\partial x}+\frac{\partial(\rho wv)}{\partial y}+\frac{\partial\left(\rho w^{2}\right)}{\partial z}=-\frac{\partial(P_{m})}{\partial z}+\rho\nu\left(\frac{\partial^{2}w}{\partial x^{2}}+\frac{\partial^{2}w}{\partial y^{2}}+\frac{\partial^{2}w}{\partial z^{2}}\right)$$

(Conservation of energy)

$$(6\text{-}3)\frac{\partial(\rho uT)}{\partial x}+\frac{\partial(\rho vT)}{\partial y}+\frac{\partial(\rho wT)}{\partial z}=\frac{\nu}{Pr}\left(\frac{\partial^{2}T}{\partial x^{2}}+\frac{\partial^{2}T}{\partial y^{2}}+\frac{\partial^{2}T}{\partial w^{2}}\right)$$

Laminar natural convection is the mechanism for heat transfer from the fin array. Radiation heat loss is neglected. The buoyancy forces representation is based on the Boussinesq approximation. The flow is, therefore considered as essentially incompressible. The fluid properties are assumed constant and are evaluated at the average of hot surface and the ambient fluid temperature. The solution is for conditions of steady state laminar natural convection.

6-3 Boundary Conditions

All boundary conditions were implemented by the inclusion of additional source and/or sink terms in the finite volume equations for computational cells at the boundaries. In natural convection flows there is no information regarding the velocity and temperature fields before the start of

calculations. Since governing, equations are invariably coupled, the temperature field causes the velocity field to develop and in turn the velocity field affects the temperature field with the promotion of convective heat transfer. The imposed boundary conditions were as follows:

1- The fin surface (I J E GI) and base surface (G E F H G) were held at constant heat flux.
2- Symmetry boundary conditions were applied at surface ACEJILA, BDHKB and LKHGL.
3- No-slip boundary conditions were applied to fin walls to simulate the effect of laminar friction and heat transfer.
4- All the remaining surface were open surfaces where air enters and leaves the surface at the ambient temperature T_∞ and the corresponding density ρ_∞. Here the ambient pressure was used as a stagnation boundary condition with the incoming mass having T_∞.

6-4 Computational Procedure

The system of Equations [(6-1)-(6-3)] with the boundary conditions stated above is solved through a control volume to obtain a set of discretized linear algebraic equations of the form.

$$a_p \phi_p = \Sigma a_{nb} \phi_{nb} + b \qquad (6\text{-}4)$$

Equations in the format given above are called finite volume equations. Finite volume equations describe processes affecting the value of ϕ in cell P in relation to its neighbor cells together with the source term b. These equations were solved by the widely used commercial (D. Rakshit, C. Balaji, [13]) CFD package FLUENT 6 employing the SIMPLEST algorithm for the pressure correction process along with the solution procedure for the hydrodynamic

equations. The central-difference-scheme leads to a second order truncation error in the approximations, whereas the upwind-scheme gives only first-order accuracy. The discretized equations are solved by the TDMA (Tri Diagonal-Matrix-Algorithm). The same technique has been successfully applied before by Baskaya et al. [8] to a much more complex natural convection problem.

6-5 Validation and Grid independency

Due to the iterative process of the code, convergence was used as the monitor of achievement of the final solution. The criterion of convergence of the numerical solution is based on the absolute normalized residuals of the equations that were summed for all cells in the computational domain. Convergence was considered as being achieved when these residuals terms of the continuity and momentum equations were smaller than 10^{-3}, and smaller than 10^{-6} for the energy equation, which was the case for most of the dependent variables, as shown in Fig. (6-3). A grid independence test was conducted in order to determine the proper grid size for this study. Grid independency checks were made and the final simulations were achieved with cell numbers shown in table (6-1) below in the *x–y–z* coordinate directions, depending on the actual physical dimensions used.

Table (6-1) Mesh density applied for 3-D finite volume model.

Aspect ratio (H/L)	Grid number $(i \times j \times k)$
0.322	$3 \times 151 \times 94$
0.215	$3 \times 101 \times 94$
0.161	$3 \times 76 \times 94$
0.08	$3 \times 39 \times 94$

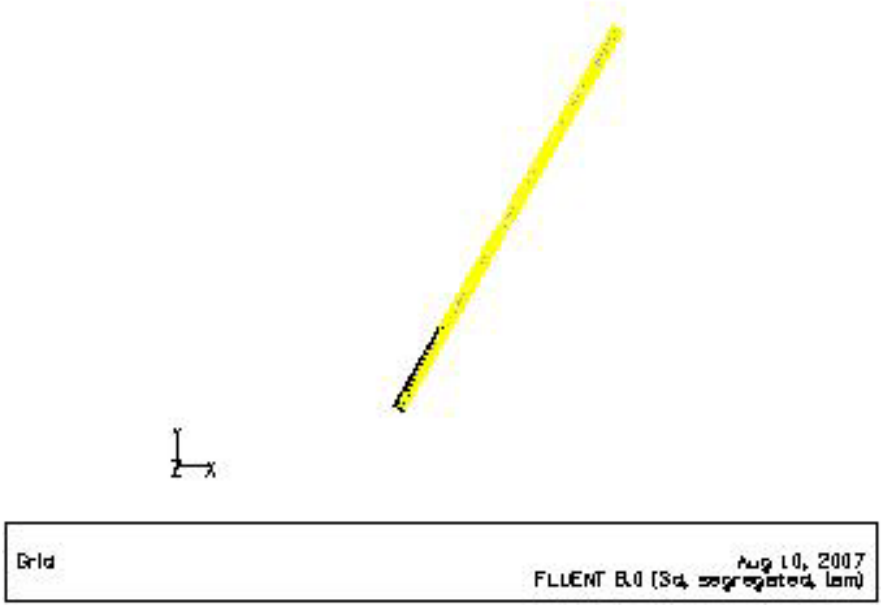

Fig. 6-3. Representative grid system

Coarser grid distributions were not able to give accurate results in agreement with experimental results and data from the literature.

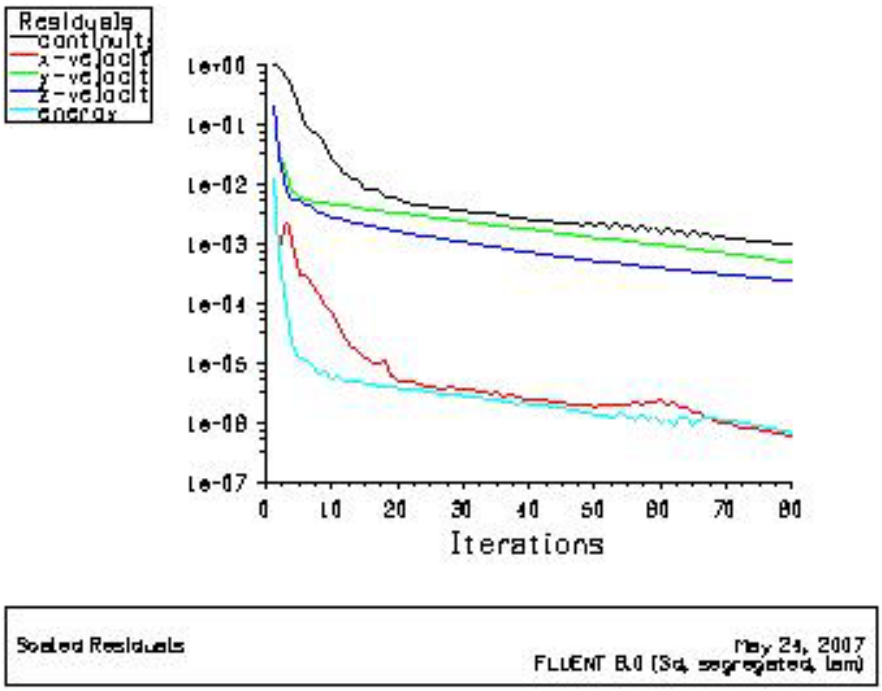

Fig. 6-4. Convergence of residual terms of continuity, momentum and energy eqns.

Fig. (6-4) shows a comparison between the experimental and numerical results for orientation angle Φ = 0 °, H = 60 mm and S = 6.5 mm. Figure shows a good agreement between the experimental and numerical results with a deviation of 1.352 ٪.

The deviation was calculated from Equation :

$$\% \, Deviation = \frac{\sum_{i=1}^{N} \left| \left[(h_i)_{cal} - (h_i)_{\exp} \right] / (h_i)_{\exp} \right|}{N} \times 100 \qquad (6\text{-}5)$$

Where the subscripts "exp" and "cal" are denoted the experimental and calculated values of heat transfer coefficient (h) and N is the number of measurements.

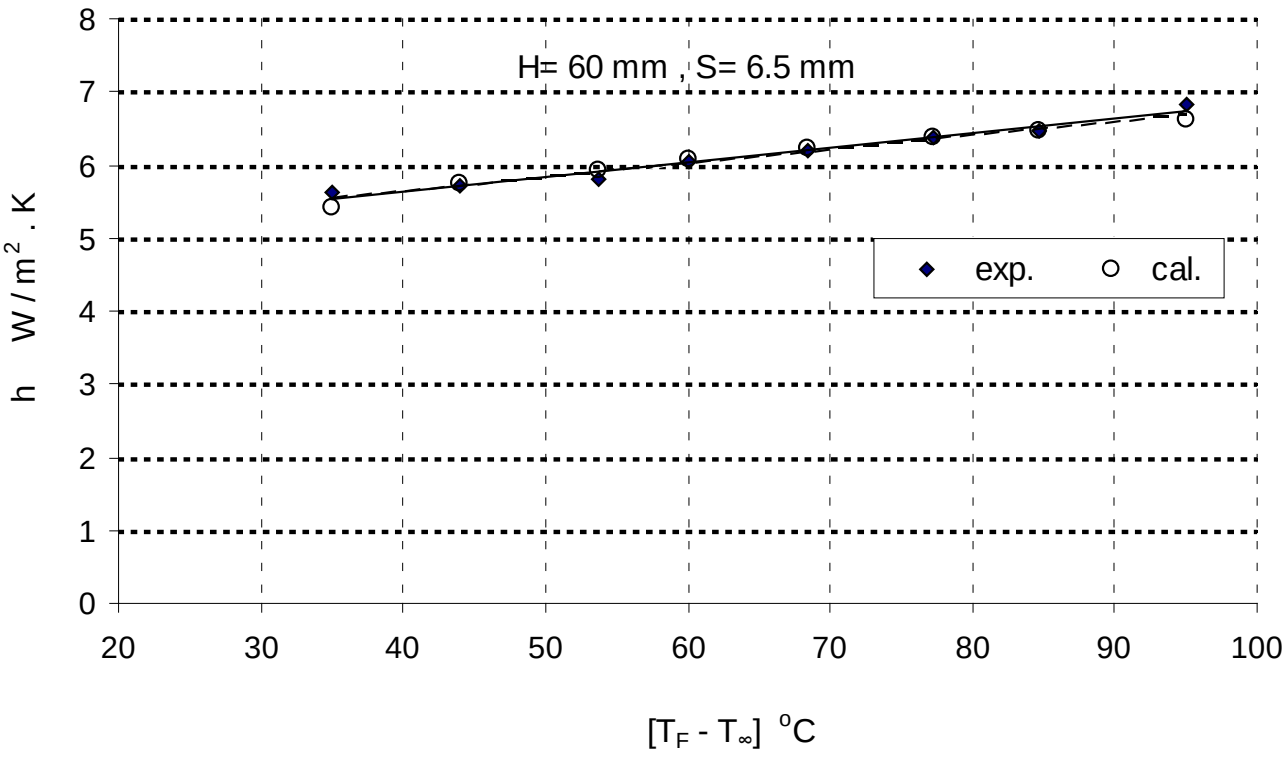

Fig.(6-5) Comparison between the experimental and numerical results for Φ = 0°, H = 60 mm and S=6.5 mm.

Fig. (6-5) shows a comparison between the experimental and numerical results for orientation angle Φ = 0 °, H = 60 mm, S = 6.5 mm with data in ref.[9]. At H = 3.8 mm, S = 6.4 mm L = 127 mm, Figure shows a good agreement between the present study and data in REF.[9] with a deviation of 12 ٪.

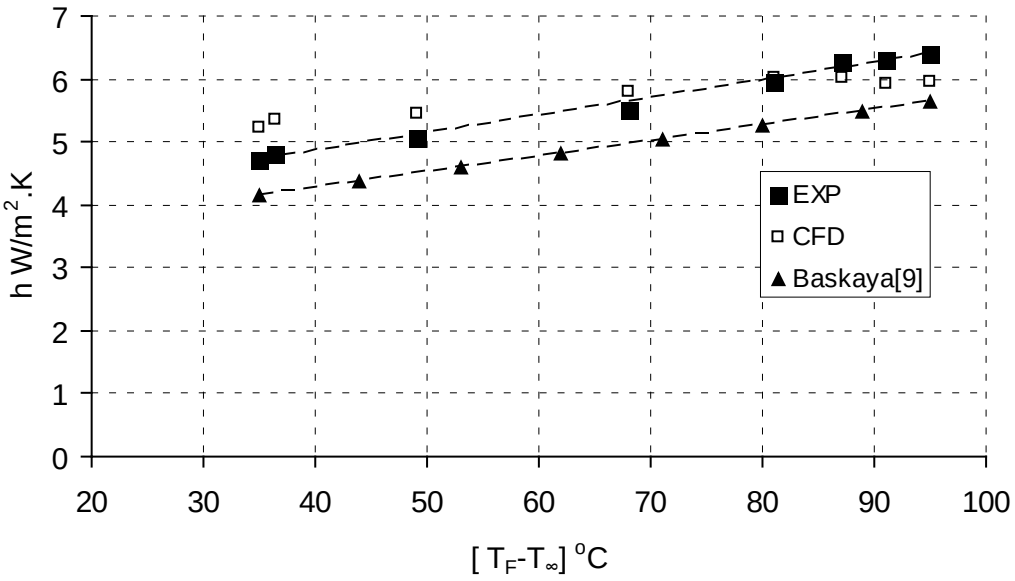

Fig.(6-6) Comparison between the experimental and numerical results for Φ = 0°, H = 40 mm and S=6.5 mm with reference [9].

العنوان:	Experimental and Numerical Study of Natural Convection Heat Transfer from Rectangular Fin Arrays
المؤلف الرئيسي:	Mohamad, Hamza Ashur Milad
مؤلفين آخرين:	Abd Allatif, Ahmed Mohamed، El Bakoush, Taib A(Advisor، Co-Advisor)
التاريخ الميلادي:	2007
موقع:	Al Khums
الصفحات:	1 - 155
رقم MD:	766381
نوع المحتوى:	رسائل جامعية
اللغة:	English
الدرجة العلمية:	رسالة ماجستير
الجامعة:	جامعة المرقب
الكلية:	كلية الهندسة
الدولة:	ليبيا
قواعد المعلومات:	Dissertations
مواضيع:	المصفوفة ، الحاسب الآلي، الحمل الحراري
رابط:	https://search.mandumah.com/Record/766381

CHAPTER 7

RESULTS AND DISCUSSION

RESULTS AND DISCUSSION

7.1 Introduction

Experimental and numerical investigations have been performed to study the natural convection heat transfer from a rectangular fin arrays at different orientation angles. An experimental test rig was built to be used for these investigations. Effects of fin spacing, fin height, model orientation angle, and temperature difference between fin and surroundings on the free convection heat transfer from fin arrays were studied. During the experiments, the fin spacing (S) was varied from 3.3 to 33 mm, fin height (H) from 15 to 60 mm, orientation angle (Φ) from 0° to 180°, and temperature difference between fin and surrounding (ΔT) from 35 to 95 °C.

Numerical model (Fluent) was used to understand the general flow patterns dominating flows from fin arrays. The three-dimensional elliptic governing equations solved using finite volume based computational fluid dynamics (CFD) code. A large number of runs were carried out for a systematic theoretical investigation of the effects of fin spacing, fin height, orientation angle and temperature difference between fin and surroundings on the heat transfer processes involved.

A comparison between the experimental and numerical results were performed to verification the numerical code. General correlations between Nussult number, Rayighly number, fin spacing, fin height, orientation angle, temperature difference between the fin and surroundings developed.

7.2 Experimental Results

7.2.1 Effect of Temperature difference

Variation of heat transfer coefficient (h) with temperature difference $(T_F - T_\infty)$ at different values of orientation angle (Φ) and fin height (H) are shown in Figures [(7-1)-(7-4)]. These figures are presented at constant value of fin spacing S = 3.375 mm. It is seen that from the figures, the heat transfer coefficient increases with increasing the temperature difference ΔT for all values of orientation angle (Φ) and fin height (H). This due to, with increase the temperature difference between the fluid adjacent to the hot fin surface and the fluid a way from it, the buoyancy force increases and a stronger natural convection currents, and thus the heat transfer coefficient increases.

7.2.2 Effect of fin height

Figures. [(7-5)-(7-9)] show variation of heat transfer rate per unit base area (Q/A_b) with fin height (H) at various orientation angles (Φ) and different values of fin spacing (S). These Figures show that the heat transfer per unit base area increases with increase in fin height (H) for all values of orientation angle and fin spacing. The reason is that, any increase of fin height increases the array surface area and thereby entails a larger heat transfer rate.

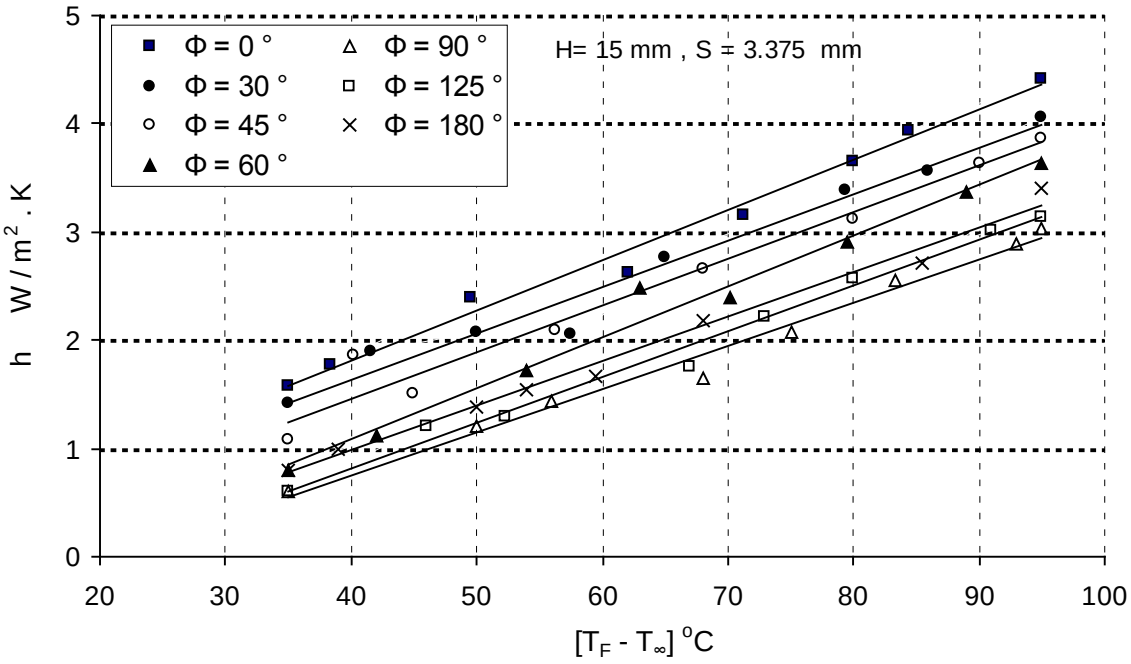

Fig. 7-1. Variation of heat transfer coefficient with temperature difference ΔT at H = 15 mm S = 3.375 mm.

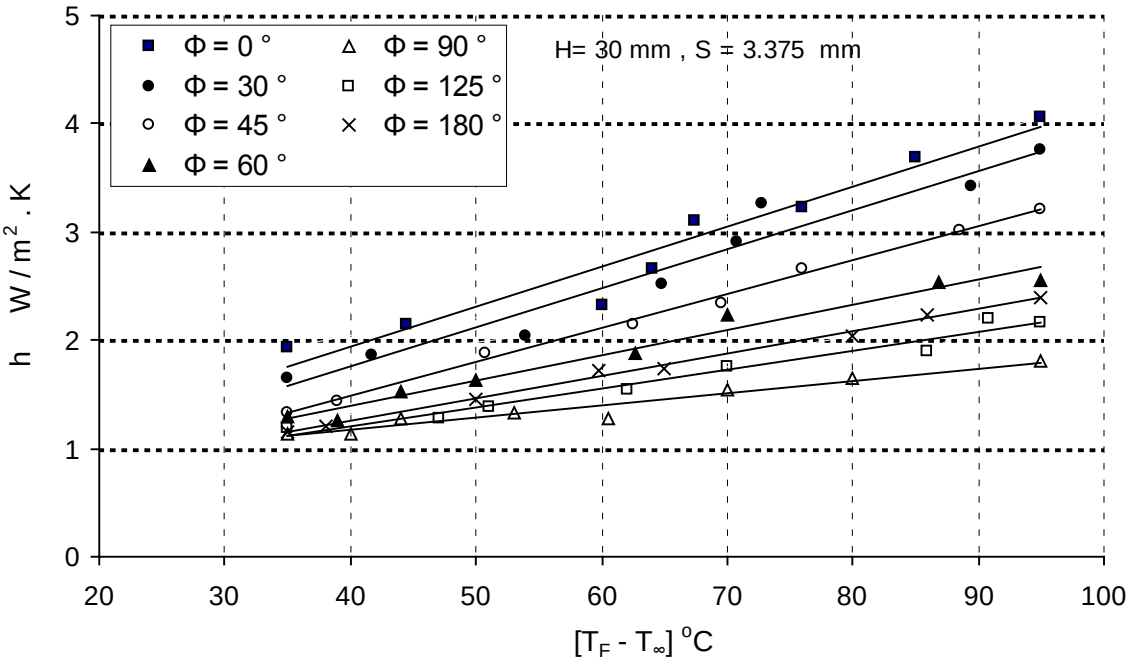

Fig. 7-2. Variation of heat transfer coefficient with temperature difference ΔT at H = 30 mm S = 3.375 mm.

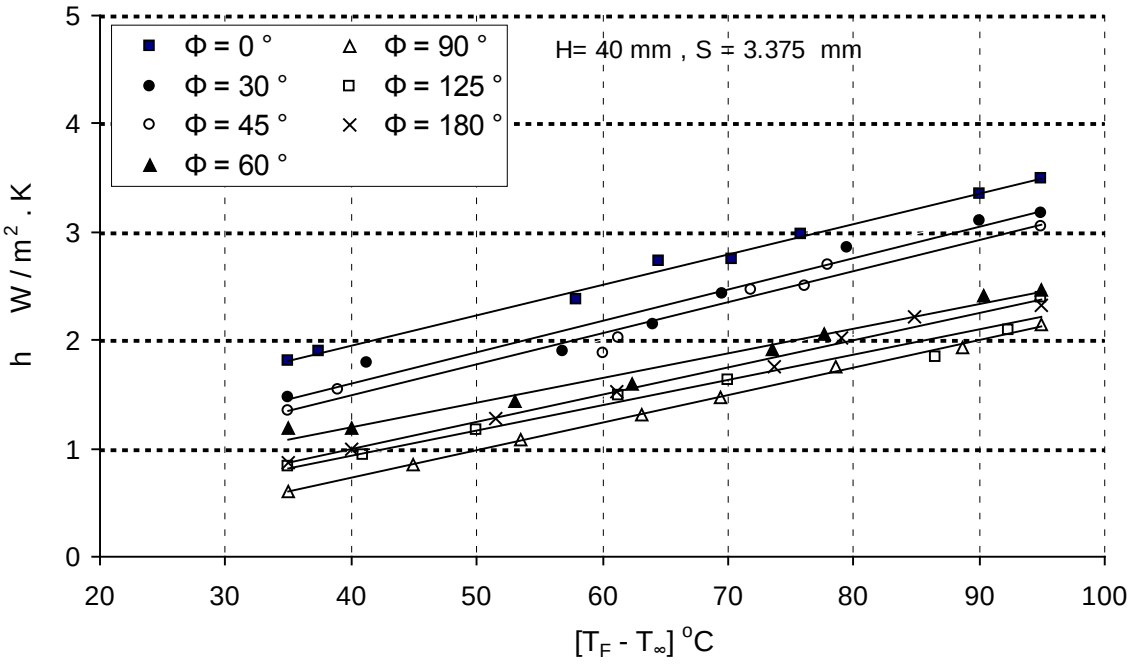

Fig. 7-3. Variation of heat transfer coefficient with temperature difference ΔTat H = 40 mm S = 3.375 mm.

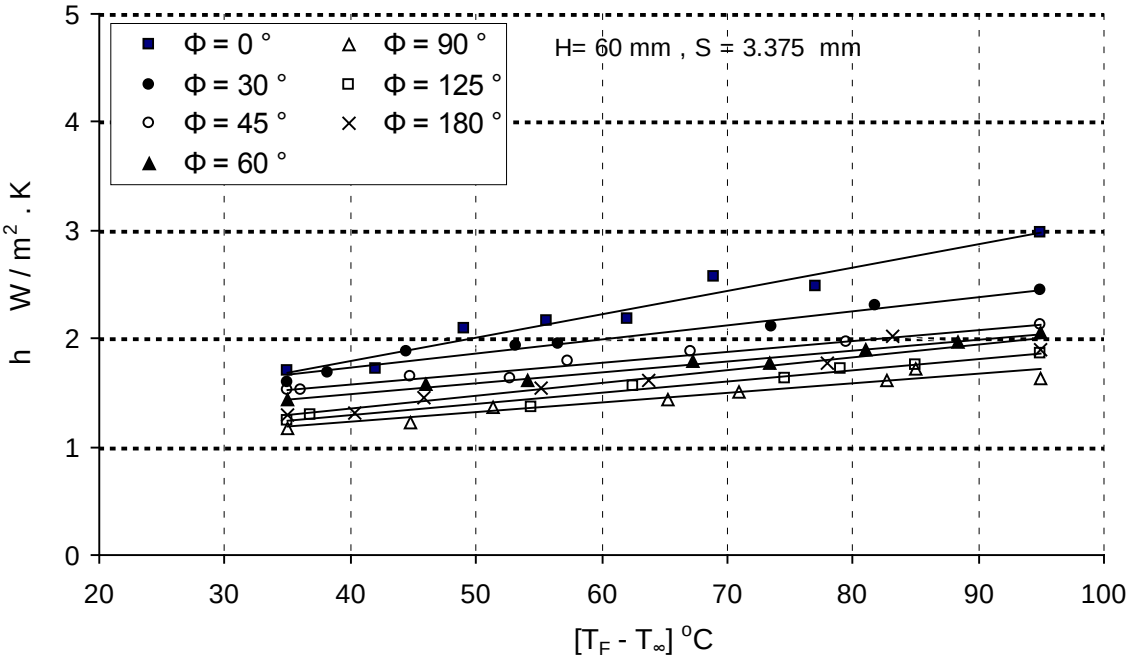

Fig. 7-4. Variation of heat transfer coefficient with temperature difference ΔT at H = 60 mm S = 3.375 mm.

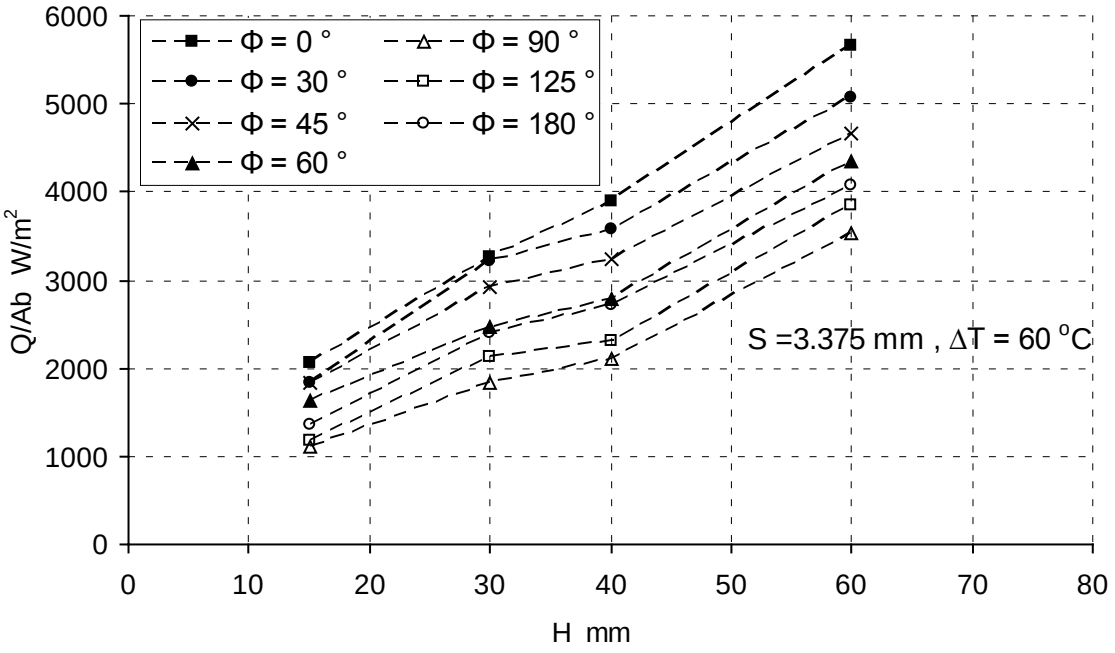

Fig. 7-5. Variation of heat transfer rate per unit base area with fin height at various Φ (S = 3.375 mm, ΔT = 60 ^{O}C).

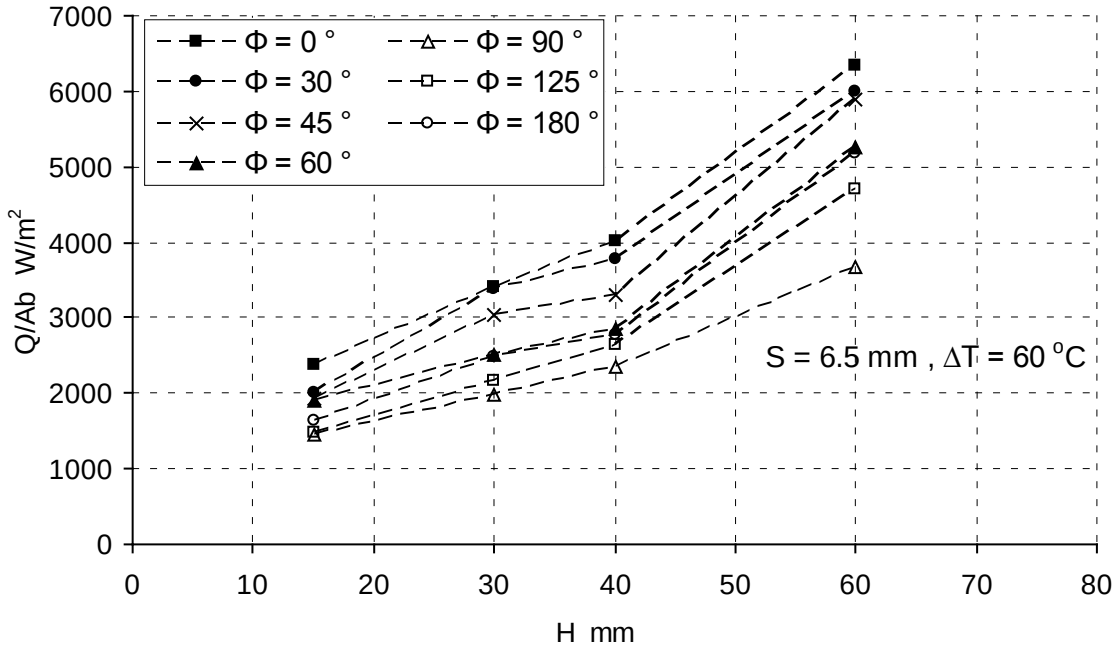

Fig. 7-6. Variation of heat transfer rate per unit base area with fin height at various Φ (S = 6.5 mm, ΔT = 60 ^{O}C).

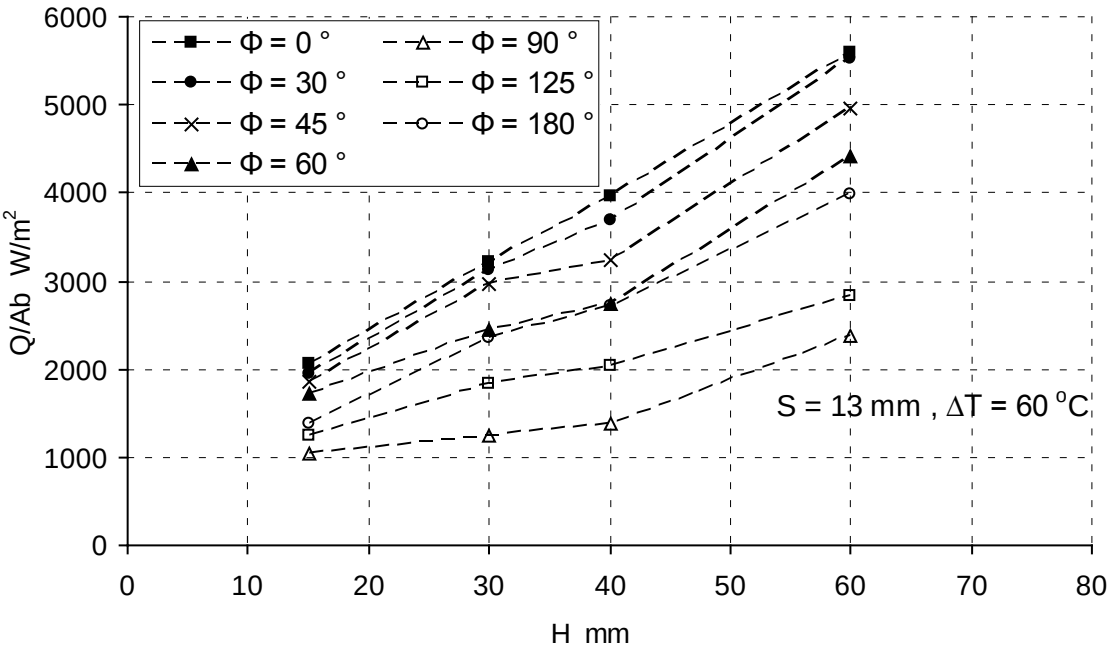

Fig. 7-7. Variation of heat transfer rate per unit base area with fin height at various Φ (S = 13 mm, ΔT = 60 ^{O}C).

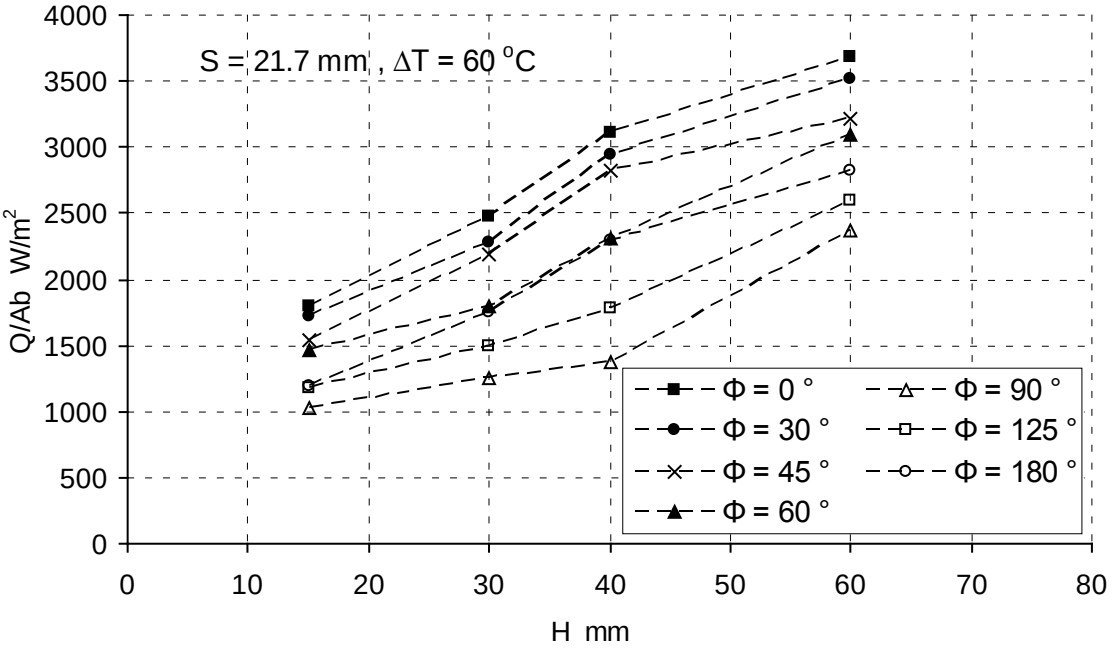

Fig. 7-8. Variation of heat transfer rate per unit base area with fin height at various Φ (S = 21.7 mm, ΔT = 60 ^{O}C).

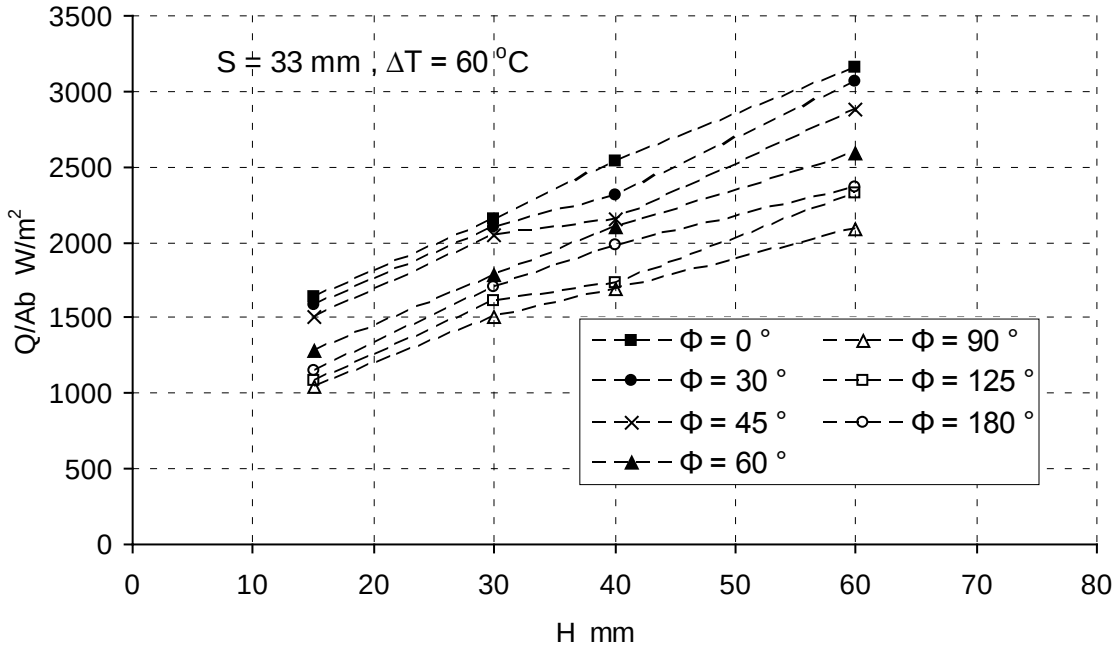

Fig. 7-9. Variation of heat transfer rate per unit base area with fin height at various Φ (S = 33 mm, ΔT = 60 ^{O}C).

7.2.3 Effect of fin spacing

The fin spacing plays an important role in determining the array heat transport capability. Figures. [(7-10)-(7-13)] show the effect of fin spacing on heat transfer rate per unit base area at various orientation angle and fin spacing. It is seen that the heat transfer rate per unit base area increases with increasing the fin spacing to reache a maximum value and then decreases with farther increase in the fin spacing. On each curve, clearly, the maximum volumetric heat dissipation occurs at optimal spacing $S_{opt} = 6.5$ mm.

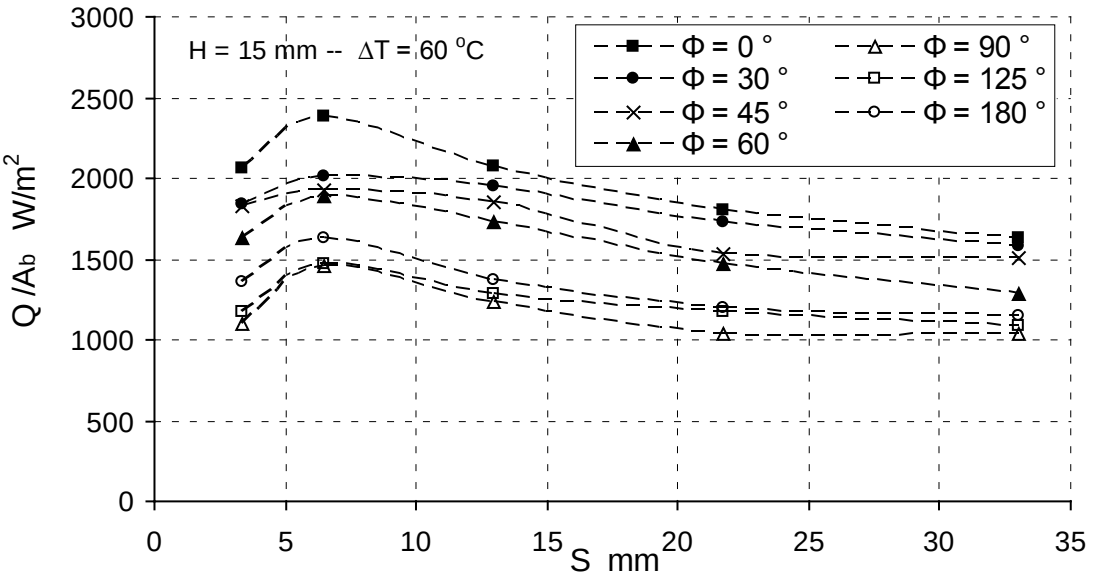

Fig. 7-10. Effects of fin spacing on heat transfer rate per unit base area, at different values of orientation angles (H = 15 mm, ΔT = 60 °C).

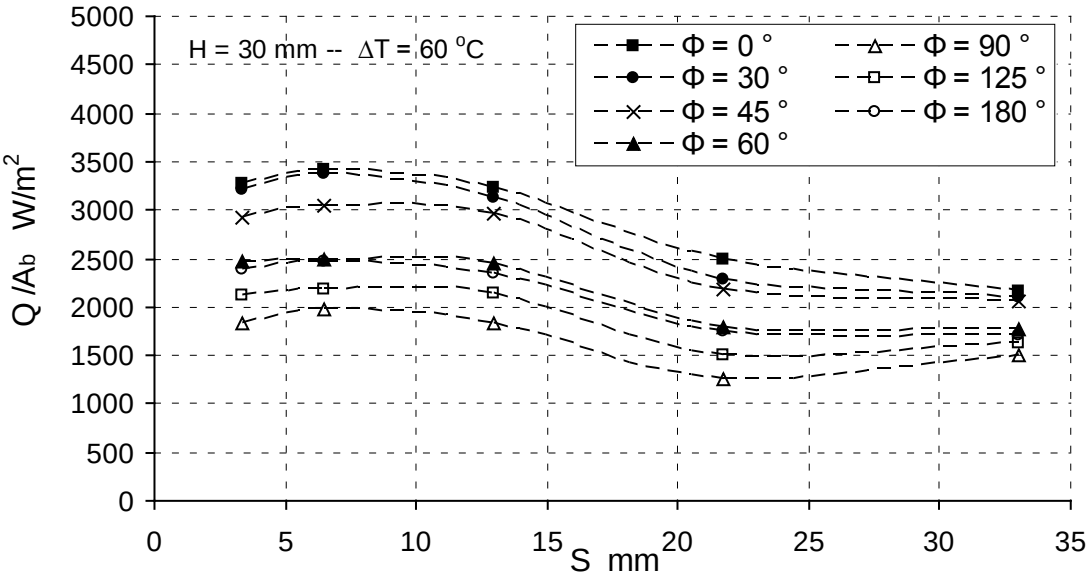

Fig. 7-11. Effects of fin spacing on heat transfer rate per unit base area, at different values of orientation angles (H = 30 mm, ΔT = 60 °C).

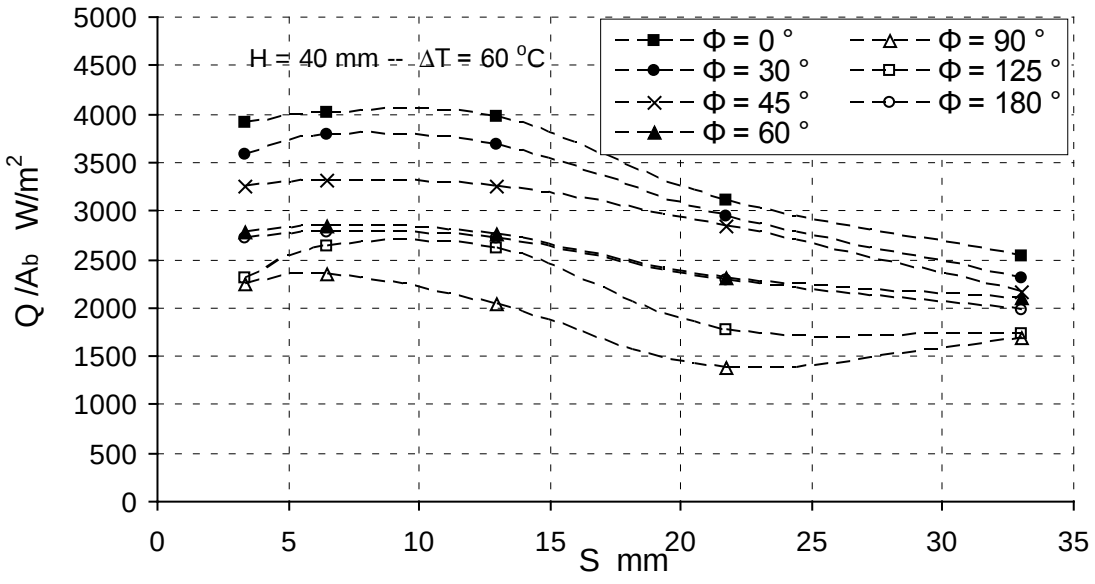

Fig. 7-12. Effects of fin spacing on heat transfer rate per unit base area, at different values of orientation angles (H = 40 mm, ΔT = 60 °C).

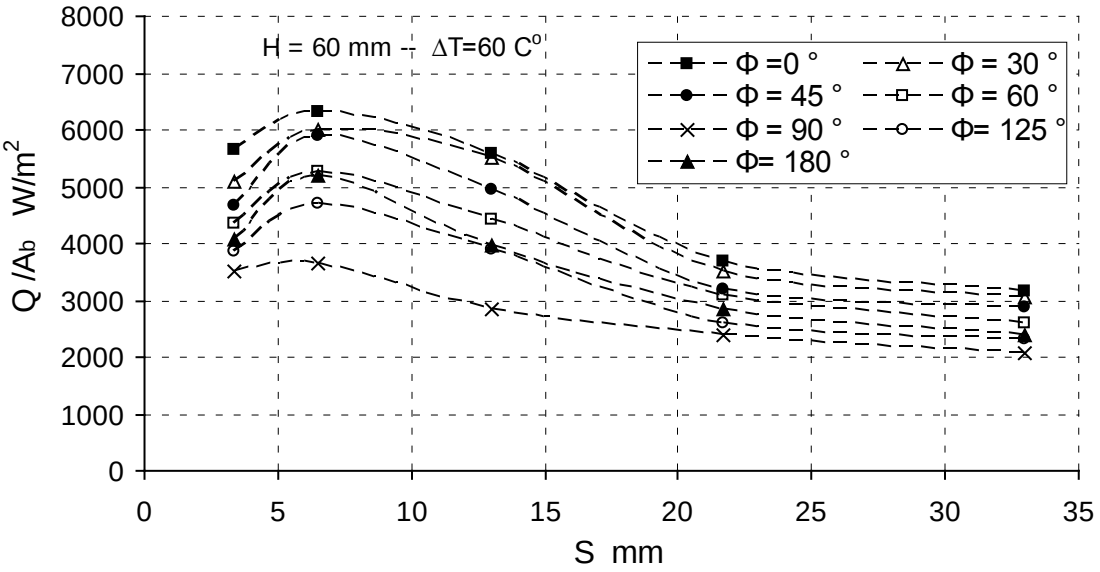

Fig. 7-13. Effects of fin spacing on heat transfer rate per unit base area, at different values of orientation angles (H = 60 mm, ΔT = 60 °C).

7.2.4 Effect of orientation angle

Effects of orientation angle (Φ) on the heat transfer coefficient are shown in Figs. [(7-14)-(7-17)]. These Figures are presented at different values of fin spacing. It is seen from the figures that the average heat transfer coefficient has a maximum value at Φ = 0° and reduce with the increase in (Φ) to reaches a minimum value at Φ = 90°and thus increase with farther increase in Φ .

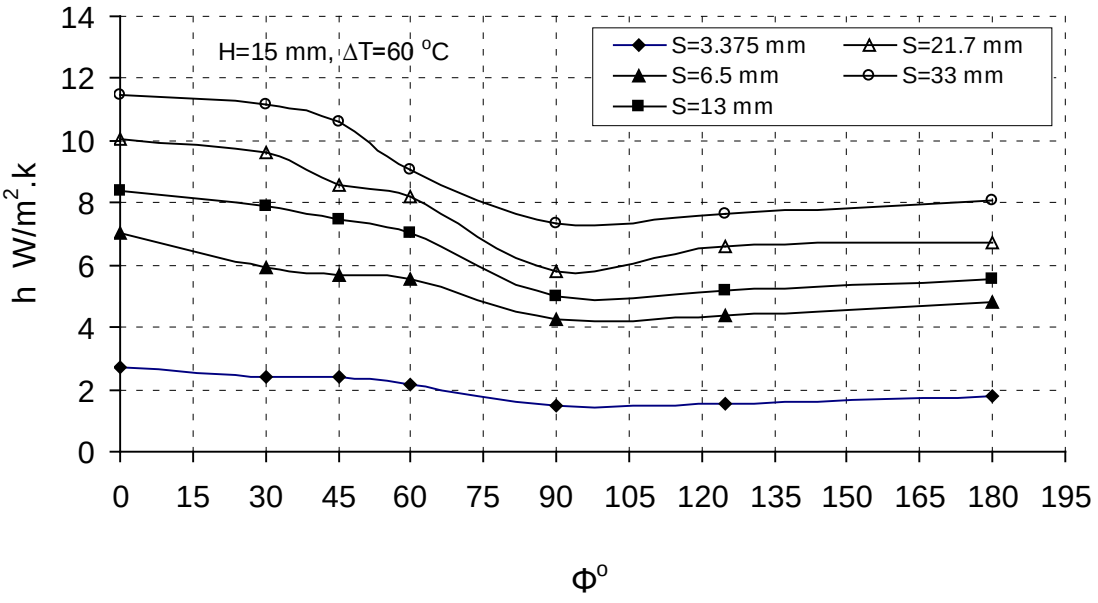

Fig. 7-14. The dependence of heat transfer coefficient h on the orientation angles at various fin spacing (H = 15 mm, ΔT = 60 °C).

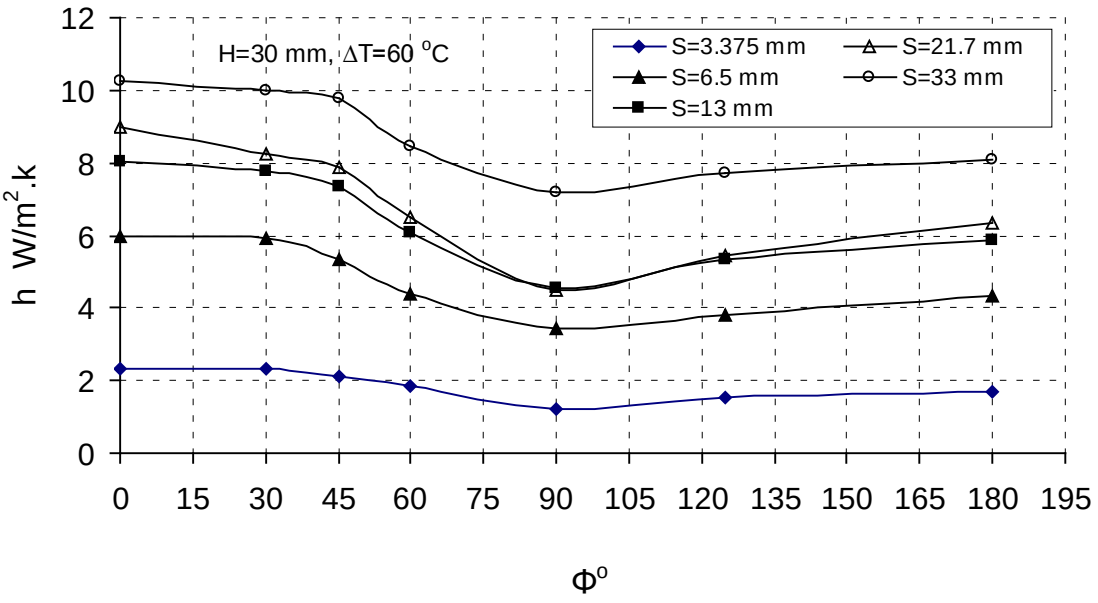

Fig. 7-15. The dependence of heat transfer coefficient h on the orientation angles at various fin spacing (H = 30 mm, ΔT = 60 °C).

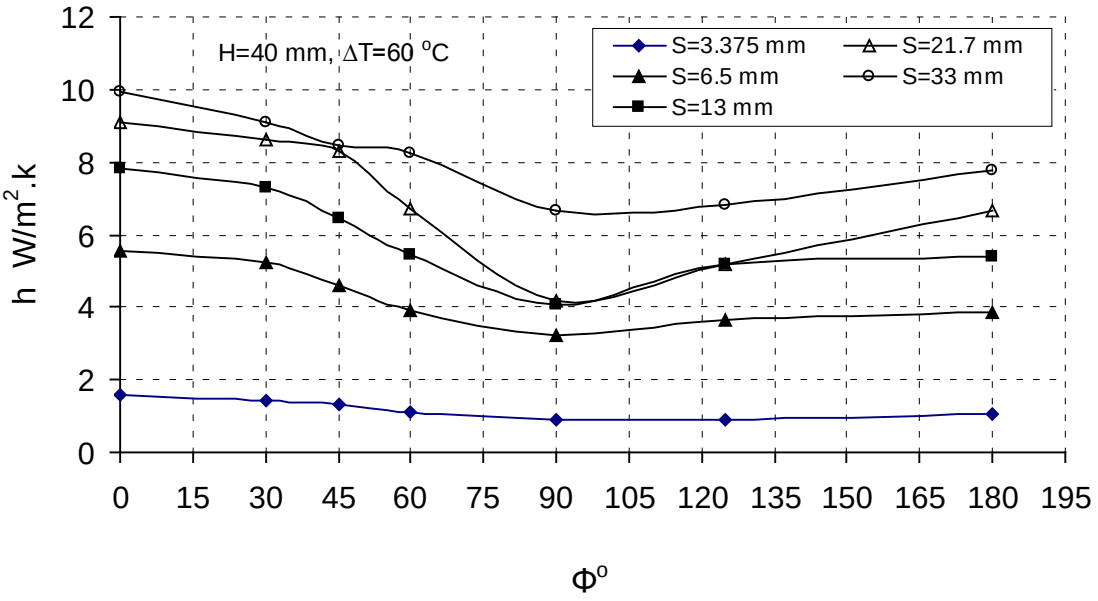

Fig. 7-16. The dependence of heat transfer coefficient h on the orientation angles at various fin spacing (H = 40 mm, ΔT = 60 °C).

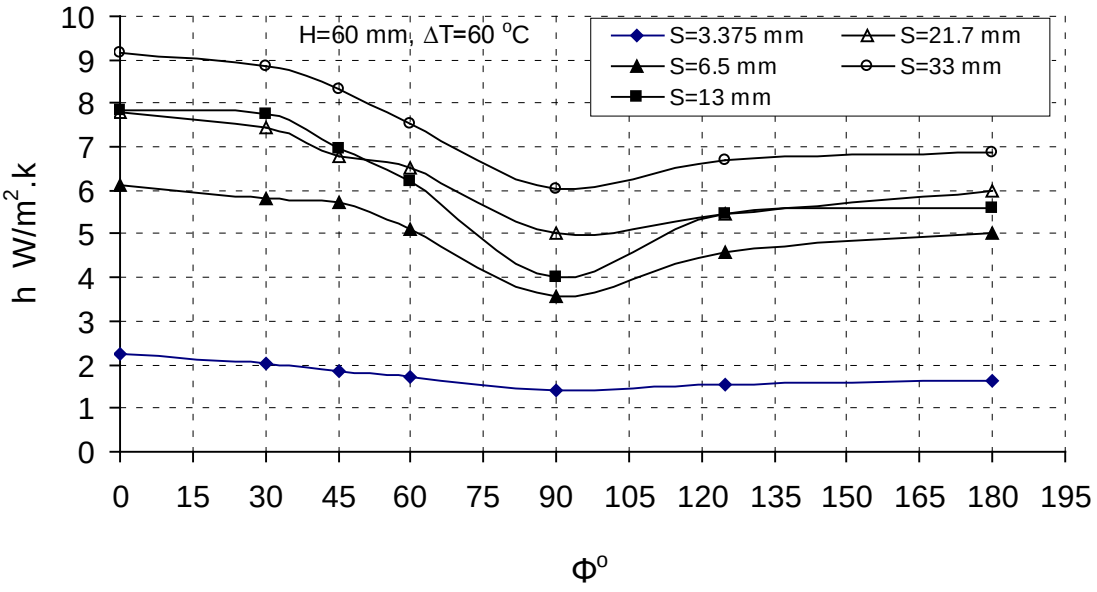

Fig. 7-17. The dependence of heat transfer coefficient h on the orientation angles at various fin spacing (H = 60 mm, ΔT = 60 °C).

At Φ = 0°, the surrounding fluid enters the fin region from the open ends and develops a vertical component of velocity as the air heated. The resulting chimney being only a fraction of the width of the fin array and the buoyancy forces exclusively induce the fluid motion in the upward direction [(See Fig. (7-18)]Consequently, higher heat transfer is expected. On the other hand, if the fin is inclined with respect to gravity (Φ = 30°. Φ = 45°, Φ = 60°) the buoyancy has a component normal, as well parallel, to the fin surface. With a reduction in buoyancy force parallel to the surface and the fluid velocities along the fin are reduced and there is attendant reduction in convection heat transfer compared with vertical fin position (Φ = 0°).

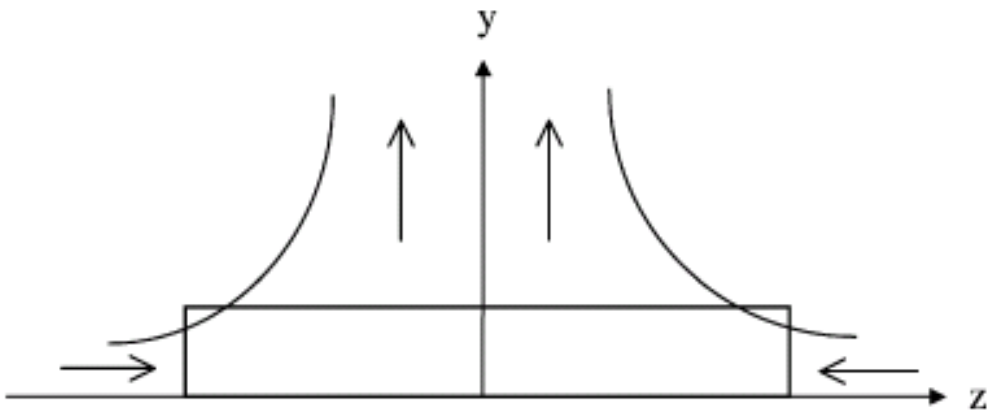

Fig. 7-18. Schematic illustration of chimney flow pattern Ref.[9].

At Φ = 180°, the ambient air flow rises from below upward and towards the surface center. At certain distance from the surface the air flow reverses its lateral movement direction and flows towards the surface edges, as indicated in Fig.(7-19). The flow is confined between the fins and the base plate and moves towards the surface edges while portraying some boundary layer characteristics. Similarly, a thermal boundary layer is also formed and thus a reduction of heat transfer rate will be occurred.

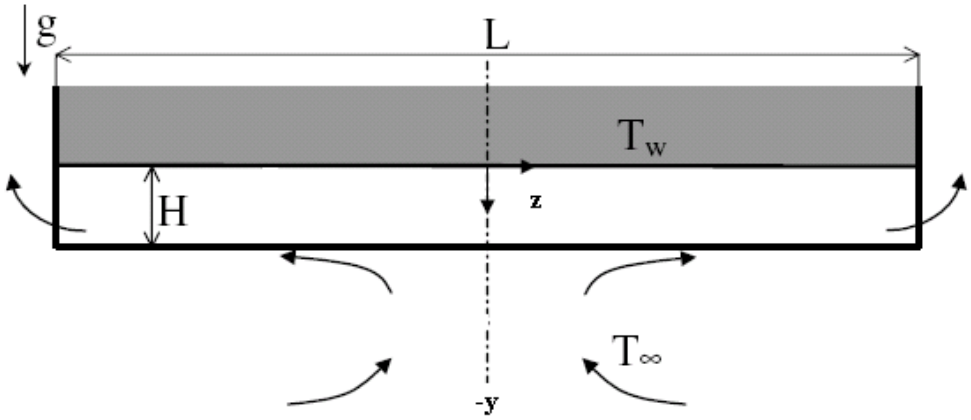

Fig. (7-19) Schematic description of natural convection at Φ = 180°.Ref[12].

As mention before, Figures [(7-14)-(7-17)] show a minimum values of heat transfer coefficient at Φ = 90°. This due to a thermal boundary layer devolved through a vertical length of fins and thus reduces the heat transfer coefficient.

Figures [(7-20)-(7-23)] show that the heat transfer coefficient increases with increase in fin spacing. These figures show also a variation of heat transfer coefficient with orientation angle (Φ) at various fin height. It is seen that, the heat transfer coefficient has a maximum values at Φ = 0°,while has a minimum values at Φ = 90°for all values of H. Inspection of the influence of the fin height on the averaged heat transfer coefficient indicates that it is quite small.

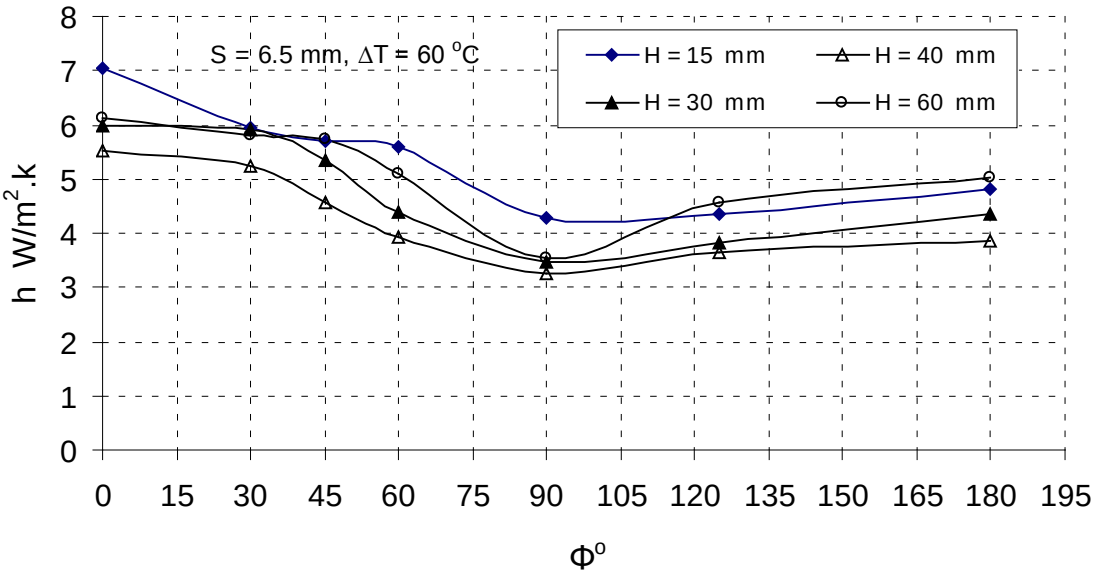

Fig. 7-20. The dependence of heat transfer coefficient h on the orientation angles at various fin height (S = 6.5 mm, ΔT = 60 °C, N=14 fins).

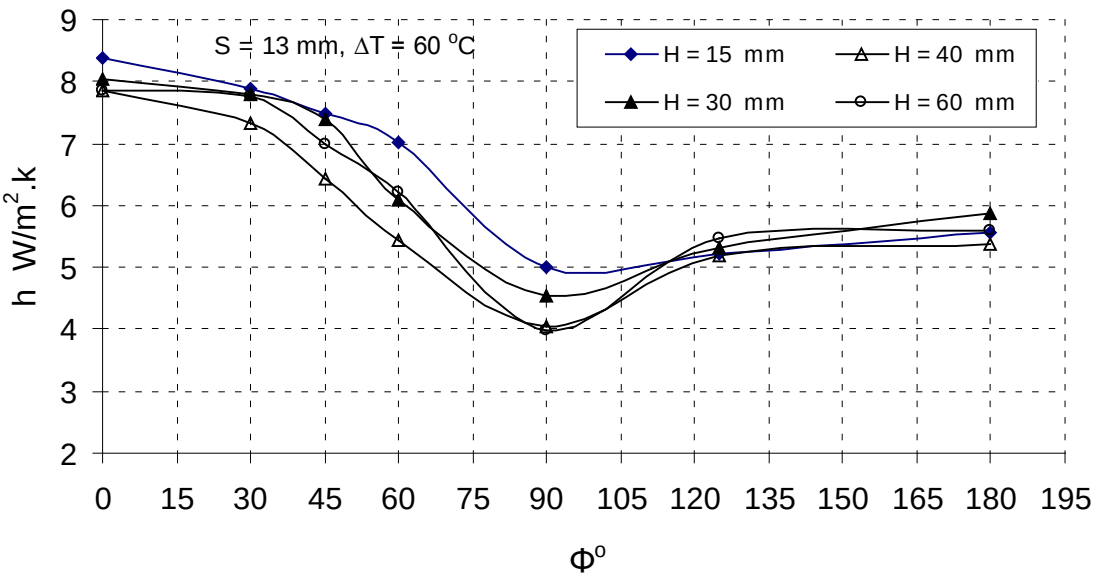

Fig. 7-21. The dependence of heat transfer coefficient h on the orientation angles at various fin height (S = 13 mm, ΔT = 60 °C, N=11 fins).

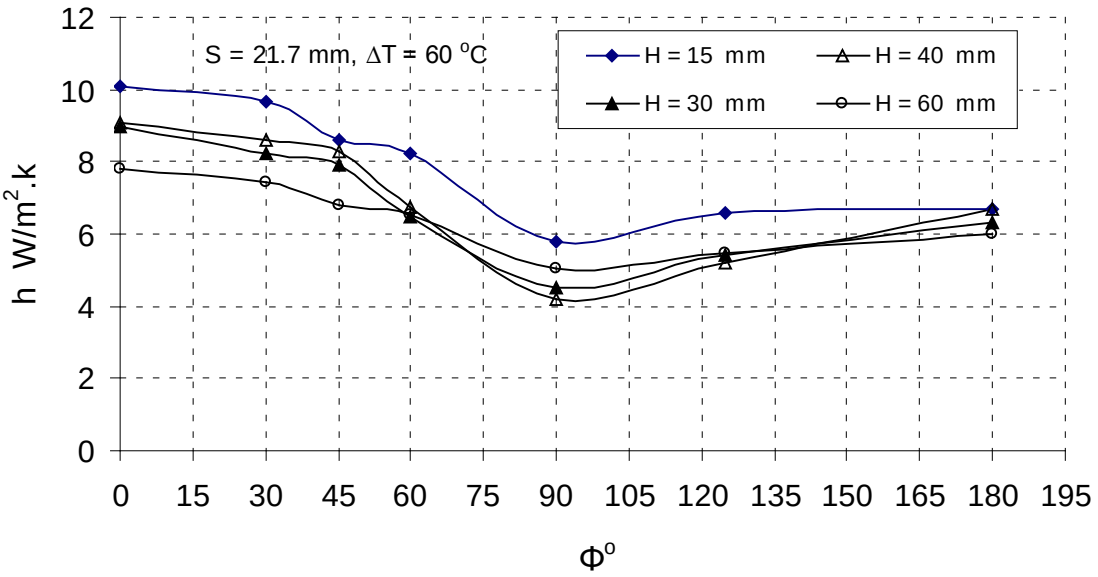

Fig. 7-22. The dependence of heat transfer coefficient h on the orientation angles at various fin height (S = 21.7 mm, ΔT = 60 °C, N= 8 fins).

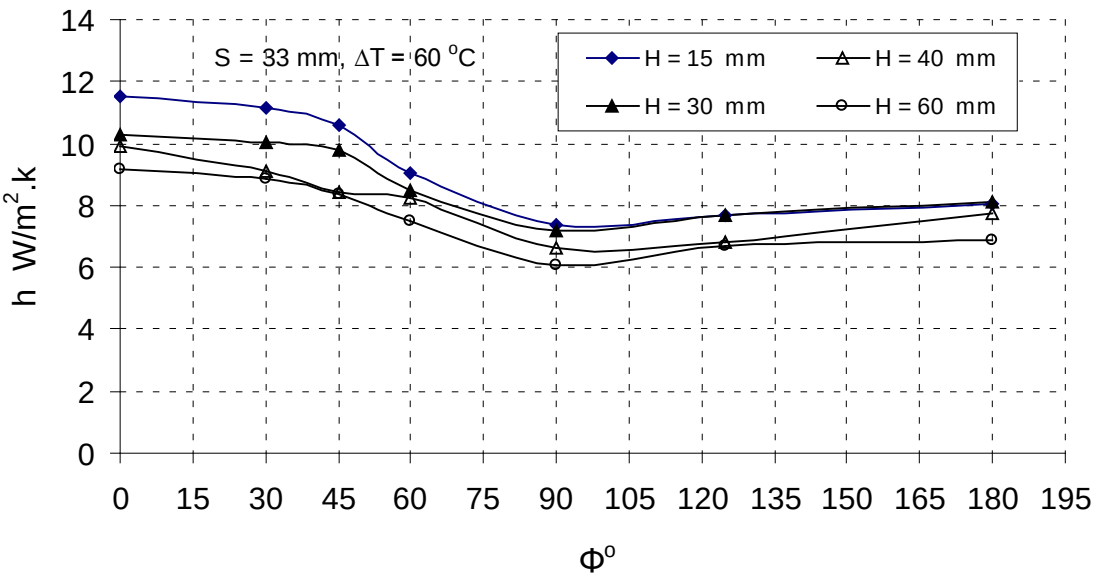

Fig. 7-23. The dependence of heat transfer coefficient h on the orientation angles at various fin height (S = 33 mm, ΔT = 60 °C, N= 6 fins).

7.3 Numerical Results

It is important to understand the general flow patterns dominating flows from fin arrays. In natural convection flows there is no information regarding the velocity and temperature field, the temperature field cases the velocity field to develop and turn the velocity field affects the temperature field with the promotion of convection heat transfer. Figures (7-24) and (7-25) show streamline and temperature contours for orientation angle $\Phi = 0°$, at Rayleigh number1.31×10^{7}. As mention before, the surrounding fluid enters the fin region from the open ends and develops vertical component of velocity as the air is heated. A chimney type flow pattern is observed, above the fin surface, whereas the fluid situated far from the fin surface is stagnant.

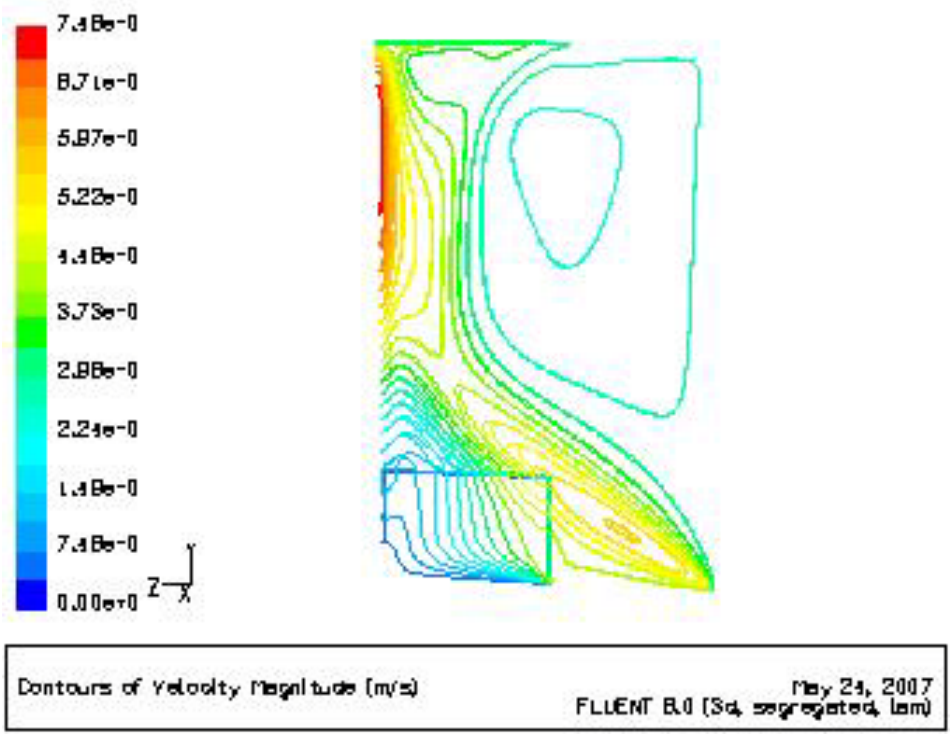

Fig. 7-24. Streamline contours at Rayleigh number 1.31×10^{7}

S = 6.5 mm, H = 60 mm, $\Phi = 0°$.

Temperature contours Fig. (7-25) show the temperatures above and near the fin surface are higher than these far from the fin.

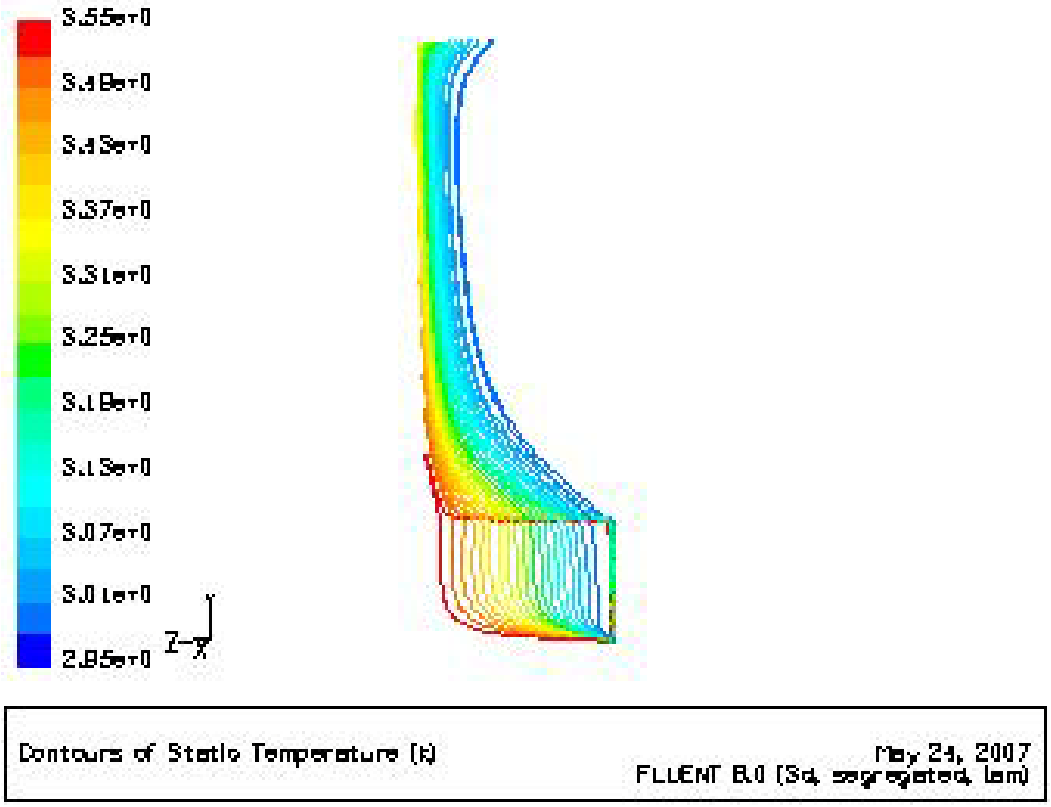

Fig. 7-25. Temperature contours at Rayleigh number 1.31×10^{7}

S = 6.5mm, H = 60 mm, $\Phi = 0°$.

Effect of temperature difference ΔT on average heat transfer coefficient at various orientation angle and different values of fin spacing S are shown in figures [(7-26)-(7-29)]. Also, it is seen that the average heat transfer coefficient increases with increasing ΔT for all values of orientation angle Φ. It is clear also, the heat transfer coefficient increases with decreasing orientation angle.

Comparisons between experimental and numerical results are presented in Figures [(7-30)-(7-33)]. From these figures, it is seen that a good a

agreement between experimental and numerical results with a maximum deviation of 13 ٪. Table (7-1) shows a deviation of the experimental results from numerical results at S = 6.5 mm, ΔT = 35°C to 95°C.

Table 7-1. Deviation of the CFD prediction from experimental results.

Orientation angle Φ	H = 60 mm	H = 40 mm	H = 30 mm	H = 15 mm
Φ = 0°	1.3٪	6.5 ٪	2.8 ٪	5.6 ٪
Φ = 30°	5.1 ٪	9.8 ٪	4.8 ٪	10 ٪
Φ = 45°	5.4 ٪	3 ٪	6.3 ٪	7.4 ٪
Φ = 60°	11.6 ٪	8.1 ٪	12.5 ٪	5.7 ٪
Φ = 90°	6.2 ٪	7.4٪	8.4 ٪	12 ٪
Φ = 125°	6.7 ٪	8.3 ٪	5.7 ٪	13 ٪
Φ = 180°	7.33 ٪	8 ٪	12 ٪	8.7 ٪

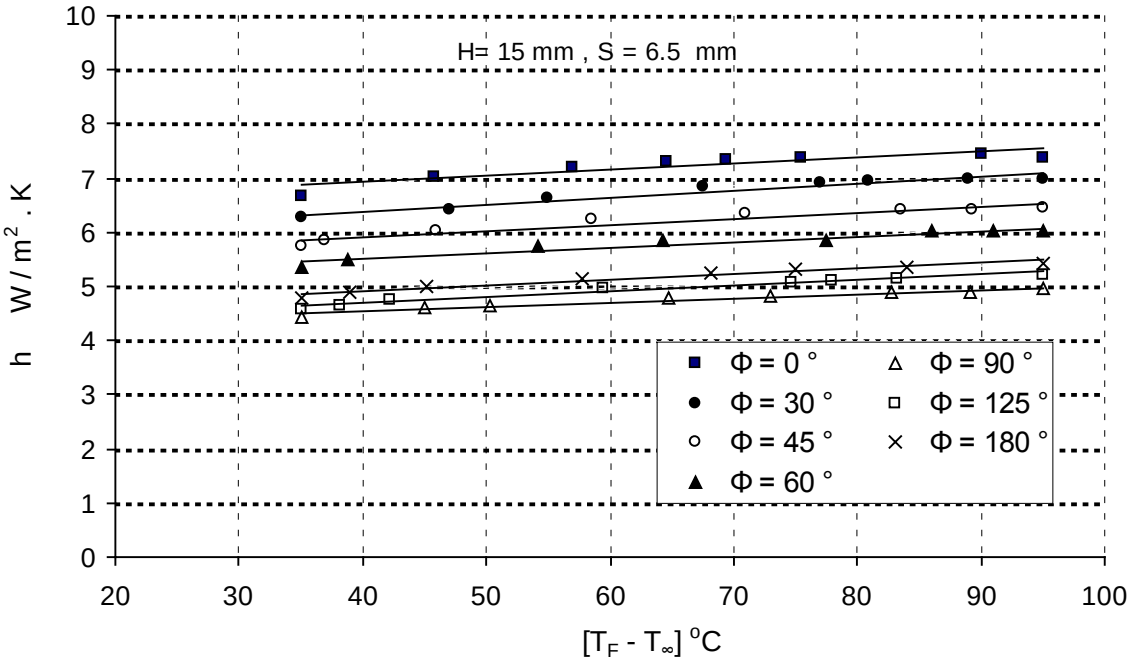

Fig. 7-26. Variation of heat transfer coefficient with temperature difference ΔT at H = 15 mm, S = 6.5 mm.

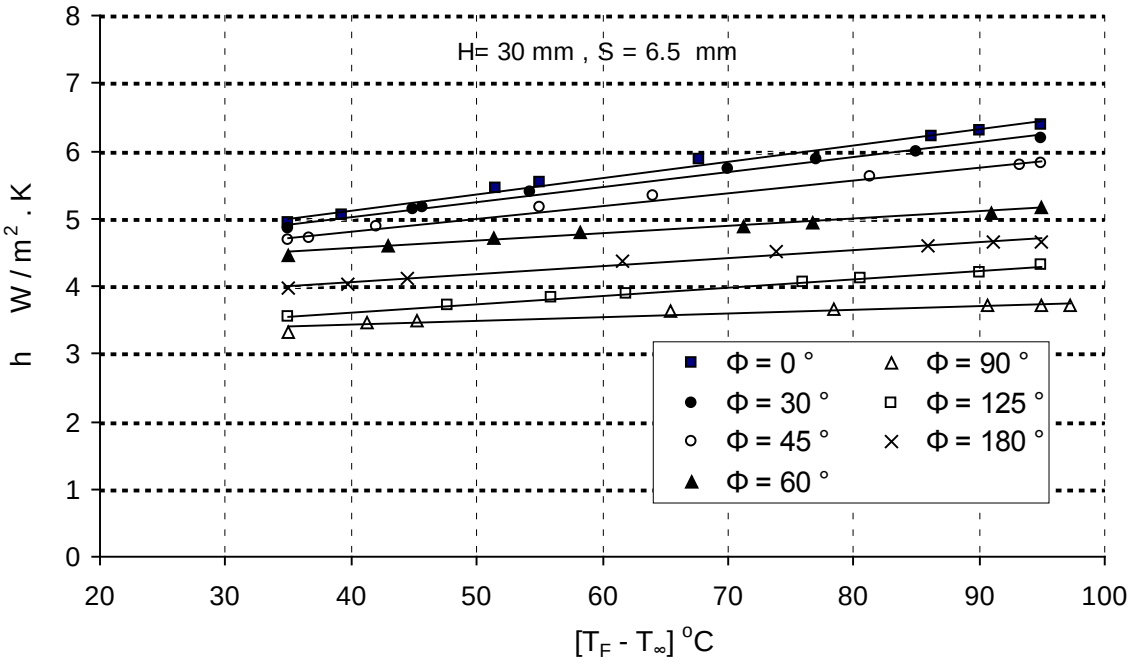

Fig. 7-27. Variation of heat transfer coefficient with temperature difference ΔT at H = 30 mm, S = 6.5 mm.

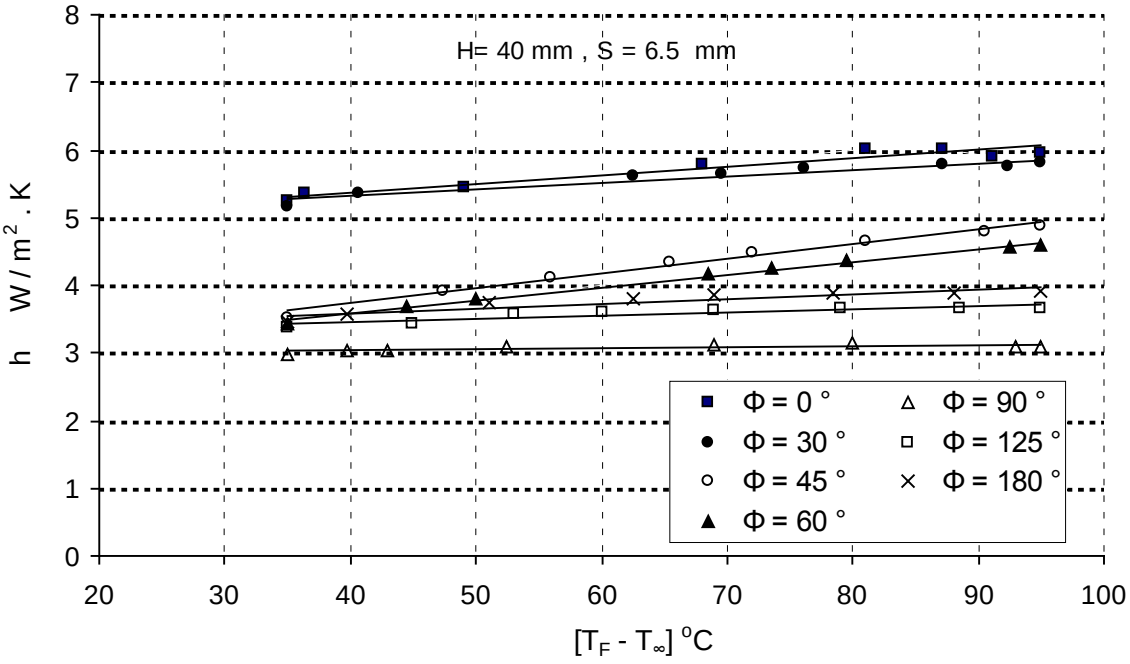

Fig. 7-28. Variation of heat transfer coefficient with temperature difference ΔT at H = 40 mm, S = 6.5 mm.

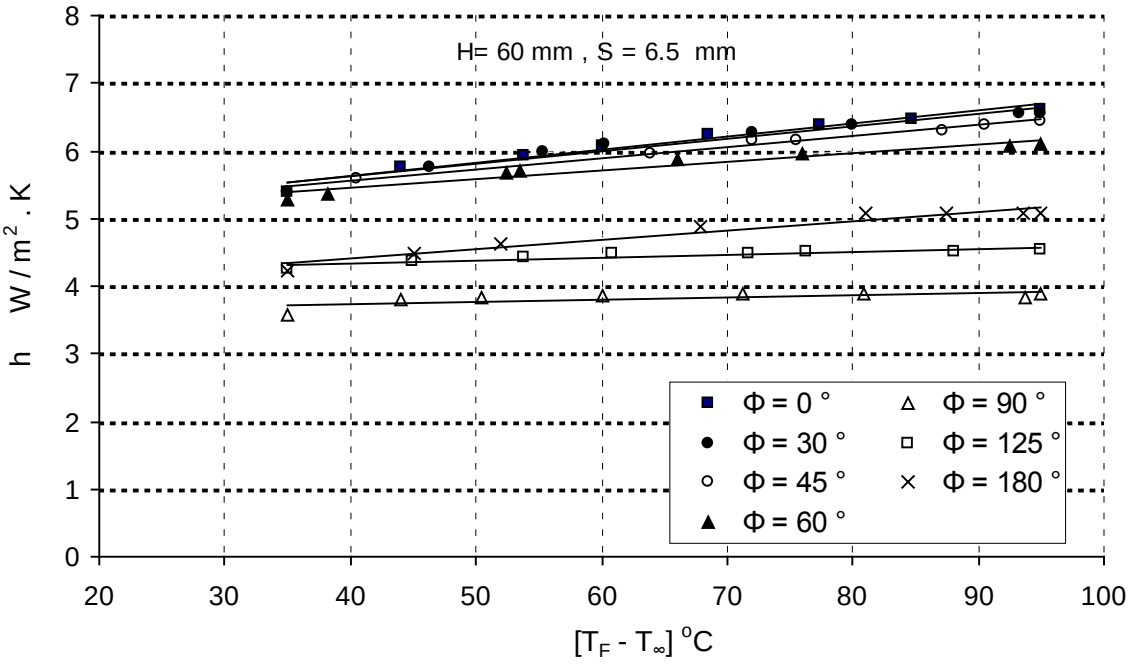

Fig. 7-29. Variation of heat transfer coefficient with temperature difference ΔT at H = 60 mm, S =6.5

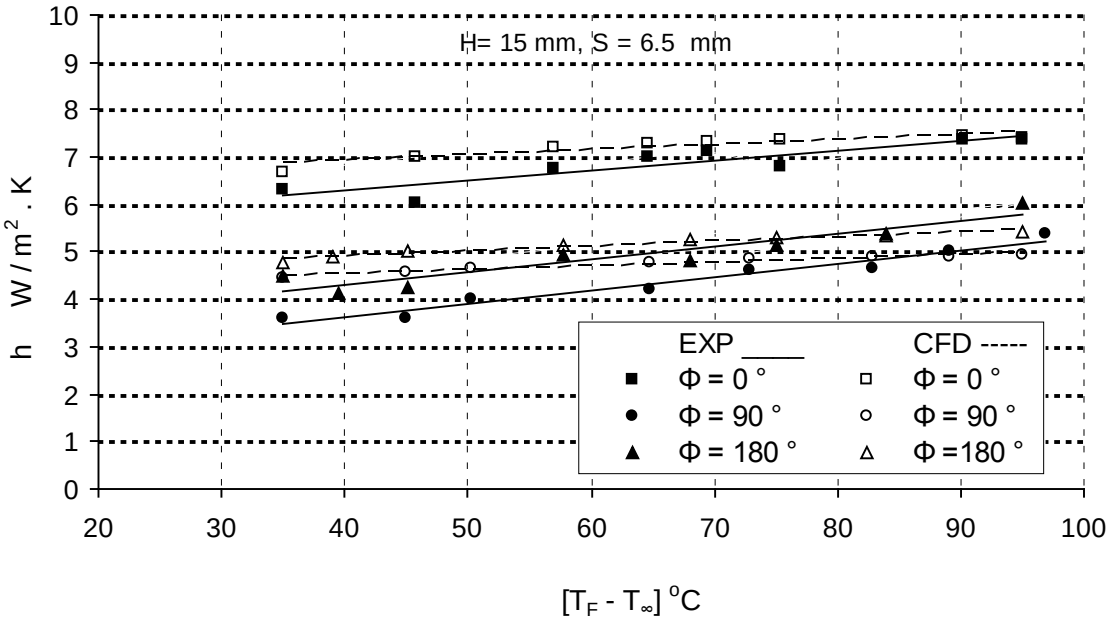

Fig. 7-30. Validation of the computational approach: present study CFD results compared with experimental data.

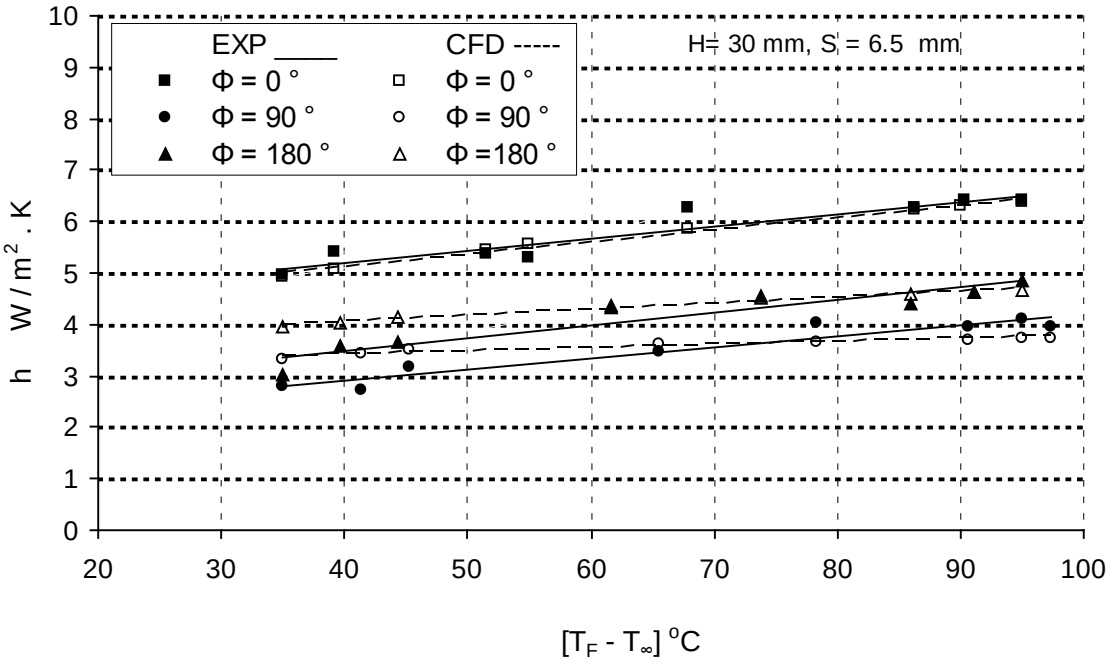

Fig. 7-31. Validation of the computational approach: present study CFD results compared with experimental data.

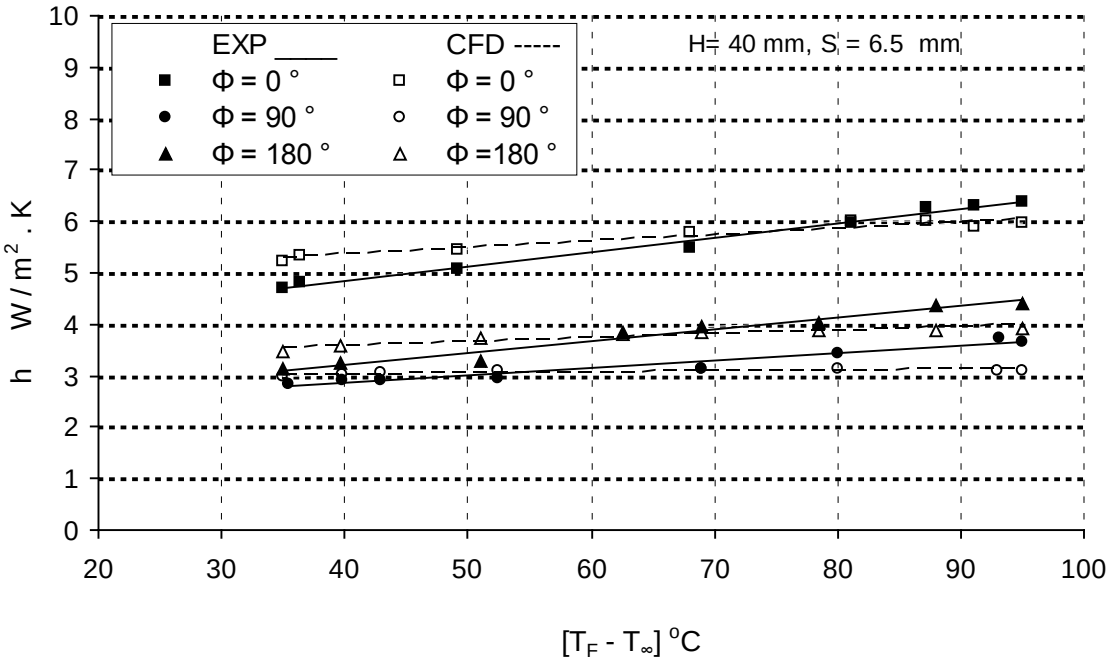

Fig. 7-32. Validation of the computational approach: present study CFD results compared with experimental data.

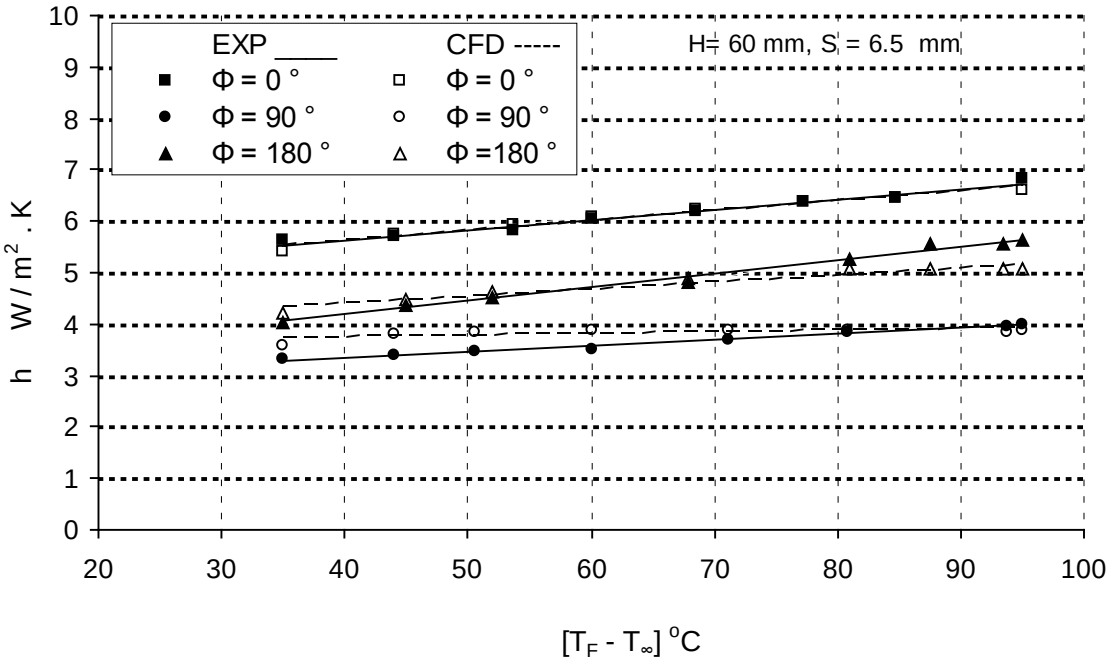

Fig. 7-33. Validation of the computational approach: present study CFD results compared with experimental data.

7-4 Empirical Equations

Four empirical equations are derived to correlate the mean Nusselt number as a function of Rayleigh number, fin spacing ratio, fin height ratio, and orientation angle as follows:

$$Nu_L = 3.36\times10^{-6}\left[Ra_L\left(\frac{S}{H}\right)\right]^{0.7}\left(\frac{S}{L}\right)^{-1.613}\left(\frac{H}{L}\right)^{-0.277}(\cos\phi)^{6.31} \qquad (7\text{-}1)$$

$$0^\circ \le \phi < 90°$$

$$Nu_L = 0.000234\left[Ra_L\left(\frac{S}{H}\right)\right]^{0.6786}\left(\frac{S}{L}\right)^{-0.8357}\left(\frac{H}{L}\right)^{1.8334} \qquad \Phi = 90° \qquad (7\text{-}2)$$

$$\Phi = 125° \qquad (7\text{-}3)\ Nu_L = 0.000422\left[Ra_L\left(\frac{S}{H}\right)\right]^{0.662}\left(\frac{S}{L}\right)^{-0.918}\left(\frac{H}{L}\right)^{2.07}$$

$\Phi = 180°$ (7-4) $$Nu_L = 0.000716\left[Ra_L\left(\frac{S}{H}\right)\right]^{0.64}\left(\frac{S}{L}\right)^{-1.04}\left(\frac{H}{L}\right)^{2.323}$$

These equations are valid for tested finned model with thickness t = 6 mm, fin height H 15 to 60 mm, and fin spacing S 3.375 to 33 mm, Rayleigh number ranged from 3.12×10^{7} to 1.67×10^{8} and at constant fin length L, with relative error = $\pm10.3\%$ for eqn. (7-1), $\pm11.3\%$ for eqn. (7-2), , $\pm11.9\%$ for eqn. (7-3) and $\pm10.7\%$ for eqn. (7-4).

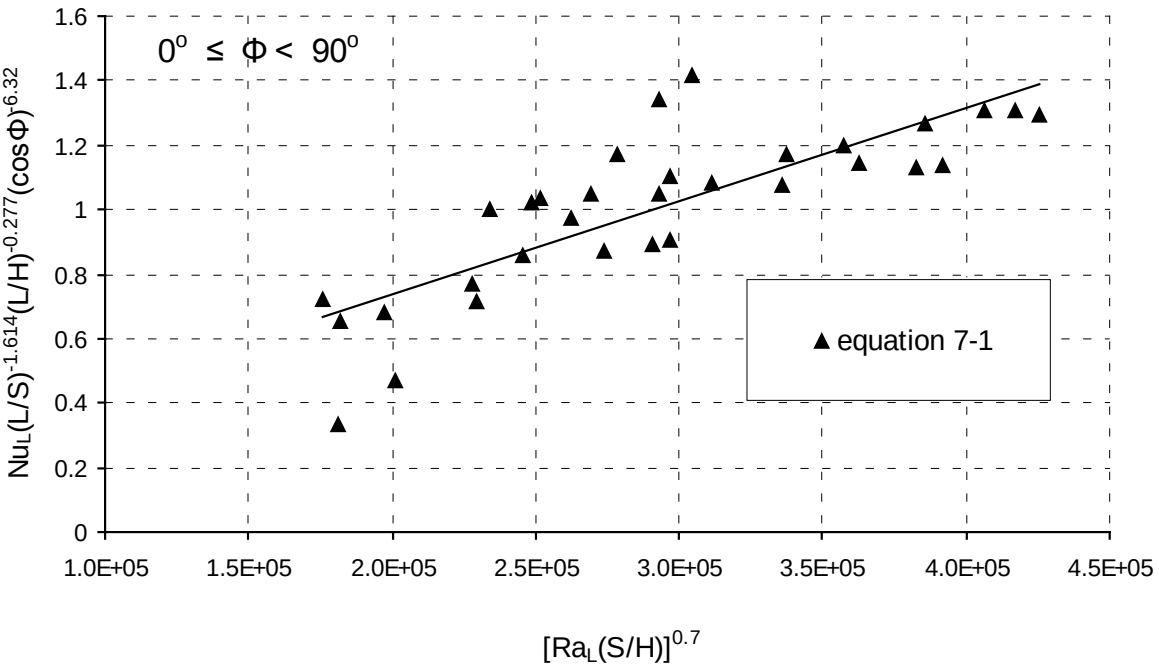

Fig. 7-34. Correlation obtained from the present study.

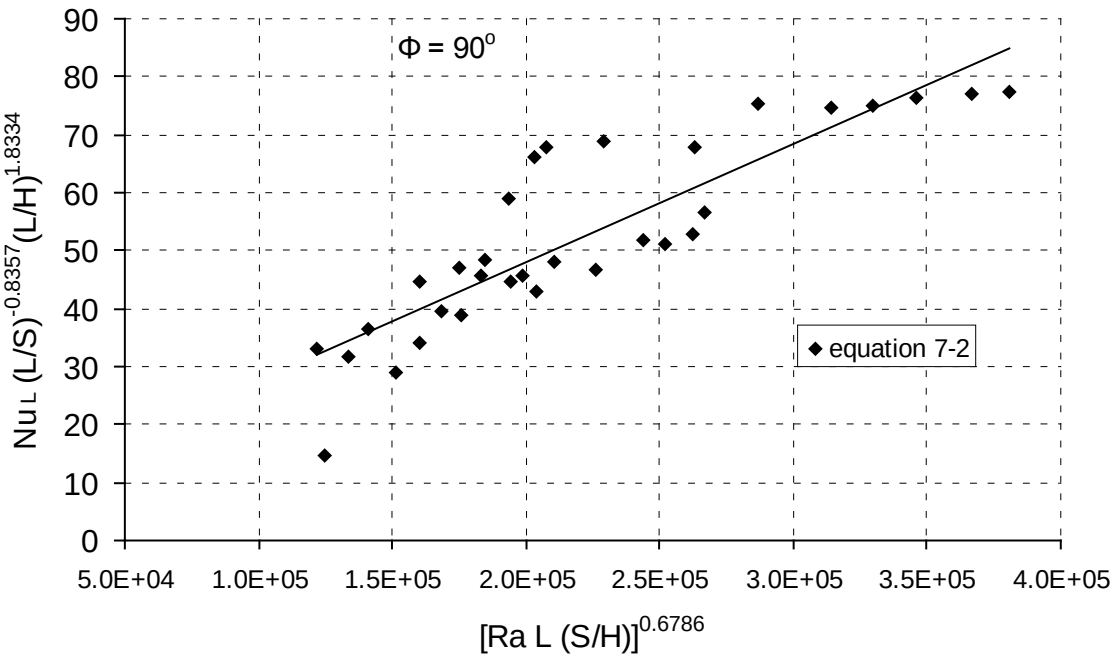

Fig. 7-35. Correlation obtained from the present study.

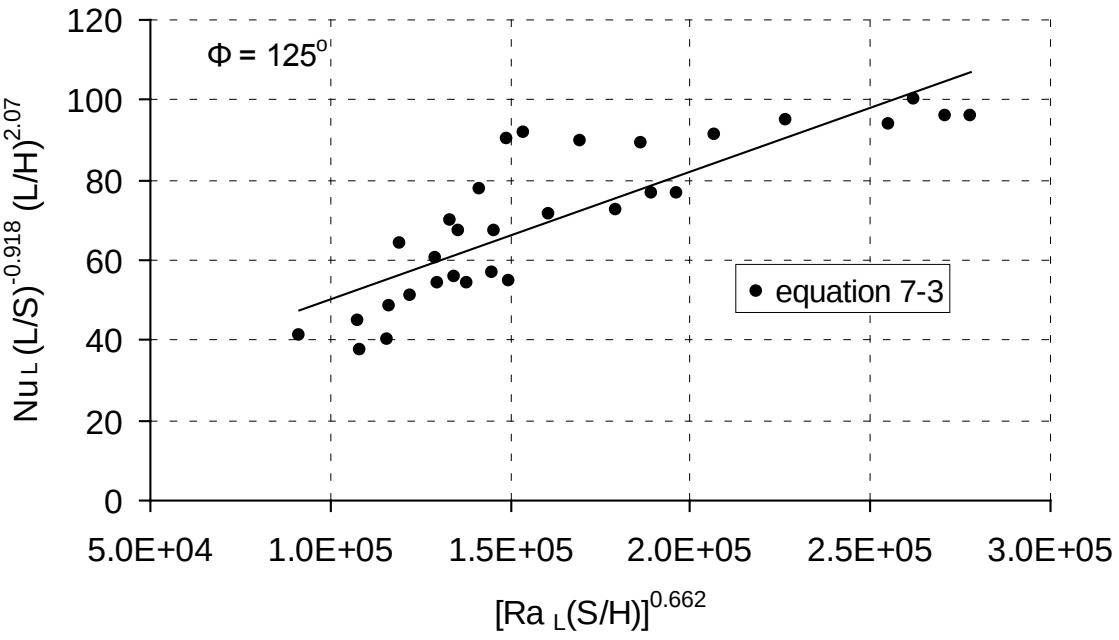

Fig. 7-36. Correlation obtained from the present study.

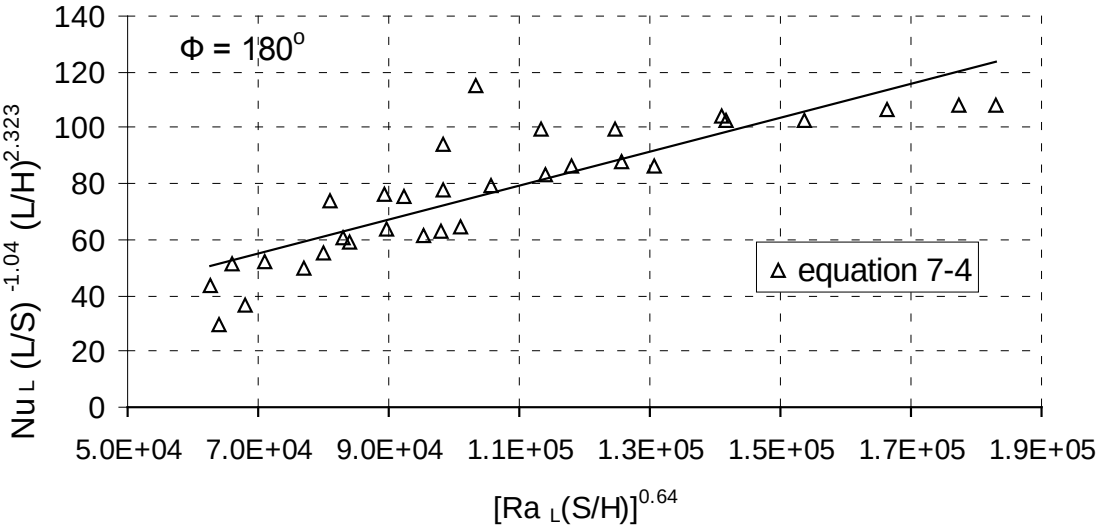

Fig. 7-37. Correlation obtained from the present study.

Figs.[(7-34)-(7-37)] shows the correlation obtained from the present study. In Fig. (7-34) the data are correlated with relative error ±10.3٪, in Fig. (7-35) the data are correlated with relative error ٪11.3، in Fig. (7-36) the data are correlated with relative error ±11.9٪, in Fig. (7-37) the data are correlated with relative error ±10.7٪.

العنوان:	Experimental and Numerical Study of Natural Convection Heat Transfer from Rectangular Fin Arrays
المؤلف الرئيسي:	Mohamad, Hamza Ashur Milad
مؤلفين آخرين:	Abd Allatif, Ahmed Mohamed، El Bakoush, Taib A(Advisor، Co-Advisor)
التاريخ الميلادي:	2007
موقع:	Al Khums
الصفحات:	1 - 155
رقم MD:	766381
نوع المحتوى:	رسائل جامعية
اللغة:	English
الدرجة العلمية:	رسالة ماجستير
الجامعة:	جامعة المرقب
الكلية:	كلية الهندسة
الدولة:	ليبيا
قواعد المعلومات:	Dissertations
مواضيع:	المصفوفة ، الحاسب الآلي، الحمل الحراري
رابط:	https://search.mandumah.com/Record/766381

ABSTRACT

Experimental and numerical investigations have been performed to study the natural convection heat transfer from a rectangular fin arrays at different orientation angles. For such purpose, an experimental test rig was manufactured to be used for these investigations. It is basically consists of base plate, an array of parallel longitudinal fins, heating unit and layers of thermal insulation. A number of factors affecting the convective heat transfer coefficient h, have been considered in the study. These include fin spacing, fin height, model orientation angle, and temperature difference between fin and surroundings on the free convection heat transfer from fin arrays were carried out. During the experiments, the fin spacing (S) was varied from 3.4 to 33 mm, while the fin height (H) from 15 to 60 mm. the orientation angle (Φ) was changed from 0° to 180°, and temperature difference between fin and surrounding (ΔT) from 35 to 95 °C.

A Numerical model commercial CFD package FLUENT, was used to understand the general flow patterns dominating flows from fin arrays. The three-dimensional elliptic governing equations were solved using finite volume based on computational fluid dynamics (CFD) code. A large number of runs were carried out for a systematic theoretical investigation of the effects of fin spacing, fin height, orientation angle and temperature difference between fin and surroundings on the heat transfer processes involved.

A comparative study between the experimental and numerical results was performed to verification the numerical code. It was found that the heat transfer rate per unit base area increases with the increase in the fin spacing and reaches a maximum value then decreases with farther in the fin spacing. The maximum volumetric heat dissipation occurs at optimal spacing $S_{opt} = 6.5$ mm. Moreover, the average heat transfer coefficient was found to have a maximum value at Φ =

0° and reduce with the increase of (Φ) to reaches a minimum value at Φ = 90°. This max value at Φ = 0°, is due to the surrounding fluid that enters the fin region from the open ends and develops a vertical component of velocity as the air heated. The resulting chimney being only a fraction of the width of the fin array and the buoyancy forces exclusively to induce the fluid motion in the upward direction.

Empirical correlations between Nussult number, Rayighly number fin spacing, fin height, orientation angle, temperature difference between the fin and surroundings were derived.

العنوان:	Experimental and Numerical Study of Natural Convection Heat Transfer from Rectangular Fin Arrays
المؤلف الرئيسي:	Mohamad, Hamza Ashur Milad
مؤلفين آخرين:	Abd Allatif, Ahmed Mohamed، El Bakoush, Taib A(Advisor، Co-Advisor)
التاريخ الميلادي:	2007
موقع:	Al Khums
الصفحات:	1 - 155
رقم MD:	766381
نوع المحتوى:	رسائل جامعية
اللغة:	English
الدرجة العلمية:	رسالة ماجستير
الجامعة:	جامعة المرقب
الكلية:	كلية الهندسة
الدولة:	ليبيا
قواعد المعلومات:	Dissertations
مواضيع:	المصفوفة ، الحاسب الآلي، الحمل الحراري
رابط:	https://search.mandumah.com/Record/766381

LIST OF CONTENTS

CHAPTER 3

CHAPTER 4

CHAPTER 5

CHAPTER 8

العنوان:	Experimental and Numerical Study of Natural Convection Heat Transfer from Rectangular Fin Arrays
المؤلف الرئيسي:	Mohamad, Hamza Ashur Milad
مؤلفين آخرين:	Abd Allatif, Ahmed Mohamed، El Bakoush, Taib A(Advisor، Co-Advisor)
التاريخ الميلادي:	2007
موقع:	Al Khums
الصفحات:	1 - 155
رقم MD:	766381
نوع المحتوى:	رسائل جامعية
اللغة:	English
الدرجة العلمية:	رسالة ماجستير
الجامعة:	جامعة المرقب
الكلية:	كلية الهندسة
الدولة:	ليبيا
قواعد المعلومات:	Dissertations
مواضيع:	المصفوفة ، الحاسب الآلي، الحمل الحراري
رابط:	https://search.mandumah.com/Record/766381

AL-MERGEB UNIVERSITY

Faculty of Engineering

Mechanical Engineering Department

Experimental and Numerical Study of Natural Convection Heat Transfer from Rectangular Fin Arrays

M.Sc Thesis in Mechanical Engineering

By
HAMZA ASHUR MILAD MOHAMAD

A thesis submitted in partial fulfillment of requirements for the masters degree of science in Mechanical Engineering

Supervised by
Dr. AHMED ABDEL-LATIF
Dr. TAIB EL-BAKOUSH

2007

ACKNOWLEDGEMENTS

The author is enormously in debt to the gratitude of Dr.Ahmed Abdel-Latif and Dr.Taib El-Bakoush, without whose technical help and knowledge this thesis would have been incomplete. The author is extremely thankful to him for taking all the strain and pain in attending to every detail and accuracy and extending immense hospitality.

The author also wishes to thank Prof.Sobeih Selim, for his tremendous efforts in materializing this work.

The author appreciates the support of his friends and his family especially to his mother for her continuous invocation to Allah for him.

Last but by no means least, the author is especially beholden to his wife and children for their continuous support, help, and sacrifice, which enabled him to finalize this work.

الإهداء

إلى أبى الشيخ عاشور ميلاد الشعافى

ABSTRACT

Experimental and numerical investigations have been performed to study the natural convection heat transfer from a rectangular fin arrays at different orientation angles. For such purpose, an experimental test rig was manufactured to be used for these investigations. It is basically consists of base plate, an array of parallel longitudinal fins, heating unit and layers of thermal insulation. A number of factors affecting the convective heat transfer coefficient h, have been considered in the study. These include fin spacing, fin height, model orientation angle, and temperature difference between fin and surroundings on the free convection heat transfer from fin arrays were carried out. During the experiments, the fin spacing (S) was varied from 3.4 to 33 mm, while the fin height (H) from 15 to 60 mm. the orientation angle (Φ) was changed from 0° to 180°, and temperature difference between fin and surrounding (ΔT) from 35 to 95 °C.

A Numerical model commercial CFD package FLUENT, was used to understand the general flow patterns dominating flows from fin arrays. The three-dimensional elliptic governing equations were solved using finite volume based on computational fluid dynamics (CFD) code. A large number of runs were carried out for a systematic theoretical investigation of the effects of fin spacing, fin height, orientation angle and temperature difference between fin and surroundings on the heat transfer processes involved.

A comparative study between the experimental and numerical results was performed to verification the numerical code. It was found that the heat transfer rate per unit base area increases with the increase in the fin spacing and reaches a maximum value then decreases with farther in the fin spacing. The maximum volumetric heat dissipation occurs at optimal spacing $S_{opt} = 6.5$ mm. Moreover, the average heat transfer coefficient was found to have a maximum value at Φ =

0° and reduce with the increase of (Φ) to reaches a minimum value at Φ = 90°. This max value at Φ = 0°, is due to the surrounding fluid that enters the fin region from the open ends and develops a vertical component of velocity as the air heated. The resulting chimney being only a fraction of the width of the fin array and the buoyancy forces exclusively to induce the fluid motion in the upward direction.

Empirical correlations between Nussult number, Rayighly number fin spacing, fin height, orientation angle, temperature difference between the fin and surroundings were derived.

LIST OF CONTENTS

CHAPTER 3

CHAPTER 4

CHAPTER 5

CHAPTER 8

LIST OF FIGURES

LIST OF TABLES

LIST OF NOTATIONS

A area

g acceleration due to gravity

h Q/A ΔT /, heat transfer coefficient

H fin height

k thermal conductivity

L fin length

Nu_S = hS=k, Nusselt number based on S

Nu_L = hL=k, Nusselt number based on L

P_m motion pressure

Pr Prandtl number

Q heat transfer rate

q'' heat flux

$Ra_S = g \beta (T_F - T_\infty) S^3 / \alpha\nu$, Rayleigh number based on S

$Ra_L = g \beta (T_F - T_\infty) L^3 / \alpha\nu$, Rayleigh number based on L

S fin spacing

T temperature

u v, w velocity components

x, y , z Cartesian coordinates

Greek symbols αβ∇Δδ

α thermal diffusivity

β coefficient of thermal expansion

Δ difference

ν kinematic viscosity

ρ density

Subscripts

∞ ambient

b fin base

F fin

L fin length

S surface

opt optimum value

CHAPTER 1

INTRODUCTION

INTRODUCTION

1.1 Background

The needs for buoyancy driven ventilation appear in a variety of engineering applications, ranging from cooling of electronic components and solar energy applications to cooling of nuclear reactor fuel elements. For an efficient application of natural convection to cooling processes, it is necessary to understand the mechanisms involved. In the free-convection cooling of electronic and thermoelectric devices, as well as in improving the heat transfer in radiators for air conditioning and in other heat exchangers, finned surfaces are extensively used.

Compared to a bare plate, a finned surface increases the heat transfer area. However, with the fins the flow rate reduced. Hence, if not properly designed it is possible that no improvement achieved in terms of overall heat transfer. Therefore, only if the fins properly designed, they are very attractive for these applications, since they offer an economical, trouble-free solution to the problem.

Energy dissipated by electronic equipment transferred to heat sinks by conduction and transferred from the heat sink to the ambient air by natural or forced convection, depending on the power dissipation requirements. Natural convection is the preferred mode of heat transfer since it involves no moving parts, like the electronic components themselves. However, in the natural convection mode the components are likely to run at a higher temperature and thus undermine reliability. A properly selected heat sink may considerably lower the operation temperature of the components and thus reduce the risk of failure.

Extended surfaces, which are popularly known as fins, are extensively used in air-cooled automobile engines and in air-cooled aircraft engines. Fins are also used for the cooling of computer processors, and other electronic devices. Fins are used in the cooling of oil carrying pipe line which runs several hundreds of miles. Heat pipes are also used along with fins to enhance cooling rate.

A great deal of research effort has been developed for developing apparatus and performing experiments to define the conditions under which an augmentive technique will improve heat transfer. The more effective and feasible techniques have graduated from laboratory to full-scale industrial equipment.

The techniques of heat transfer augmentations studies are classified according to Bergles[1] classification as the following:

1- Passive methods operate without increase of the consumption. They lie in the introduction of finned, rough or otherwise developed surfaces on the side of a fluid of a low heat transfer coefficient, as well as turbulizers, rods, and swirls devices of eliminating the boundary layer.

2- Active methods of heat transfer augmentation employ supplementary external power. They employ mechanical devices to mix or to scrape the heat carrier from the surface, as well as vibration and rotation of the surfaces itself, to decrease the thickness of the boundary layer and to increase the rate of wetting, which results in heat transfer augmentation. Sound vibrations, may be introduced in the fluid, from 1 HZ to ultrasonic. An electric field may be introduced in the system, to increase convective motion of the fluid through specific forces in

the dielectric fluid. The heated fluid may be sucked a way through a porous layer.

Among the passive augmentative techniques in use today are:

1- Surface promoters, distributed, isolated, or machined.
2- Displaced promoters, by placed thin rings or discs, coil, or springs, and twisted tapes.
3- Vortex flow, which reffered to as turbulence promoters.
4- Extended surfaces, continuous or interrupted, internal or external, and straight or spiral.

1.2 Objectives

The objective of this thesis is to study the natural convection heat transfer from a rectangular fin arrays. In the first part of the present work, experimental investigations were performed to determine the heat transfer characteristics from a longitudinal fin arrays. Effects of fin spacing, fin height, model orientation angle, and temperature difference between fin and surroundings on the free convection heat transfer from fin arrays were carried out. During the experiments, the fin spacing (S) was varied from 3.4 to 33 mm, fin height (H) from 15 to 60 mm, orientation angle (Φ) from 0° to 180°, and temperature difference between fin and surrounding (ΔT) from 35 to 95 °C.

In the second part of present work, numerical model (Fluent) to predict the fluid motion that occurs in natural convection heat transfer from fin arrays. The three-dimensional elliptic governing equations solved using finite volume based computational fluid dynamics (CFD) code. A large number of runs were carried out for a systematic theoretical investigation of the effects of fin spacing, fin height, orientation angle and temperature

difference between fin and surroundings on the heat transfer processes involved.

In the third part of the present work is to compare the experimental results with the numerical results verification the numerical solution, and to derive empirical correlations between Nussult number, Rayighly number fin spacing, fin height, orientation angle, and temperature difference between the fin and surroundings.

CHAPTER 2

THEORETICAL BACKGROUND

THEORITICAL BACKGROUND

2.1 Introduction

This chapter presents a review of the theoretical analysis and equations of heat transfer especially for convection heat transfer on surfaces.

2.2 Natural Convection Mode

In natural convection, or free convection, the fluid flows “naturally” (by itself), as it is driven by the affect of buoyancy. This effect is distributed throughout the fluid, and is associated with the general tendency of fluids to expand, when heated at constant pressure. The layer that feels the warm vertical wall (see Fig. 2-1) becomes lighter than the rest of the fluid. Its lightness forces it to flow upward, to sweep the wall and to collect heat transfer from the wall in a manner that reminds us of the boundary layer of this time; however, the flow is a vertical. Jet parallel to the wall, whereas the fluid situated far from the wall is stagnant.[33]

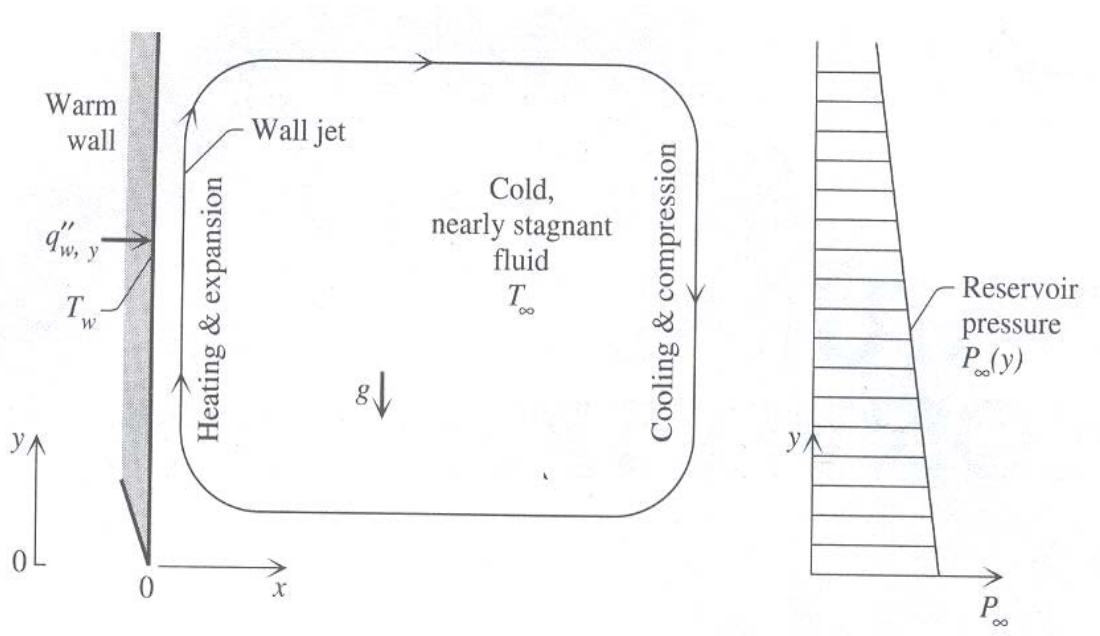

Fig. 2-1. Wall jet driven by buoyancy along a heated wall, and the pressure distribution in the reservoir of stagnant fluid.

العنوان:	Experimental and Numerical Study of Natural Convection Heat Transfer from Rectangular Fin Arrays
المؤلف الرئيسي:	Mohamad, Hamza Ashur Milad
مؤلفين آخرين:	Abd Allatif, Ahmed Mohamed، El Bakoush, Taib A(Advisor، Co-Advisor)
التاريخ الميلادي:	2007
موقع:	Al Khums
الصفحات:	1 - 155
رقم MD:	766381
نوع المحتوى:	رسائل جامعية
اللغة:	English
الدرجة العلمية:	رسالة ماجستير
الجامعة:	جامعة المرقب
الكلية:	كلية الهندسة
الدولة:	ليبيا
قواعد المعلومات:	Dissertations
مواضيع:	المصفوفة ، الحاسب الآلي، الحمل الحراري
رابط:	https://search.mandumah.com/Record/766381

CHAPTER8

CONCLUSIONS

CONCLUSIONS

Experimental and numerical investigations have been performed to study the natural convection heat transfer from a rectangular fin arrays at different orientation angles. An experimental test rig was manufactured to be used for these investigations. Numerical model (Fluent) was used to understand the general flow patterns dominating flows from fin arrays.

The following conclusions can be obtained from the heat transfer results:

1- The heat transfer rate per unit base area increases with the increase in the fin spacing to reaches a maximum value and then decreases with farther in the fin spacing.

2- The maximum volumetric heat dissipation occurs at optimal spacing $S_{opt} = 6.5$ mm.

3- The average heat transfer coefficient has a maximum value at $\Phi = 0°$ and reduce with the increase of (Φ) to reaches a minimum value at $\Phi = 90°$. This due to at $\Phi = 0°$, the surrounding fluid enters the fin region from the open ends and develops a vertical component of velocity as the air heated. The resulting chimney being only a fraction of the width of the fin array and the buoyancy forces exclusively to induce the fluid motion in the upward direction.

4- The heat transfer coefficient increases with increasing the temperature difference (ΔT) between the fin and surroundings for all values of orientation angle (Φ) and fin height (H). The reason is that, with the increase in the temperature difference between the fluid adjacent to the hot fin surface and the fluid a way from it,causes the buoyancy

force to increase with a stronger natural convection currents, and thus the heat transfer coefficient increases.

5- The heat transfers per unite base area increases with increase in fin height (H) for all values of orientation angle (Φ) and fin spacing (S).

6- A comparison between experimental data and numerical results indicates satisfactory agreement.

7- Empirical correlation were derived to correlate the Nusselt number as a function of Rayleigh number, fin spacing ratio, fin height ratio, and orientation angle. The general empirical formula obtained from the present study is given in the form:

$$Nu_L = 3.5\times10^{-6}\left[Ra\frac{S}{H}\right]^{0.699}\left(\frac{S}{L}\right)^{-1.613}\left(\frac{H}{L}\right)^{-0.272}(COS\phi)^{6.31}$$

$$\text{at } 0^{\circ} \le \phi < 90°$$

$$Nu_L = 0.000234\left[Ra\frac{S}{H}\right]^{0.6786}\left(\frac{S}{L}\right)^{-0.8357}\left(\frac{H}{L}\right)^{-1.8334} \quad \text{at} \quad \Phi = 90°$$

$$Nu_L = 0.000422\left[Ra\frac{S}{H}\right]^{0.662}\left(\frac{S}{L}\right)^{-0.918}\left(\frac{H}{L}\right)^{-2.07} \quad \text{at} \quad \Phi = 125°$$

$$Nu_L = 0.000422\left[Ra\frac{S}{H}\right]^{0.64}\left(\frac{S}{L}\right)^{-0.1.04}\left(\frac{H}{L}\right)^{2.323} \quad \text{at} \quad \Phi = 180°$$

العنوان:	Experimental and Numerical Study of Natural Convection Heat Transfer from Rectangular Fin Arrays
المؤلف الرئيسي:	Mohamad, Hamza Ashur Milad
مؤلفين آخرين:	Abd Allatif, Ahmed Mohamed، El Bakoush, Taib A(Advisor، Co-Advisor)
التاريخ الميلادي:	2007
موقع:	Al Khums
الصفحات:	1 - 155
رقم MD:	766381
نوع المحتوى:	رسائل جامعية
اللغة:	English
الدرجة العلمية:	رسالة ماجستير
الجامعة:	جامعة المرقب
الكلية:	كلية الهندسة
الدولة:	ليبيا
قواعد المعلومات:	Dissertations
مواضيع:	المصفوفة ، الحاسب الآلي، الحمل الحراري
رابط:	https://search.mandumah.com/Record/766381

REFERENCES

References

1. A. E. Bergles, In Hand book of transfer, Section 10W. M. Rohasenow and J. P. Hartnett. Eds., Mc Graw- Hill, New York, (1972).
2. B. Rich, (1953), "An investigation of heat transfer from an inclined flat plate in free convection", Trans. ASME, No. 75. pp. 489.
3. McAdams, (1954), "Heat transmission", 3rd ed., Mc-Graw-Hill, New York, Chap. 7.
4. Churchill, chu, (1975), "Correlating equation for laminar and turbulent free convection from a vertical plate", International Journal Heat and Mass Transfer, No, 18, pp. 1323-1975.
5. A. Bar-Cohn, W.M. Rohsenow, (1984), "Thermally optimum spacing of vertical natural convection cooled parallel plates", Journal of Heat Transfer, No. 106, pp. 116.
6. C.J.M. Lasane, (1986), “Numerical simulation of natural convection heat transfer in a television Set”, Centre for Manufacturing Technology, Philips, the Netherlands.
7. C.W. Leung, S.D. Probert, (1997), "Heat–Exchanger performance: influence of gap width between consecutive vertical rectangular fin arrays", International Journal Applied Energy, vol. 56, No. 1, pp. 1-8.
8. A.D. Vollaro, S. Grignaffini, F. Gugliermo, (1999), "Optimum design of vertical rectangular fin arrays", International Journal Thermal Science, No. 38, pp. 525-529.

9. S. Baskaya, M. Sivrioglu, M. Ozek, (2000), “Parametric study of natural convection heat transfer from horizontal rectangular fin arrays”, International Journal Thermal Science, No. 39, pp. 797-805.
10. S. Narasimham, J. Majdalani, (2001), “Characterization of compact heat sink models in natural convection”, International Electronic Packaging Technical Conference and Exhibition, ASME, July 8-13, Kauai, Hawaii, USA.
11. A. Giri, G.S.V.L. Narasimham, M.V.K. Murthy, (2002), “Combined natural convection of heat and mass transfer from vertical fin arrays”, International Journal of Heat and Fluid Flow, No. 24, pp. 100-113.
12. A. Dayan, R. Kushnir, G. Mittelman, A. Ullman, (2004), “Laminar free convection underneath a downward facing hot fin array”, International Journal Heat and Mass Transfer, No. 47, pp. 2849-2860.
13. D. Rakshit, C. Balaji, (2004), “Evaluation of candidate approaches in the study of conjugate convection from a fin array”, International Communications in Heat and Mass Transfer, No. 32, pp. 529-538.
14. F. Bobaru, S. Rachakonda, (2004), “Boundary Layer in shape optimization of convective fins using a mesh free approach", International Journal for Numerical Methods in Engineering, No. 60, pp. 1215-1236.
15. S.P Liaw, R.H Yeh, W.T. Yeh, (2005), "A simple design of fins for boiling heat transfer", International Journal of Heat and Mass Transfer, No. 48, pp. 2493-2502.
16. D.W. Mueller, H.I. Abu-Mulaweh, (2005), "Prediction of the temperature in a fin cooled by natural convection and

radiation", Applied Thermal Engineering, No. 3, pp.445-460.

17. C.J. Kobus, T. Oshio, (2005), "Predicting the thermal performance characteristics of staggered vertical pin fin array heat sinks under combined mode radiation and mixed convection with impinging flow", International Journal of Heat and Mass Transfer, No. 48, pp. 2684-2696.
18. V. D. Rao, S.V. Naidu, B. G. Rao, (2006), "Heat transfer from a horizontal fin array by natural convection and radiation –A conjugate", International Journal of Heat and Mass Transfer, No. 49, pp. 3379-3391.
19. Z. Zhao, C.T. Avedisan, (1997), "Enhancing forced air convection heat transfer from an array of parallel plate fins using a heat pipe", International Heat Mass Transfer, Vol. 40, No. 13, pp. 3135-3147.
20. R.H. Yeh, (1997), "An analytical study of the optimum dimensions of rectangular fins and cylindrical pin fins", International Heat Mass Transfer, Vol. 40, No. 15, pp. 3607-3615.
21. L.Tsai-Yu, C.K. Chen, (1998), "Application of Taylor transformation to optimize rectangular fins variable thermal parameters", Applied Mathematical Modeling, No. 22, pp. 11-21.
22. A. Hachemi, (1998), "Experimental study of thermal performance of offset rectangular plate fin absorber-plates", Renewable Energy, No. 17, pp. 371-384.
23. Z.X. Yua, W.Q. Tao, Q.W. Wang, (1998), "Numerical predication for laminar forced convection heat transfer in

parallel-plate channels with streamwise-periodic rod disturbances", International Journal for Numerical Methods in Fluids, No. 28, pp. 1371-1387.

24. C.V.M. Braga, F.E.M. Saboya, (1999), "Turbulent heat transfer pressure drop and fin efficiency in annular regions with continuous longitudinal rectangular fins", Experimental Thermal and Fluid Science, No. 20, pp. 55-65.
25. S. Dong, S. Liu, H. Su, (2001), "An experimental investigation of heat transfer in pin fin array", Heat Transfer –Asian Research, Vol. 7, No. 30, pp. 533-541.
26. O.N. Sara, T. Pekdemir, S. Yapici, M. Yilmaz, "Enhancement of heat transfer from a flat surface in a channel flow by attachment of rectangular blocks", (2001), International Journal of Energy Research, No. 25, pp. 563-576.
27. E.Velayati, M. Yaghoubi, (2002), "Numerical study of convection heat transfer from an array of parallel", International Journal of Heat and Fluid Flow, No. 26, pp. 80-91.
28. K. Bilen, U. Akyol, S. Yapici, (2002), "Thermal performance of a tube finned surface", International Journal of Energy Research, No. 26, pp. 321-333.
29. A. Al-Sarkhi, (2005), "Comparison between variable and constant height shrouded fin array subjected to forced convection heat transfer", International Communication in Heat and Mass Transfer, No. 32, pp. 548-556.

30. U. Akyol, K. Bilen, (2005), "Heat transfer and thermal performance analysis of a surface with hollow rectangular fins", Applied Thermal Engineering, No. xxx, pp. xxx.
31. N. Sahiti, A. Lemouedda, D. Stojkovic, F. Durst, E. Franz, (2005), "Performance comparison of pin fin in-duct flow arrays with various pin cross-section", Applied Thermal Engineering, No. xxx, pp. xxx.
32. S.V. Patankar, (1980), "Numerical heat transfer and fluid flow", Second Edition, Taylor and Francis, USA.
33. J.A. Jones, (1993), "Heat Transfer", John Wiley and Sons, USA, Chap. 7.
34. F.P. Incropera, D.P. Dewitt, (1996), "Fundamentals of heat and mass transfer", Fourth Edition, John Wiley and Sons, USA, Chap. 9.
35. Y.A. Cengel, (2003), "Heat Transfer", Second Edition, McGRAW-Hill, USA, Chap. 9.
36. Y. Jaluria, K.E. Torrance, (2003), "Computational heat transfer", Second Edition, Taylor and Francis, USA, Chap. 3.
37. J. P. Holman, (1994), "Experimental methods for engineers", Sixth Edition, McGRAW-Hill, USA, Chap. 3. McGRAW-Hill, USA

العنوان:	Experimental and Numerical Study of Natural Convection Heat Transfer from Rectangular Fin Arrays
المؤلف الرئيسي:	Mohamad, Hamza Ashur Milad
مؤلفين آخرين:	Abd Allatif, Ahmed Mohamed، El Bakoush, Taib A(Advisor، Co-Advisor)
التاريخ الميلادي:	2007
موقع:	Al Khums
الصفحات:	1 - 155
رقم MD:	766381
نوع المحتوى:	رسائل جامعية
اللغة:	English
الدرجة العلمية:	رسالة ماجستير
الجامعة:	جامعة المرقب
الكلية:	كلية الهندسة
الدولة:	ليبيا
قواعد المعلومات:	Dissertations
مواضيع:	المصفوفة ، الحاسب الآلي، الحمل الحراري
رابط:	https://search.mandumah.com/Record/766381

APPENDIX

Calibration Table 4-1

$T_{ture} = 1.0441\ T_{measured} + 0.7561$

Heating		Cooling	
$T_{measured}$ °C	T_{ture} °C	$T_{measured}$ °C	T_{ture} °C
39	41.5	35	37.2
43	45.5	37	39.3
49	51.5	45	47
50	52.5	52	55
53	55.5	55	58.2
56	59	60	63.4
65	69	63	66.6
78	82.5	70	73.9
82.5	89	80	84.4
90.5	95	82	86.5
30	32	26	27.5
25	27	22	23.6
20	22	94	99.1
100	104	99	104.4

EXPERMENTAL DATA :

Table 7-1 **H= 60mm and S=3.375mm**

angle =0		angle =30		angle =45		angle =60	
TF-Ta	h	TF-Ta	h	TF-Ta	h	TF-Ta	h
35	1.6969	35	1.59	35	1.5247	35	1.4426
42	1.72005	38.2	1.691168	36	1.528977	46	1.57048
49.1	2.094015	44.5	1.8812	44.8	1.655223	54.1	1.618122
55.7125	2.15433	53.2	1.933058	52.7	1.624707	67.3	1.783404
62	2.182291	56.5	1.95568	57.3	1.794573	73.4	1.765429
69	2.570486	73.5	2.101732	67.1	1.874247	81	1.8991
77.1	2.474728	81.8	2.309283	79.5	1.966754	88.3	1.965507
95	2.977	95	2.445	95	2.1344	95	2.0567

angle =90		angle =135		angle =180	
TF-Ta	h	TF-Ta	h	TF-Ta	h
35	1.1702	35	1.2367	35	1.2871
44.8	1.229183	36.8	1.287706	40.3	1.318274
51.3	1.371651	54.3625	1.36451	45.8	1.452105
65.3	1.428374	62.5	1.554036	55.2	1.551066
71	1.502197	74.6	1.635166	63.7	1.614321
82.7	1.613662	79	1.713501	78	1.775
95	1.631	85	1.753	95	1.889
85	1.7216	95	1.8538	83.2	2.0129

Table 7-2 **H= 60mm and S=6.5mm**

angle =0		angle =30		angle =45		angle =60	
TF-Ta	h	TF-Ta	h	TF-Ta	h	TF-Ta	h
35	5.6173	35	5.1343	35	4.8647	35	4.3585
44	5.725129	46.25	5.631606	40.5	5.1002	38.25	4.726725
53.75	5.8035	60.2	5.733017	63.925	5.738933	52.375	4.811083
60.125	6.05358	72	6.08577	71.95	5.936778	53.5	4.910161
84.75	6.456906	93.325	6.692711	75.5	5.693862	66.025	5.141055
95	6.8232	95	6.6943	87.125	6.25531	76	5.620753
68.5	6.20805	80	6.3249	90.5	6.0123	92.5	5.86211
77.3	6.38317	55.3	5.70493	95	6.4007	95	6.0385

angle =90		angle =135		angle =180	
TF-Ta	h	TF-Ta	h	TF-Ta	h
35	3.3368	35	3.5449	35	4.0427
60	3.505962	44.875	4.089349	45.025	4.382785
80.875	3.855182	53.75	4.306528	67.875	4.821459
93.75	3.968558	60.875	4.454982	87.5	5.543525
95	3.9788	71.75	4.543181	93.5	5.572292
44	3.3977	76.3	4.668109	95	5.6387
71.2	3.70956	88.075	5.0082024	52	4.5088
50.5	3.47565	95	5.0069	81	5.2773

Table 7-3

H= 60mm and S=13mm

angle =0		angle =30		angle =45		angle =60	
TF-Ta	h	TF-Ta	h	TF-Ta	h	TF-Ta	h
35	6.8136	35	6.6162	35	6.0252	35	5.4136
40.5	7.0154	40	6.6721	46.5	6.565247	40.4	5.872391
48.625	7.53977	45.6	6.959649	57.2	6.764063	52.5	5.813129
63.525	7.852605	60.75	7.764626	65.4	7.161522	62.5	6.186837
71.025	8.554187	71.475	8.024595	74.4	7.068322	65.6125	6.205119
83.125	8.98175	80.725	8.366871	82	7.324484	80.5	6.719386
90.7	9.21528	89.95	8.5338	90.9	7.766521	88.5	7.359231
95	9.4476	95	8.7882	95	7.9212	95	7.3156

angle =90		angle =135		angle =180	
TF-Ta	h	TF-Ta	h	TF-Ta	h
35	3.2925	35	4.3803	35	4.7812
40	3.4	43.6	4.662136	40	5
44.5	3.577328	49.25	4.81685	45.4	5.083439
48.625	3.829702	58.125	5.132392	57.5	5.488447
60.25	3.935435	74.5	5.735374	67.425	5.677823
66.075	3.89344	83.5	6.05311	71.5	5.741399
80.3	4.514087	91.375	6.27415	82.625	6.443992
95	4.9065	95	6.4863	95	6.7512

Table 7-4

H= 60mm and S=21.7mm

angle =0		angle =30		angle =45		angle =60	
TF-Ta	h	TF-Ta	h	TF-Ta	h	TF-Ta	h
35	6.636	35	6.2066	35	5.456746	35	5.6392
46.9	7.166471	36.5	6.008897	43.3	5.686895	38	5.7154
60.3	7.658893	41	6.115877	47	6.312652	50.7	6.09244
67.5	7.907235	50.3	7.037943	55	6.77787	60	6.2742
79.5	8.464297	63.8	7.448651	66	6.814362	72.7	6.59895
93.9	8.887052	80.3	7.763089	79	7.148229	85	6.911744
95	9.008	93.4	7.635805	88	7.233856	92	7.087
90	8.8022	95	8.0485	95	7.6944	95	7.1632

angle =90		angle =135		angle =180	
TF-Ta	h	TF-Ta	h	TF-Ta	h
35	3.6847	35	4.8817	35	5.4677
57.4	3.663242	41	5.348922	36.2	5.438395
73.9	4.485851	47.2	5.313323	42.2	5.729196
87.9	4.435394	53.3	5.042151	58.1	5.783353
95	4.7527	73.2	5.44872	69.8	6.357319
40	3.6431	80.5	5.958372	84	6.458215
55.5	3.9372	95	6.1707	91.8	6.594145
65	4.1164	63.5	5.50485	95	6.756724

Table 7- 5 **H= 60mm and S=33mm**

angle =0		angle =30		angle =45		angle =60	
TF-Ta	h	TF-Ta	h	TF-Ta	h	TF-Ta	h
35	8.4453	35	7.837	44.6	7.53786	39.2	7.002325
44.5	8.82015	40.5	8.162936	54.075	7.977078	49.9	7.308365
51.7	9.002068	47.75	7.978169	63	8.361481	63.7	7.471975
59.8	9.092908	57.125	8.632375	78.5	8.641426	72.9	7.52847
68.5	9.596577	71.8	9.210554	87.5	8.710838	87.9	8.415288
83.875	10.09376	86.5	9.526852	35	7.4267	35	6.8308
87.525	10.12068	89.5	9.584077	95	9.0407	95	8.3728
95	10.4673	95	9.829	71.5	8.40785	82	8.0394

angle =90		angle =135		angle =180	
TF-Ta	h	TF-Ta	h	TF-Ta	h
45	5.341758	35	6.151	35	6.3246
63.8	5.964023	41.5	6.201052	41.8	6.432568
88.9	6.354802	50.8	6.390287	53.9125	6.755723
78.3	6.216417	61.7	6.715697	54	6.744776
53.3	5.979456	80.9	6.711577	64.2	6.804558
35	5.3703	85.5	7.206173	77.2	7.109345
95	6.5343	93	6.984363	90.1	7.277467
70.2	6.05378	95	7.123	95	7.4756

Table 7- 6 **H= 40mm and** **S=3.375mm**

angle =0		angle =30		angle =45		angle =60	
TF-Ta	h	TF-Ta	h	TF-Ta	h	TF-Ta	h
35	1.817	35	1.464	39	1.546522	35	1.1845
37.5	1.905133	41.3	1.79572	35	1.3553	40	1.1925
57.9	2.380821	56.8	1.889828	60	1.881597	53	1.44
64.5	2.737888	64.1	2.149519	61.3	2.022277	62.4	1.587851
70.4	2.744	69.5	2.420452	71.8	2.459263	73.6	1.910303
75.8	2.986664	79.5	2.847016	76.1	2.502194	77.6	2.061474
90	3.3567	90	3.099154	78	2.689604	90.4	2.412413
95	3.4991	95	3.175	95	3.05	95	2.4727

angle =90		angle =135		angle =180	
TF-Ta	h	TF-Ta	h	TF-Ta	h
35	0.5976	95	2.388266	35	0.8683
63.1	1.306348	92.3	2.092778	40	0.9933
69.4	1.466897	86.5	1.84918	51.5	1.27917
78.6	1.75292	61.3	1.480907	61.1	1.531124
88.7	1.927721	41	0.931661	73.7	1.75751
95	2.140103	35	0.826	79.00625	2.024782
53.5	1.075207	70	1.638	84.9	2.210187
44.9	0.849698	50	1.1702	95	2.3164

Table 7- 7 **H= 40mm and** **S=6.5mm**

angle =0		angle =30		angle =45		angle =60	
TF-Ta	h	TF-Ta	h	TF-Ta	h	TF-Ta	h
35	4.7087	35	4.2979	35	3.5245	35	3.177545
36.4	4.815814	40.7	4.401904	47.4	3.942221	44.5	3.397781
49.1	5.080489	62.5	4.734486	55.9	3.75552	68.5	4.089693
68	5.503039	69.5	5.386383	65.5	4.697221	73.5	4.130063
81.1	5.961517	76.1	5.481694	73	4.46	79.5	4.457242
87.2	6.262492	87.2	5.634676	81	4.665234	92.5	4.590075
91.1	6.293805	92.4	5.483372	90.5	4.692045	95	4.710878
95	6.3887	95	5.7619	95	4.9825	50	3.57

angle =90		angle =135		angle =180	
TF-Ta	h	TF-Ta	h	TF-Ta	h
35.5	2.841058	35	2.9702	35	3.1222
39.8	2.924825	45	3.10828	39.7	3.228504
52.5	2.957691	53	3.447673	51	3.278391
69	3.152713	69	3.377852	62.5	3.861141
93.2	3.716079	79.1	3.835077	69	3.950206
95	3.6517	88.5	4.002801	78.5	4.016398
80	3.4354	95	4.0982	88	4.382951
43	2.9026	60	3.4304	95	4.3882

Table 7-8

H= 40mm and S=13mm

angle =0		angle =30		angle =45		angle =60	
TF-Ta	h	TF-Ta	h	TF-Ta	h	TF-Ta	h
35	7.4624	35	6.6414	35	5.8542	35	5.6281
42.5	7.403334	45	6.991549	37.9	5.77448	38.6	5.548461
51.3	8.558081	52.5	7.078853	52.3125	6.65194	51	6.072029
64.6	8.194424	58.9	7.366906	63.3	6.926723	60.5	6.379339
74.6	7.922927	68.3	7.398641	69	7.047413	83	7.15246
77.5	8.491051	80.9	7.917375	74.7	7.018317	92	6.943018
85.2	8.563219	91.2	7.893592	81.3	7.506889	95.9	6.957138
95	8.6924	95	8.1594	95.5	7.738468	71.1	6.53491

angle =90		angle =135		angle =180	
TF-Ta	h	TF-Ta	h	TF-Ta	h
35	3.6089	35	4.4839	35	4.8394
40.9	3.833836	40.2	4.254178	45	4.971655
58.95	3.950694	42.2	4.957132	59.5	5.360562
68.5	3.882772	61.5	5.188641	75.5	5.934738
87.1	4.313666	78.9	5.309679	88.5	6.086978
95.5	4.937011	90	5.663767	95	6.103
95	4.5139	95	5.7885	70	5.6315
81	4.3533	50	4.811	51	5.212

Table 7-9

H= 40mm and S=21.7mm

angle =0		angle =30		angle =45		angle =60	
TF-Ta	h	TF-Ta	h	TF-Ta	h	TF-Ta	h
34.3	7.74166	40.5	7.628449	35	6.8535	35	5.8393
35.9	7.9171	43.2	7.869309	39.7	7.001265	38.2	5.974245
50.2	8.009532	52.8	7.731861	46.6	7.162547	50.2	6.647856
54	8.710202	63.5	8.67672	54.7	7.804023	64	7.347597
65.6	8.68542	73.2	9.052768	59.6	8.204158	73.3	7.517739
70.7	9.461913	84	8.776107	75.4	8.870237	79.4	7.877069
87	9.257802	95	9.6222	90.7	8.743013	88.6	8.180676
95	9.9483	35	7.426	95	9.2548	95	8.4564

angle =90		angle =135		angle =180	
TF-Ta	h	TF-Ta	h	TF-Ta	h
39.6	3.727419	35	3.7161	36.9	5.178086
58	3.829754	46	4.018252	39.8	6.204729
62.6	4.341386	52.2	4.610924	58.7	4.840369
75.5	4.339356	56.5	4.919009	63.1	6.174728
87.7	4.938622	78.1	5.147381	77.2	6.332423
95	5.399136	86.3	5.664997	82.5	6.753031
35	2.881199	92.2	5.908242	92	7.067494
50	3.6989	95	6.0995	94.5	7.143196

Table 7- 10

H= 40mm and S=33mm

angle =0		angle =30		angle =45		angle =60	
TF-Ta	h	TF-Ta	h	TF-Ta	h	TF-Ta	h
35	8.5813	35	7.225	35	7.2232	36	6.713147
42.9	8.649446	38	7.760118	37	7.145784	65	8.742093
55.5	8.867901	55	8.950247	58.5	8.544131	71	8.210336
57.5	9.191786	58.46875	9.1993	71.5	9.324241	93	9.7
67.5	9.42989	70	9.2864	76.3	9.127739	35	6.7444
76.2	10.44845	85	9.895359	88.5	9.848954	95	9.8135
82.3	10.68768	92.7	10.3816	94.5	10.02552	50	7.5114
94.8	11.60524	95	10.189	95	10.189	82	9.1465

angle =90		angle =135		angle =180	
TF-Ta	h	TF-Ta	h	TF-Ta	h
39	5.613043	49	5.8513	43.3	6.813099
50.3	6.004226	52	6.103712	64.2	7.66421
72.1	7.029444	89	7.999077	72.5	8.89125
84.5	6.798816	35	5.9579	77.5	7.223708
87.9	7.40426	95	7.8599	93.5	8.513647
92.8	8.079573	65	6.7946	95	8.76
35	5.4236	72.1	7.07383	35	6.5825
62.2	6.47594	81.2	7.43146	80	8.1633

Table 7-11

H= 30mm and S=3.375mm

angle =0		angle =30		angle =45		angle =60	
TF-Ta	h	TF-Ta	h	TF-Ta	h	TF-Ta	h
35	1.9331	35	1.6469	35	1.3317	35	1.289
44.5	2.145618	41.7	1.862575	39	1.441497	39	1.257898
60	2.322187	54	2.031954	50.7	1.882345	44	1.520085
64.1	2.658003	64.8	2.519116	62.6	2.151077	50	1.6399
67.4	3.109934	70.8	2.909892	69.5	2.348023	62.7	1.888
76	3.218648	72.8	3.270695	76	2.663212	70	2.228917
85	3.6965	89.5	3.417019	88.6	3.008765	86.8	2.537036
95	4.0634	95	3.7561	95	3.2023	95	2.561868

angle =90		angle =135		angle =180	
TF-Ta	h	TF-Ta	h	TF-Ta	h
40	1.138826	35	1.1792	35	1.1457
44	1.278237	47	1.273909	38	1.198764
53	1.322306	51	1.383709	50	1.4556
60.6	1.28	62	1.540728	59.8	1.715942
95	1.800623	70	1.7561	65	1.732549
35	1.1428	85.9	1.900089	80	2.040785
70	1.5417	90.8	2.190088	86	2.230045
80	1.6558	95	2.1669	95	2.3908

Table 7-12 **H= 30mm and S=6.5mm**

angle =0		angle =30		angle =45		angle =60	
TF-Ta	h	TF-Ta	h	TF-Ta	h	TF-Ta	h
35	4.9449	35	4.7453	35	4.4109	35	3.4901
39.2	5.424629	44.9	5.28113	36.6	4.041816	51.3	4.036883
51.5	5.373206	45.7	4.975699	42	4.227664	58.2	4.065978
55	5.29882	54.3	5.185069	64	5.409046	71.2	4.366928
67.8	6.278672	70	4.93724	81.3	5.53578	76.8	4.825978
86.2	6.257081	77.2	6.023229	93.2	5.732634	91	5.064612
90.3	6.409109	95	6.24	95	5.9699	95	5.1881
95	6.4157	95.3	6.44299	55.4	4.80126	43	3.7165

angle =90		angle =135		angle =180	
TF-Ta	h	TF-Ta	h	TF-Ta	h
35	2.8072	35	3	35	3.012
41.3	2.721204	47.7	3.299523	39.7	3.598156
45.2	3.154582	55.9	3.610716	44.4	3.664717
65.5	3.45699	61.9	3.821444	61.6	4.326391
78.4	4.027362	76	4.220062	73.8	4.556782
90.7	3.969952	95	4.3	86	4.420445
95	4.0912	80.5	4.1421	91.1	4.609674
97.3	3.953154	90	4.3617	95	4.8418

Table 7-13

H= 30mm and S=13mm

angle =0		angle =30		angle =45		angle =60	
TF-Ta	h	TF-Ta	h	TF-Ta	h	TF-Ta	h
35	7.0628	35.2	6.620428	35	6.4733	35	4.97642
45	7.714371	52.3	7.550568	40.4	6.363182	41	5.370682
63.1	7.970145	54.7	7.769549	57.8	7.14577	41.7	5.283347
69.3	8.301059	63.2	8.147366	70.2	7.851119	48.3	5.940017
76.8	8.81248	73.7	7.89295	76.3	7.614938	63.1	6.0621
81.8	9.090095	80.9	8.664092	82	7.519444	74	6.7927
95	9.4644	95	8.510001	94	7.67206	92.5	7.313355
55.5	7.8902	43	7.197	95	8.0535	95	7.2658

angle =90		angle =135		angle =180	
TF-Ta	h	TF-Ta	h	TF-Ta	h
35	3.8734	35	4.3822	35	4.5904
36.3	4.102561	35.5	4.361541	47.7	5.131119
61.6	4.353127	46.7	4.595801	59.5	5.825056
70.3	4.924282	55	4.9135	66	6.161113
93	5.786094	64.7	5.073172	70.3	5.878156
95	5.8654	73.3	5.8718	82.7	6.362792
49	4.3037	94	5.721238	87.5	6.498614
81	5.3217	95	5.9775	95	6.629885

Table 7-14

H= 30mm and S=21.7mm

angle =0		angle =30		angle =45		angle =60	
TF-Ta	h	TF-Ta	h	TF-Ta	h	TF-Ta	h
35	7.4021	35	6.7501	35	6.8349	35	4.8041
52.7	8.119145	42.3	7.399208	41	6.885013	39.3	4.834447
65.5	9.227675	49.5	8.183232	55.4	7.450333	48.2	5.373396
73.2	9.305358	58.5	8.104029	65.6	8.045575	58.3	6.02131
80.5	9.604528	73.7	8.722793	67.5	8.70439	69	7.311247
83.6	9.890772	85	9.639129	85.5	9.044374	69.7	6.467224
87.1	10.28681	92.2	9.80017	95	9.2469	81.6	7.122184
95	10.5341	95	9.9168	77	8.6266	95	7.9188

angle =90		angle =135		angle =180	
TF-Ta	h	TF-Ta	h	TF-Ta	h
35	3.2971	35	4.2466	35	4.2466
51.5	3.987039	36.4	3.955914	46.7	4.72513
54	3.945247	46.5	4.580185	65.8	5.687138
67.4	4.753512	60.3	4.80429	80.3	6.47557
73.7	5.284756	69.2	5.51727	83.1	6.626593
83.1	5.609565	82.2	6.138044	95.6	7.124481
91.6	6.01175	95	7.1446	70	5.9232
95	6.2116	88	6.519	52.3	5.0558

Table 7- 15

H= 30mm and S=33mm

angle =0		angle =30		angle =45		angle =60	
TF-Ta	h	TF-Ta	h	TF-Ta	h	TF-Ta	h
35	9.0584	35	8.484544	35	8.4519	35	8.6272
46	9.191625	44.8	9.251731	40	8.686487	41.6	8.571013
55	9.701232	55	9.5087	51	9.191498	45.2	8.323677
66	10.31873	63.5	9.850067	61	9.672549	51.4	9.134071
72.2	10.51796	67.8	10.12337	67	9.469451	61	9.3123
81	10.9031	77.5	10.69233	74.5	10.12904	74.2	9.522564
89.4	11.11764	86	10.53247	82.2	10.42469	85.7	10.42
95	11.6765	95	11.02004	95	11.05279	95	10.6143

angle =90		angle =135		angle =180	
TF-Ta	h	TF-Ta	h	TF-Ta	h
35	5.7313	35	6.4767	35	7.1542
39.6	5.704487	39.3	6.856017	37.5	7.197646
53.8	6.45125	65	7.447123	51.4	7.977418
68	7.696858	71	7.754696	64	8.154319
75	7.428	84.5	8.376013	79	8.613001
85	7.8516	89.5	8.113812	81.2	8.722763
95	8.000681	90.4	8.028701	91.9	9.113091
66	7.0454	95	8.3871	95	9.2136

Table 7- 16

H= 15mm and S=3.375mm

angle =0		angle =30		angle =45		angle =60	
TF-Ta	h	TF-Ta	h	TF-Ta	h	TF-Ta	h
35	1.5765	35	1.4245	35	1.078	35	0.7902
38.3	1.773973	41.5	1.9	40.2	1.856	42	1.1219
49.5	2.387859	50	2.0686	45	1.504197	54	1.721675
62	2.615542	57.5	2.05	56.3	2.095403	63	2.4862
71.3	3.155262	65	2.760613	68	2.658731	70.2	2.397982
80	3.6594	79.3	3.389155	80	3.123511	79.5	2.906817
84.4	3.93046	86	3.564102	90	3.6303	89	3.3728
95	4.421961	95	4.067712	95	3.8607	95	3.6345

angle =90		angle =135		angle =180	
TF-Ta	h	TF-Ta	h	TF-Ta	h
35	0.6069	35	0.6069	35	0.8028
50	1.2045	46	1.199577	39	1
56	1.433985	52.3	1.295255	50	1.3903
68	1.642742	67	1.761002	59.5	1.66586
75	2.075614	73	2.2109	68	2.18376
83.3	2.547383	80	2.573954	85.4	2.705126
93	2.888924	91	3.022017	95	3.396818
95	3.026999	95	3.139	54	1.5503

Table 7-17

H= 15mm and S=6.5mm

angle =0		angle =30		angle =45		angle =60	
TF-Ta	h	TF-Ta	h	TF-Ta	h	TF-Ta	h
35	6.312	35	5.6	37	5.7123	35	5.123
45.8	6.038355	47.2	5.8	46	5.5042	38.8	5.1921
57	6.774243	55.3	5.457052	58.5	5.441484	54.2	5.098329
64.6	7.019741	67.5	6.217208	71	5.669601	64.3	5.21
69.4	7.139682	77	5.887445	83.5	6.434726	77.5	5.9
75.4	6.794825	80.9	6.540107	89.3	6.29959	86	6.151025
90.1	7.365983	95	7.0546	35	5.0236	95	6.6016
95	7.351	89	6.7944	95	6.7196	91	6.4312

angle =90		angle =135		angle =180	
TF-Ta	h	TF-Ta	h	TF-Ta	h
35	3.6011	35	3.8121	39.5	4.121
45	3.6123	38.1	3.9123	45.1	4.261637
64.8	4.2121	42.2	3.957749	57.8	4.927899
72.9	4.601951	59.4	4.087777	68.1	4.801142
82.8	4.661284	74.7	4.82913	84	5.395134
96.9	5.372975	77.9	5.604216	95	6.016349
50.3	4.012	95	5.658775	35	4.5122
89.1	5.0061	83.2	5.3571	75	5.1587

Table 7-18

H= 15mm and S=13mm

angle =0		angle =30		angle =45		angle =60	
TF-Ta	h	TF-Ta	h	TF-Ta	h	TF-Ta	h
35	7.3	35.1	7.028091	35	6.8377	35	6.3506
43.9	7.595076	43.7	7.676952	38.3	6.95704	42	6.5434
49.8	7.8818	60	7.72	48.2	6.959879	53.1	6.691487
59.1	8.309068	60.2	7.487069	63.5	8.232656	60.9	7.45476
67.1	8.641521	76.4	8.904877	70	7.8561	73.9	7.076656
78.9	8.996495	83.7	9.188922	80	7.644735	80	7.5919
88.9	9.869466	90.7	9.676533	91.2	8.651201	88.2	7.939352
95.5	10.0769	95	9.6586	95	8.5822	95	8.0096

angle =90		angle =135		angle =180	
TF-Ta	h	TF-Ta	h	TF-Ta	h
35	2.9575	35	3.4338	38	3.871922
47.4	3.502314	43	3.862624	55.7	4.587055
65	4.3667	45.2	3.906505	71.7	5.349726
76	4.9244	55	4.4665	79.9	6.033618
81.1	6.055067	67.3	4.665123	89.4	6.494836
95	6.4005	75.5	5.72319	94.2	7.210091
96.3	6.019952	91.7	6.215822	95	6.641
87	5.8024	95	6.6409	35	3.5133

Table 7-19

H= 15mm and S=21.7mm

angle =0		angle =30		angle =45		angle =60	
TF-Ta	h	TF-Ta	h	TF-Ta	h	TF-Ta	h
35	8.442	35.5	7.297498	47	7.280889	35	5.977
41.5	8.822191	46	7.828883	56	8.445179	44.3	6.386686
53.8	10.34054	54.1	8.8	61	8.33743	55.1	7.506504
66	10.05123	66.5	9.617475	77	9.077064	76	9.037487
73.5	11.12759	74.9	10.12558	79	9.148135	87.3	9.229014
77.3	11.19554	85.2	11.27278	95	10.74475	95	9.9247
90.4	12.33394	95	10.74475	35	6.6884	65	7.9792
93.7	12.27791	40	7.6947	85	9.8328	49	6.9167

angle =90		angle =135		angle =180	
TF-Ta	h	TF-Ta	h	TF-Ta	h
35	4.010504	35	4.4446	35	5.0078
45	4.702753	43	4.9	45.8	5.399062
52	5.672403	56.1	5.6	54.8	6.029519
62.5	5.65793	63	6.14444	68.8	6.529235
73.2	6.460793	70.9	7.006756	79.5	7.593817
82.8	7.003739	83	7.131014	87.7	8.239138
86.6	6.971808	89	7.7226	95	8.1159
95	7.4992	95	8.0884	63	6.4944

Table 7- 20

H= 15mm and S=33mm

angle =0		angle =30		angle =45		angle =60	
TF-Ta	h	TF-Ta	h	TF-Ta	h	TF-Ta	h
35	9.8584	35	9.2674	35	8.9415	50.9	7.887013
43.2	10.16408	50.6	9.29726	38.5	8.645799	60.6	9.805052
54.1	10.6642	67.2	11.10125	66	10.67572	73.6	9.196163
59.8	10.33878	75.5	10.97711	69.3	11.16325	85.9	10.44519
74.3	11.47058	81.4	11.70725	77.7	10.48977	92.9	10.84564
83.5	12.02007	86.1	12.82889	87.3	12.02005	68.4	10.90786
94.1	12.27634	91.1	11.36873	88.7	11.51842	35	7.8398
95	12.6669	95.3	12.31315	95	12.1089	95	11.0919

angle =90		angle =135		angle =180	
TF-Ta	h	TF-Ta	h	TF-Ta	h
35	5.134083	35.7	6.160254	35	6.684
44.3	5.611041	57.5	7.174645	38.5	6.49448
56	7.382272	76.5	8.097532	48.5	7.993272
59.6	6.248827	92.3	9.251059	64	7.994545
60.1	7.114628	95	9.2515	77	8.433055
83.2	8.94037	64	8.383114	89.8	9.073747
87	8.714217	54.4	6.317387	90.3	10.08878
95	9.1149	50	7.977661	95	9.4509

Table 7- 21

Numerical solution H= 60mm and S=6.5mm

angle =0		angle =30		angle =45		angle =60	
TF-Ta	h	TF-Ta	h	TF-Ta	h	TF-Ta	h
35	5.4	35	5.4	35	5.4	35	5.271197
44	5.746998	46.25	5.758712	40.5	5.598102	38.25	5.363096
53.75	5.934257	55.3	5.9918289	63.925	5.97092	52.375	5.678468
60.125	6.07708	60.2	6.086696	71.95	6.1486201	53.5	5.711528
68.5	6.233842	72	6.283624	75.5	6.16145	66.025	5.869266
77.3	6.380849	80	6.3922133	87.125	6.298343	76	5.96248
84.75	6.471729	93.325	6.5412765	90.5	6.389429	92.5	6.071448
95	6.602056	95	6.554552	95	6.426398	95	6.086942

angle =90		angle =135		angle =180	
TF-Ta	h	TF-Ta	h	TF-Ta	h
35	3.5725758	35	4.259459	35	4.227167
44	3.795383	44.873	4.3778949	45.025	4.47549
50.5	3.834817	53.75	4.429509	52	4.610112
60	3.86558	60.875	4.473215	67.875	4.874681
71.2	3.882088	71.75	4.493783	93.5	5.073684
80.875	3.87248	76.3	4.524298	81	5.073684
93.75	3.842206	88.075	4.522717	87.5	5.074411
95	3.876819	95	4.531966	95	5.068008

Table 7- 22

H= 40mm and S=6.5mm

angle =0		angle =30		angle =45		angle =60	
TF-Ta	h	TF-Ta	h	TF-Ta	h	TF-Ta	h
35	5.235	35	5.16	35	3.52424	35	3.425898
36.4	5.35359	40.7	5.375256	47.4	3.914165	44.5	3.688943
49.1	5.460323	62.5	5.604689	55.9	4.121481	50	3.813318
68	5.781796	69.5	5.656915	65.5	4.337705	68.5	4.183664
81.1	6.017403	76.1	5.723589	72	4.488071	73.5	4.265533
87.2	6.021058	87.2	5.784411	81	4.639698	79.5	4.365918
91.1	5.90847	92.4	5.759552	90.5	4.807006	92.5	4.555817
95	5.964677	95	5.815085	95	4.8757553	95	4.588597

angle =90		angle =135		angle =180	
TF-Ta	h	TF-Ta	h	TF-Ta	h
35	2.98781	35	3.387279	35	3.460186
39.8	3.028098	45	3.443486	39.7	3.567203
43	3.048837	53	3.584874	51	3.735152
52.5	3.091609	69	3.644043	62.5	3.807784
69	3.122372	79	3.654665	69	3.8498
80	3.14805	88.5	3.659389	78.5	3.881474
93	3.100736	95	3.645861	88	3.896364
95	3.097257	60	3.605715	95	3.924988

Table 7- 23

H= 30mm and S=6.5mm

angle =0		angle =30		angle =45		angle =60	
TF-Ta	h	TF-Ta	h	TF-Ta	h	TF-Ta	h
35	4.923749	35	4.848985	35	4.6843	35	4.458677
39.2	5.062052	44.9	5.139011	36.6	4.711374	51.3	4.709723
51.5	5.457601	45.7	5.159356	42	4.86569	58.2	4.782188
55	5.54569	54.3	5.378556	64	5.330802	71.2	4.892572
67.8	5.86	70	5.730847	81.3	5.612003	76.8	4.933198
86.2	6.223957	77	5.862496	93.2	5.778191	91	5.07465
90	6.290636	85	5.994898	95	5.822386	95	5.171447
95	6.374906	95	6.18504	55	5.149418	43	4.602771

angle =90		angle =135		angle =180	
TF-Ta	h	TF-Ta	h	TF-Ta	h
35	3.316753	35	3.547999	35	3.969012
41.3	3.450179	47.7	3.717739	39.7	4.040824
45.2	3.490588	55.9	3.818626	44.4	4.123926
97.3	3.729032	61.9	3.8966	61.6	4.369744
65.5	3.619619	76	4.060546	73.8	4.50582
78.4	3.670899	95	4.302415	86	4.597686
90.7	3.708716	80.5	4.126714	91.1	4.640356
95	3.724969	90	4.21067	95	4.657643

Table 7- 24

H= 15 mm **S=6.5mm**

angle =0		angle =30		angle =45		angle =60	
TF-Ta	h	TF-Ta	h	TF-Ta	h	TF-Ta	h
35	6.67435	35	6.272242	37	5.833446	35	5.360157
45.8	7.008161	47	6.405346	46	6.031898	38.8	5.489649
57	7.210902	55	6.621036	58.5	6.237751	54.2	5.74998
64.6	7.296589	67.5	6.842209	71	6.350747	64.3	5.861807
69.4	7.346845	77	6.927431	83.5	6.409215	77.5	5.868467
75.4	7.385876	80.9	6.947165	89.3	6.427559	86	6.02
90.1	7.435107	89	6.985281	35	5.742846	95	6.011428
95	7.390694	95	6.973464	95	6.448156	91	6.020025

angle =90		angle =135		angle =180	
TF-Ta	h	TF-Ta	h	TF-Ta	h
35	4.45	35	4.578398	39	4.888285
45	4.592309	38.1	4.64573	45.1	5.000735
64.8	4.780507	42.2	4.759809	57.8	5.155588
72.9	4.8391	59.4	4.973638	68.1	5.256315
82.8	4.885352	74.7	5.086192	84	5.359324
95	4.950745	77.9	5.119064	95	5.412148
50.3	4.648096	95	5.2271247	35	4.791274
89.1	4.896464	83.2	5.137696	75	5.314706

Table 7- 25

S=3.37mm ΔT=60 C°

Φ	**0°**	**30°**	**45°**	**60°**	**90°**	**125°**	**180°**
H mm	**Q/A $_b$[w/m^2]**	**Q/A $_b$[w/m^2]**	**Q/A $_b$[w/m^2]**	**Q/A $_b$[w/m^2]**	**Q/A $_b$[w/m^2]**	**Q/A $_b$[w/m^2]**	**Q/A $_b$[w/m^2]**
15	2061.33	1841.895	1831	1632.8	1103.715	1175.77	1354.042
30	3265.63	3212.2	2914.9055	2478.93	1831.939466	2128.815	2389.486
40	3902.8	3570	3248.9	2778.98	2100	2302.9	2708.08
60	5655.12	5076.49	4657.9	4348.74	3521.95	3848.14	4068.68

S=6.5mm ΔT=60 C°

Φ	**0°**	**30°**	**45°**	**60°**	**90°**	**125°**	**180°**
H mm	**Q/A $_b$[w/m^2]**	**Q/A $_b$[w/m^2]**	**Q/A $_b$[w/m^2]**	**Q/A $_b$[w/m^2]**	**Q/A $_b$[w/m^2]**	**Q/A $_b$[w/m^2]**	**Q/A $_b$[w/m^2]**
15	2386.426	2017	1929.77	1890.88	1452.6	1474.93	1635.04
30	3408.705	3371.2	3045	2497.85	1969.45	2178.2929	2476.282
40	4017.38	3782	3310.119	2847.32	2350.37	2631.75	2783.3
60	6327.91	5994.86	5899.71	5258.87	3663.53	4710.25	5188.83

S=13 mm ΔT=60 C°

Φ	**0°**	**30°**	**45°**	**60°**	**90°**	**125°**	**180°**
H mm	**Q/A $_b$[w/m^2]**	**Q/A $_b$[w/m^2]**	**Q/A $_b$[w/m^2]**	**Q/A $_b$[w/m^2]**	**Q/A $_b$[w/m^2]**	**Q/A $_b$[w/m^2]**	**Q/A $_b$[w/m^2]**
15	2069.389	1947.656	1846.22	1730.13	1234.98	1286.25	1373.58
30	3225.806	3130.6	2962.06	2443.21	1825.9	2136.34	2353.42
40	3961	3692.4	3246.09	2750	2042.3	2613.11	2718.6
60	5590.32	5514.4	4958.212	4420.56	2840.3	3882.45	3976.466

S=21.7mm ΔT=60 C°

Φ	0°	30°	45°	60°	90°	125°	180°
H mm	Q/A $_b$[w/m^2]	Q/A $_b$[w/m^2]	Q/A $_b$[w/m^2]	Q/A $_b$[w/m^2]	Q/A $_b$[w/m^2]	Q/A $_b$[w/m^2]	Q/A $_b$[w/m^2]
15	1799.57	1722.89	1535.087	1469.98	1033.79	1178.1	1197.02
30	2480.08	2281.4	2184.65	1794.463	1247.4765	1499.409	1753.25
40	3112.62	2949.43	2829.655	2302.215	1377.4	1776.163	2286.83
60	3678.55	3515.85	3208.33	3090.67	2372.05	2590.767	2826.027

S=33mm ΔT=60 C°

Φ	0°	30°	45°	60°	90°	125°	180°
H mm	Q/A $_b$[w/m^2]	Q/A $_b$[w/m^2]	Q/A $_b$[w/m^2]	Q/A $_b$[w/m^2]	Q/A $_b$[w/m^2]	Q/A $_b$[w/m^2]	Q/A $_b$[w/m^2]
15	1632.186	1579.97	1502.414	1282.5	1042.68	1088.571	1142.94
30	2150.537	2098.6	2050.76	1778.39	1508.49	1615.83	1699.022
40	2533.61	2313.457	2150.54	2100	1694.36	1734.87	1975.769
60	3160.638	3058.89	2876.69	2594.91	2085.9	2318.11	2368.82

Table 7- 26

H=15 mm ΔT=60 C°

s=3.375		**s=6.5 mm**		**s=13 mm**		**s=21.7 mm**	
Φ dgree	hw/m^2.k	Φ dgree	hw/m^2.k	Φ dgree	hw/m^2.k	Φ dgree	hw/m^2.k
0	2.707979	0	7.037099	0	8.376958	0	10.07746
30	2.419706	30	5.947734	30	7.884178	30	9.648055
45	2.405393	45	5.69051	45	7.473562	45	8.596372
60	2.145017	60	5.575831	60	7.003626	60	8.231778
90	1.449956	90	4.28343	90	4.999241	90	5.789147
125	1.544615	125	4.349277	125	5.206784	125	6.597272
180	1.778811	180	4.82141	180	5.560299	180	6.703222

s=33 mm

Φ dgree	hw/m^2.k
0	11.50046
30	11.13254
45	10.58608
60	9.036555
90	7.3467721
125	7.670122
180	8.053209

H=30 mm ΔT=60 C°

s=3.375		**s=6.5 mm**		**s=13 mm**		**s=21.7 mm**	
Φ dgree	hw/m^2.k	Φ dgree	hw/m^2.k	Φ dgree	hw/m^2.k	Φ dgree	hw/m^2.k
0	2.322187	0	5.980993	0	8.030643	0	8.965612
30	2.3	30	5.915186	30	7.793627	30	8.247374
45	2.09	45	5.342828	45	7.374047	45	7.897618
60	1.83525	60	4.382786	60	6.08237	60	6.487072
90	1.2	90	3.455643	90	4.545577	90	4.509689
125	1.51245	125	3.822083	125	5.318417	125	5.420438
180	1.715942	180	4.344942	180	5.858838	180	6.338085

s=33 mm

Φ dgree	hw/m^2.k
0	10.25698
30	10.00927
45	9.781095
60	8.482027
90	7.194739
125	7.706697
180	8.103481

H=40 mm **ΔT=60 C^o**

s=3.375		**s=6.5 mm**		**s=13 mm**		**s=21.7 mm**	
Φ dgree	hw/m^2.k	Φ dgree	hw/m^2.k	Φ dgree	hw/m^2.k	Φ dgree	hw/m^2.k
0	1.5607399	0	5.525877	0	7.84677	0	9.10159
30	1.4276523	30	5.225365	30	7.314672	30	8.624407
45	1.2992435	45	4.573308	45	6.430528	45	8.274174
60	1.1113213	60	3.933898	60	5.4477	60	6.73189
90	0.894842	90	3.247305	90	4.045811	90	4.186552
125	0.9209357	125	3.636063	125	5.17659	125	5.193665
180	1.0829682	180	3.845447	180	5.385567	180	6.686903

s=33 mm

Φ dgree	hw/m^2.k
0	9.942472
30	9.07854
45	8.439216
60	8.240886
90	6.64906
125	6.808031
180	7.753374

H=60 mm **ΔT=60 C^o**

s=3.375		**s=6.5 mm**		**s=13 mm**		**s=21.7 mm**	
Φ dgree	hw/m^2.k	Φ dgree	hw/m^2.k	Φ dgree	hw/m^2.k	Φ dgree	hw/m^2.k
0	2.261497	0	6.134506	0	7.862596	0	7.781726
30	2.030102	30	5.811635	30	7.755817	30	7.437545
45	1.862706	45	5.719393	45	6.973557	45	6.787007
60	1.739073	60	5.09814	60	6.217368	60	6.538105
90	1.408437	90	3.551559	90	3.994786	90	5.017913
125	1.538881	125	4.566287	125	5.460534	125	5.480594
180	1.627076	180	5.03024	180	5.592765	180	5.978271

s=33 mm

Φ dgree	hw/m^2.k
0	9.1573
30	8.862506
45	8.334619
60	7.518219
90	6.043467
125	6.716248
180	6.86317

العنوان:	Experimental and Numerical Study of Natural Convection Heat Transfer from Rectangular Fin Arrays
المؤلف الرئيسي:	Mohamad, Hamza Ashur Milad
مؤلفين آخرين:	Abd Allatif, Ahmed Mohamed، El Bakoush, Taib A(Advisor، Co-Advisor)
التاريخ الميلادي:	2007
موقع:	Al Khums
الصفحات:	1 - 155
رقم MD:	766381
نوع المحتوى:	رسائل جامعية
اللغة:	English
الدرجة العلمية:	رسالة ماجستير
الجامعة:	جامعة المرقب
الكلية:	كلية الهندسة
الدولة:	ليبيا
قواعد المعلومات:	Dissertations
مواضيع:	المصفوفة ، الحاسب الآلي، الحمل الحراري
رابط:	https://search.mandumah.com/Record/766381

AL-MERGEB UNIVERSITY

Faculty of Engineering

Mechanical Engineering Department

Experimental and Numerical Study of Natural Convection Heat Transfer from Rectangular Fin Arrays

M.Sc Thesis in Mechanical Engineering

By
HAMZA ASHUR MILAD MOHAMAD

A thesis submitted in partial fulfillment of requirements for the masters degree of science in Mechanical Engineering

Supervised by
Dr. AHMED ABDEL-LATIF
Dr. TAIB EL-BAKOUSH

2007